ChemPubSoc Europe

DOI: 10.1002/chem.201804225

CHEMISTRY
A European Journal
Review

Materials Science

Nonconjugated Hydrocarbons as Rigid-Linear Motifs: Isosteres for Material Sciences and Bioorganic and Medicinal Chemistry

Gemma M. Locke, Stefan S. R. Bernhard, and Mathias O. Senge*[a]

Dedicated to Professor Philip E. Eaton

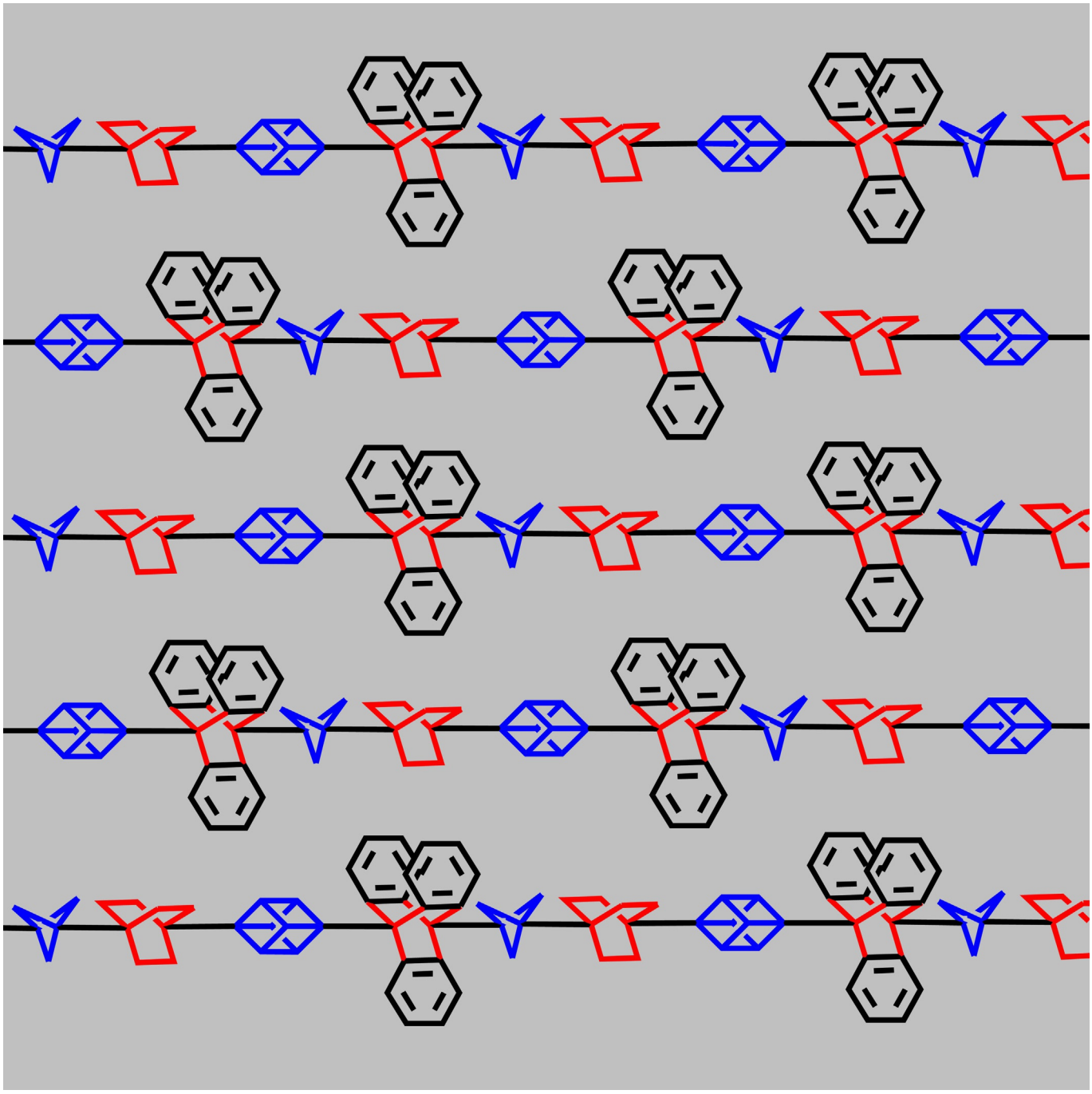

Abstract: Nonconjugated hydrocarbons, like bicyclo[1.1.1]-pentane, bicyclo[2.2.2]octane, triptycene, and cubane are a unique class of rigid linkers. Due to their similarity in size and shape they are useful mimics of classic benzene moieties in drugs, so-called bioisosteres. Moreover, they also fulfill an important role in material sciences as linear linkers, in order to arrange various functionalities in a defined spatial manner. In this Review article, recent developments and usages of these special, rectilinear systems are discussed. Furthermore, we focus on covalently linked, nonconjugated linear arrangements and discuss the physical and chemical properties and differences of individual linkers, as well as their application in material and medicinal sciences.

1. Introduction

Arranging functionalities in a linear fashion enables the alteration of the distance between functionalities without affecting the overall geometry of the molecule, and this is of high importance in medical and material sciences. This can be achieved with nonconjugated rigid hydrocarbons (NRHs) which share three main features for their usage in biological and material sciences: 1) they are rigid, that is, all conformational changes are frozen; 2) they are linear, where the arrangement of the different functionalities happens in a defined spatial manner, in this case a 180° fashion; 3) they are nonconjugated, as the formal sp^3-hybridized carbon center interrupts electronic communication (even though this is only partially true, as will be discussed in detail vide infra).

Over the years, linear linking has been a classic field of *para*-substituted benzenes and alkynes, due to the plethora of well-established cross-coupling reactions.[1] Recently however, certain other hydrocarbons, such as cubane or bicyclo[1.1.1]pentane (BCP) have begun to draw attention due to their remarkable properties.[2,3] Besides these highly strained, rather unusual hydrocarbons more common moieties are in use, such as bicyclo[2.2.2]octane (BCO) and triptycene (Figure 1). In particular, the use of triptycene as a molecular rotor has received much interest, propelled by the Nobel prize in chemistry for molecular machines awarded in 2016.[4]

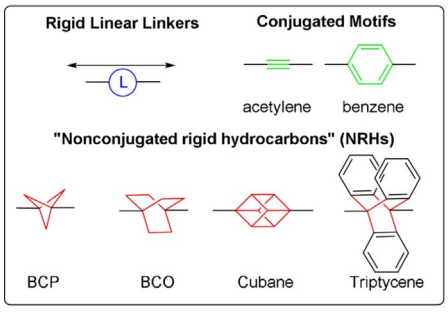

Figure 1. Nonconjugated rigid hydrocarbons (NRHs).

This Review aims at identifying the origins of rigid-linear-aliphatic hydrocarbons and their use in functional materials, while tying together the chemistry, differences and commonalities between these groups and outlining the missing components of those dormant groups. While there are many aspects that govern the structural composition and behavior of a compound, such as quantum mechanics (e.g., London dispersion), this review will focus solely on the physical bond connections within the four selected NRH linkers, taking a structural engineering viewpoint.

2. General Aspects

2.1. Bicyclo[1.1.1]pentane (BCP)

Bicyclo[1.1.1]pentane (BCP) is the smallest member of bicyclic bridged alkanes. It was first synthesized by Wiberg et al. in 1964 (Scheme 1).[5,6] The synthesis was achieved by an anti-Markovnikov addition of hydrogen bromide to methylenecyclobutane **1**, followed by hydrolysis of the methylester **2** and decarboxylative bromination in the presence of mercury(II)oxide. The final ring-closure was achieved by a Wurtz reaction of the dibromide **3** in dioxane to form BCP **4**.

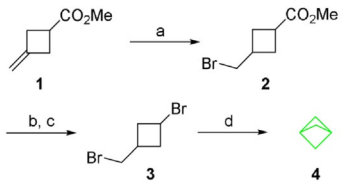

a) HBr; b) H_2O, NaOH; c) HgO, Br_2; d) Na, dioxane

Scheme 1. Synthesis of BCP according to Wiberg et al.[5]

Different approaches for the synthesis of substituted and unsubstituted BCPs are known in the literature.[7] The methods involve cyclizations, ring-expansions, and ring-contractions. Today, most chemistry of the BCP scaffold arises from the bridged [1.1.1]propellane intermediate **6** by utilizing strain relief as the main driving force. Usually the generation of the reactive [1.1.1]propellane intermediate is carried out according

[a] *G. M. Locke, Dr. S. S. R. Bernhard, Prof. Dr. M. O. Senge*
School of Chemistry, SFI Tetrapyrrole Laboratory
Trinity Biomedical Sciences Institute, Trinity College Dublin
The University of Dublin, 152–160 Pearse Street, Dublin 2 (Ireland)
E-mail: sengem@tcd.ie

The ORCID identification number(s) for the author(s) of this article can be found under: https://doi.org/10.1002/chem.201804225.

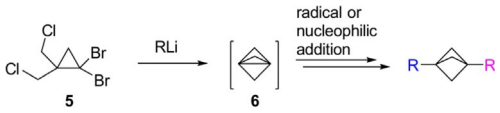

Scheme 2. Preparation of [1.1.1]propellane **6**.

to an optimized and improved procedure developed by Szeimies and co-workers that employs the tetrahalide **5** as the starting material (Scheme 2).[8] The term propellane was first coined by Ginsburg et al. in 1966, to trivialize the lengthy names tricyclic systems require.[9]

The molecular structure of the parent BCP hydrocarbon shows some notable peculiarities. Electron diffraction in the vapor phase confirmed the symmetric shape (D_{3h}) and shows one of the shortest nonbonded carbon–carbon interactions (interbridgehead distance of 1.845[10]/1.874 Å[11]). This 1,3-nonbonded repulsion of the bridgehead carbon atom leads to a destabilization of the BCP cage in the ground state. Moreover, it even is considered to be one major aspect of the overall ring strain.[12] The inverted tetrahedral geometry of BCP is represented by the high strain energy of 68 kcal mol^{-1} (Table 1).[13]

Table 1. Physical properties of bicyclo[1.1.1]pentane.

Molecular formula	C_5H_8
boiling point [°C][7]	36
appearance	colorless clear liquid
decomposition [°C][21]	>280
heat of formation [kcal mol^{-1}] [13]	51
strain energy [kcal mol^{-1}][13]	68
C_1–C_2 bond length [Å]	1.545[10]/1.557[11]
C–H bond length [Å]	1.100[10]/1.109[11]
bridgehead distance [Å]	1.845[10]/1.874[11]

Decreasing the electron density of the relevant orbitals, for example, by the introduction of electron-withdrawing substituents at the bridgehead, leads to a reduction of the 1,3-nonbonding repulsion and a shorter distance between the bridgehead carbon atoms.[14] Interestingly, this repulsion is further relieved by the introduction of an internal carbon–carbon bond, an unexpected stability of [1.1.1]propellane. Due to the high *s*-character, the intercaged carbon–carbon bonds are very short (according to Bent's rule).[15] Therefore, the true character of the central inverted bridgehead–bridgehead bond still remains enigmatic (Scheme 3). A refined electron density analysis of [1.1.1]propellane by intense synchrotron primary radiation measurements revealed significant electron density, which is characteristic of a covalent bond, but no charge accumulation

Scheme 3. Valence bond structures for the internal bond in [1.1.1]propellane.

at the bond critical point,[16] as a positive Laplacian was evident.[17] A positive Laplacian usually is interpreted as a typical signature of charge shift bond, a bond in which the covalent–ionic resonance energy is the main factor.[18]

In addition, systematic theoretical studies of the $^1J_{(13C–13C)}$ nuclear spin–spin coupling of the bridgehead–bridgehead carbon atoms reflected strong through-cage electronic interactions, but with higher *p*-character of the central bond.[19] The inverted carbon geometry of the bridgehead–bridgehead bond, no matter of the actual bond character itself–which most likely will stay unrevealed–still tests current theoretical calculations of energy and bond lengths (Table 1).[20] Further information about BCP and related propellanes can be found in other very comprehensive reviews.[3,7,22]

Gemma Locke obtained her BSc in Medicinal Chemistry at Trinity College Dublin (TCD) in 2014. During this time, she did a three-month internship in the University of North Carolina at Chapel Hill (UNC), working on N-centered radicals under the supervision of Prof. Dr. Erik Alexanian. She is currently a PhD student under the mentorship of Prof. Dr. Mathias O. Senge carrying out research on electron-transfer mimics with both cubane and triptycene porphyrin complexes.

Dr. Stefan Berhard studied chemistry at the Johannes Gutenberg-University Mainz, Germany. He completed his doctoral studies on the synthesis of optically active crinine-type alkaloid precursors under the supervision of Prof. Udo Nubbemeyer in 2015. In the same year he joined the group of Prof. Dr. Mathias O. Senge at the Trinity College Dublin as a postdoctoral researcher. His current research is focused on cross-coupling chemistry with highly strained alkanes and the functionalization of porphyrins.

Mathias O. Senge, Dipl.-Chem., MA, Dr rer. nat., FTCD, studied chemistry and biochemistry in Freiburg, Amherst, Marburg, and Lincoln. After a PhD from the Philipps Universität Marburg (1989) and postdoctoral studies with K. M. Smith at UC Davis he received his habilitation in Organic Chemistry in 1996 from the Freie Universität Berlin. From 1996 on he was a Heisenberg fellow at FU Berlin and UC Davis and held visiting professorships in Greifswald and Potsdam. In 2002 he was appointed Professor of Organic Chemistry at the Universität Potsdam and since 2005 holds the Chair of Organic Chemistry at Trinity College Dublin. He was the recipient of fellowships from the Studienstiftung des Deutschen Volkes, the Deutsche Forschungsgemeinschaft, and Science Foundation Ireland (Research Professor 2005–2009).

2.2. Bicyclo[2.2.2]octane (BCO)

The first synthesis of bicyclo[2.2.2]octane (BCO) **10** was achieved by Alder and Stein in 1934 (Scheme 4).[23] They utilized their prior findings, a Diels–Alder reaction, for the generation of the

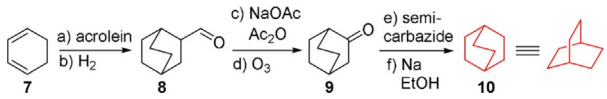

Scheme 4. Synthesis of bicyclo[2.2.2]octane.

bridged bicyclo[2.2.2]octane-2-carbaldehyde **8**.[24] After ozonolysis of the enolacetate to ketone **9**, they were able to reduce the corresponding semicarbazide to the parent hydrocarbon **10**.

In comparison to the fairly stable [1.1.1]propellane, the corresponding [2.2.2]propellane **12** is only of minor importance for further synthetic modifications. The first synthesis of the unsubstituted parent hydrocarbon was achieved by Wiberg et al. in 1974.[25] However, the pure material could not be isolated and was trapped as the addition product of chlorine **13** (Scheme 5). The [2+2]-cycloreversion to the 1,4-dimethylenecy-

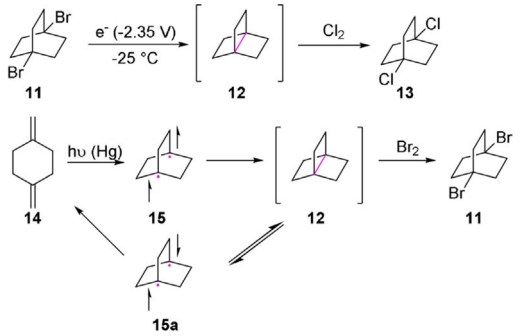

Scheme 5. Synthesis of [2.2.2]propellane.

clohexane **14** proceeds at low temperatures by the singlet radical. Interestingly, the opposite approach, populating the triplet state via irradiation, can also be used to generate [2.2.2]propellane **12**. Again, the reactive intermediate was trapped by the addition of bromine to give **11**.[26]

Both experiments proved earlier predictions regarding the instability of the [2.2.2]propellane system through calculations by Stohrer and Hoffmann.[27] The actual conformation of BCO was a topic of a long discussion during the 1960s.[28,29] The large heat of hydrogenation from bicyclo[2.2.2]octene to bicyclo[2.2.2]octane, was interpreted by Turner et al. as proof for a twisted D_3-structure,[30] in accordance with previous strain-minimization calculations by Hendrickson (Figure 2).[31] In contrast, the analysis of IR, Raman, and microwave spectra indicated an eclipsed conformation with D_{3h}-symmetry.[32] Due to a formation of a large super-cell with a complex diffraction pattern, the preferred conformation could not be proven.[33] Only the

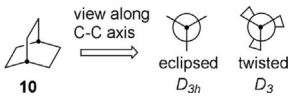

Figure 2. Conformation of BCO.

analysis of substituted derivatives gave clear indication that the stable conformation is indeed the eclipsed D_{3h} one.[29,34] The measured bond distances and angles are in good agreement with the theoretical considerations of Gleicher and Schleyer, both supporting the D_{3h}-symmetry.[35]

The high melting of BCO is attributed to the dense, approximately spherical packing (Table 2).

Table 2. Physical properties of bicyclo[2.2.2]octane.

Molecular Formula	C_8H_{14}
boiling point [°C][36]	116 (5 mbar)
melting point [°C][23]	169–170
heat of formation [kcal mol^{-1}][15]	−24.3
strain energy [kcal mol^{-1}][15]	7.4
C_1–C_2 bond length [Å][a]	1.542[29]
C_2–C_3 bond length [Å][a]	1.544[29]
C_1–C_4 distance [Å][a,b]	2.597 Å[29]

[a] Data in reference to the 1,4-dicarboxylic acid derivative, since no data for the parent compound is available. [b] Bridgehead-to-bridgehead distance.

2.3. Triptycene and barrelene

Highly related to the BCO system is the triple benzannulated tripycene, the simplest representative of the so-called iptycenes.[37,38] Triptycene—named after "triptych" (*τρίπτυχον* Greek. "*threefold*"), a painting or book with three leaves hinged on a common axis—was first synthesized by Bartlett et al. in 1942 (Scheme 6).[39] A Diels–Alder reaction was used to install the threefold geometry, by reacting anthracene **16** with quinone in refluxing xylene. The final defunctionalization of the quinone intermediate was obtained by isomerization, oxidation to the corresponding quinone **17**, substitution with hydroxylamine hydrochloride, and a subsequent reduction to the diamine **18**. The bis-diazoniumtriptycene was afforded through

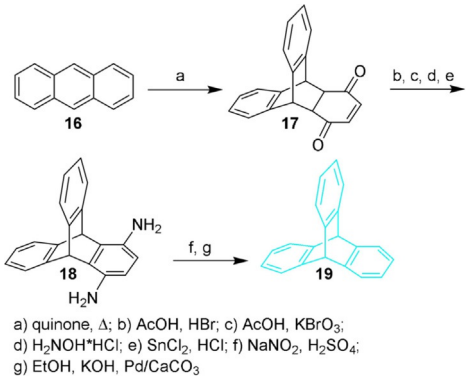

Scheme 6. Synthesis of triptycene according to Bartlett et al.[39]

diazotization with sodium nitrite and reduction of the corresponding chloride in the presence of potassium hydroxide and palladium on calcium carbonate, to yield triptycene **19**. This synthetic route enabled access to a series of substituted BCO derivatives, to study the nucleophilic substitution at the bridgehead carbon center and thus investigate the reactivity of structures, which cannot undergo the Walden inversion.[40,41] A further insight into the chemistry of those bridgeheads will be given at a later stage. Up to now, using a Diels–Alder reaction with anthracene derivatives is still the most valid method for the introduction of functionalities in the bridgehead positions, especially with the usage of aryne coupling partners, generating the (functionalized)-triptycene unit in a single step.[42]

The missing link from BCO to triptycene is bicyclo[2.2.2]octa-2,5,7-triene, the so-called barrelene **24**. Its first synthesis was achieved by Zimmerman and Paufler in 1960 (Scheme 7).[43]

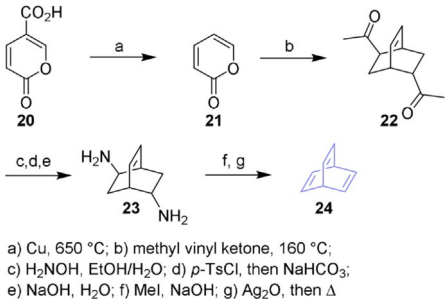

Scheme 7. Synthesis of barrelene by Zimmerman et al.[43]

Coumalic acid **20** was decarboxylated over copper at 650 °C to α-pyrone **21**. Afterwards the labile diene was heated under reflux with two equivalents of methyl vinyl ketone, generating the bicyclo[2.2.2]octene **22** skeleton in a double Diels–Alder reaction with loss of carbon dioxide. Generation of the bis-oxime, and a subsequent second-order Beckmann rearrangement under alkaline conditions of the bis-tosylate, yielded the diamine **23**. Exhaustive methylation and Hofmann elimination of the quaternary ammonium salts led to the introduction of the two missing double bonds, finalizing the synthesis of barrelene **24**.

The photochemical isomerization of barrelene represents one of the most fundamental and general photoprocesses; a di-π-methane rearrangement is observed which initiated different general mechanistic discussions (Scheme 8).[44,45]

Different pathways are observed depending on the presence of an additional photosensitizer. Direct irradiation results in a photochemical isomerization to cyclooctatetraene **30** by the intramolecular [2+2]-cycloadduct **29**. In the presence of a suitable photosensitizer, the triplet excited state reacts with the diradical **28a**. Ring-opening of the cyclopropane intermediate to the stabilized allylradical **28b** results in the subsequent formation of semibullvalene **31**.[46] Consideration of the bond structure, according to Hückel's rule, suggests barrelene **24** is an aromatic compound. Although the π-bonds are not coplanar, the p orbitals show some homoconjugative overlap with a

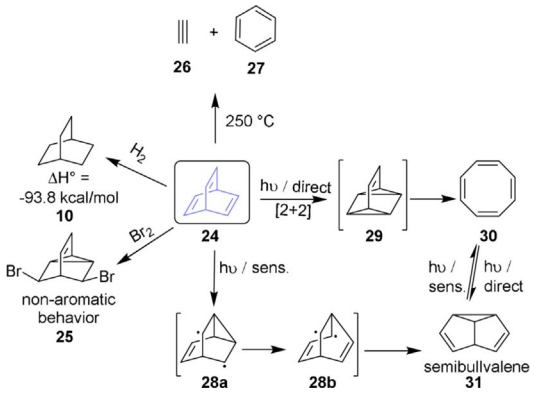

Scheme 8. Reactivity and photochemistry of barrelene.

Figure 3. Barrelene as a Möbius aromatic system.

phase shift, a characteristic phenomenon for Möbius-type aromatic structures (Figure 3).[47,48]

However, the chemistry and reactivity of **24** indicate a rather non-aromatic behavior. Hydrogenation of the double bonds results in the saturated BCO **10** (Scheme 8). Thereby, comparison to other hydrocarbons suggests a destabilization of about 10 kcal mol^{-1} due to angular strain.[49] The addition of bromine leads to a transannular bond formation yielding **25**, showing typical nonaromatic behavior as well.[47] Despite its theoretical interest, little use of barrelene **24** as a building block is reported in the literature.[50] The existence of the even more bizarre propellene analogue, [2.2.2]propellatriene, is a topic of speculation and for now remains at the realms of theoretical chemists.[51]

2.4. Cubane

Cubane **37**, a constitutional isomer to barrelene (C_8H_8) **24**, was synthesized in 1964 by P. E. Eaton and T. W. Cole.[52,53] Despite its fascinating simple structure of eight methine units in perfect cubic arrangement, this synthesis is considered a milestone of organic chemistry,[54] challenging the concept of carbon hybridization. Cubane was considered impossible due to the significant deviation in geometry of each carbon atom from the tetrahedral angle (109.5° of sp^3-carbon vs. 90° in a cubic arrangement).[55] Its high strain notwithstanding, cubane shows a remarkable high thermal stability; due to the lack of orbital symmetry-allowed ring opening, the thermal rearrangement does not occur below 200 °C.[56]

Eaton's original synthesis of the carbon skeleton of cubane **37** is still the basis of most practical approaches to install the caged structure.[57] Just two cycloadditions, a diastereoselective Diels–Alder reaction, and a subsequent [2+2]-photocyclization, are necessary to setup the backbone of cubane, which then can undergo a double ring contraction under Favorskii conditions (Scheme 9).[53]

Other approaches to generate substituted cubanes, make use of [2+2]-cycloadditions of substituted tricy-

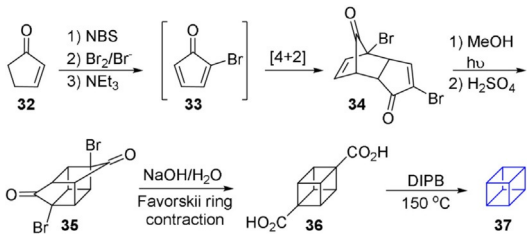

Scheme 9. Eaton and Cole's synthesis of the cubane core.[53,57] DIPB = 1,4-diisopropylbenzene; NBS = *N*-bromosuccinimide.

clo[4.2.0.0^{2,5}]octa-3,7-diene derivatives **38**, a method not suitable for unsubstituted cubanes, due to the large separation of the involved π-orbitals (3.05 Å), the sizeable difference in strain energy between the educt and product, and a dominance of through-bond interaction, as π^+ lies above π^- for both sets of MOs (Scheme 10).[58] Dissimilarly to the quite stable [1.1.1]pro-

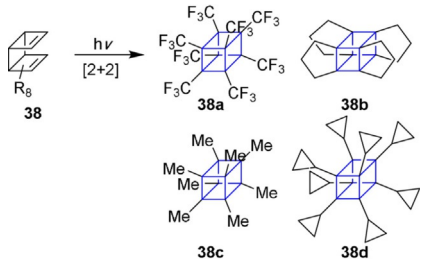

Scheme 10. Persubstituted cubanes.

pellane, the reaction of 1,4-diiodocubane **39** with *tert*-butyllithium, is proposed to have three plausible reactive intermediates, the cubane-diyl **40 a**, the "cubane-propellane" **40 b**, and the cubane–diene **40 c** (Scheme 11).[59] Due to an orbital mis-

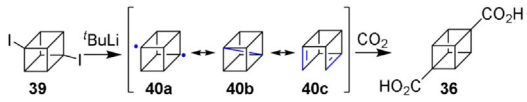

Scheme 11. Reactive intermediates in the synthesis of compound **36**.

match the long length of the internal bond would be rather weak and calculations could rule out the likelihood of a "cubane-propellane" intermediate and strengthen the possibility of a singlet diradical species.[60,61] The cubane–diene intermediate **40 c**, a supposedly excellent dienophile, could not be quenched in the presence of Diels–Alder dienes.

Due to the unusual structure of cubane its physical properties are quite different from other hydrocarbons (Table 3). The perfect cubic arrangement of the carbon atoms results in an octahedral point group O_h, with a high density of 1.29 g cm^{-3}.[62] The carbon–carbon distance of 1.571 Å is slightly longer than in unstrained alkanes (1.54 Å) and in cyclobutane (1.55 Å).[63] Further information can be deduced in comprehensive reviews[2,62,69] and book chapters,[70] each delivering a unique view onto chemistry's platonic body *par excellence*.

Table 3. Physical properties of cubane.

Molecular formula	C_8H_8
shape[64,65]	O_h point group
appearance	transparent, rhombic crystals[64]
decomposition [°C][66]	> 220
density [g cm^{-3}][62]	1.29
heat of formation [kcal mol^{-1}] [67]	144
strain energy [kcal mol^{-1}][68]	161.5
C–C bond lengths [Å][63]	1.571
C–H bond lengths [Å][63]	1.109
C_1–C_4 distance [Å][62]	2.72

3. Physical Properties

To understand the different chemical behavior during the synthesis and the resulting properties of the NRHs a closer look into some specific physical detail is necessary. This chapter identifies common trends and differences from a physical perspective between the different groups and combines it with additional information about the specific bond situation given for the individual linker motif.

3.1. Size and dimension

The structural properties of the NRHs have been studied by X-ray diffraction, electron diffraction and other types of spectroscopy. Even though the geometry for each linker is linear, there is a remarkable variety in size and, therefore, in the length of the linker unit (Figure 4). While acetylene **26** is rather small with a C–C distance of 1.20 Å,[71] the size increases gradually from BCP **4** (1.85 Å),[10] to BCO **10** (2.60 Å),[29] to triptycene **19** (2.61 Å),[72] to cubane **37** (2.72 Å),[73] which is very close to the largest representative benzene **27** (2.79 Å).[74]

The highly strained BCP system is influenced the most by electronic and steric effects. Different substituents on the bridgehead positions alter the internal C–C distance. This

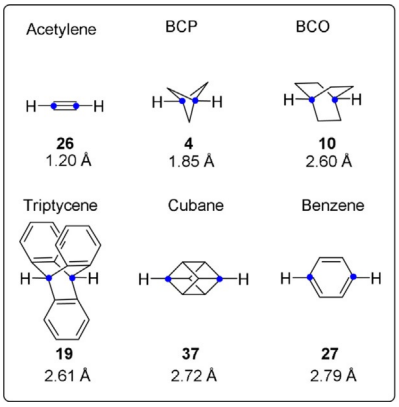

Figure 4. Bond length and internal C–C distance for the bridgehead carbon atoms.

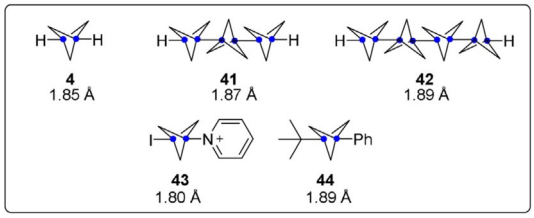

Figure 5. Substitution effects on internal C–C bond length of BCP-derivatives.

effect is contributed to the increased *s* character of the exocyclic bond (Bent's rule[15]) and is even visible in the oligoBCP compounds **41** and **42**, so-called *n*-staffanes (Figure 5). Here, the distance between the two bridgehead carbon atoms increases with the amount of additional BCP-monomer units.[75] The same effect results in rather long internal distances for alkyl- and aryl-substituted BCPs.[76] On the other hand, the opposite effect occurs in quaternary pyridinium salts **43**.[77] Here the very short nonbonding contact of 1.80 Å, is almost as short as the longest observed direct C–C-bond is long (1.70 Å).[78]

3.2. Bond considerations, electronic communication, and ring strain

Bridgehead hybridization and distances are not only important for the electronic communication of linear attached functionalities of the target molecule, they also indicate the reactivity of the compound. ^{1}H and ^{13}C NMR shifts and coupling constants are a powerful tool to determine the formal character of a bond.[79] The chemical shifts for unstrained hydrocarbons like acetylene **26**, benzene **27** and cyclohexane **45** are referred here as standards (Figure 6).[80] Within those molecules the carbon–hydrogen coupling represents the classic hybridization (50% = sp, 33% = sp^2, 25% = sp^3). A different situation occurs for the nonconjugated-linear linkers. While the rather unstrained triptycene **19** and BCO **10** show the expected chemical shifts,[81] the degree of s-character is already significantly higher compared to cyclohexane.[82] This effect further increases for BCP **4** and cubane **37**.[83,84] Here the formal bond situation is closer to sp^2 than to sp^3. The extraordinary s-character of the exocyclic C–H-orbitals in cubane, and, therefore, the p-rich character of the cage C–C-orbitals, are further reflected in the high acidity of the C–H bond.[85,86] The kinetic acidity of cubane is 6.6×10^{-4} that of benzene and 6.3×10^{4} that of cyclohexane.[86] This result is quite similar to other strained hydrocarbons, for example, the kinetic acidity for cyclopropane is 7.1×10^{4} that of cyclohexane, and both, cyclopropane and cubane, have a similar degree of hybridization (32 vs. 31%).[87]

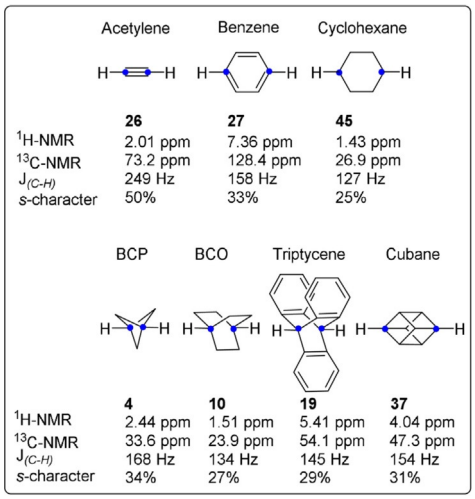

Figure 6. NMR and hybridization data for bridgehead carbon atoms; the s-character is calculated via Mueller and Pritchard's empirical relationship: %s = 1/5 $J_{(C-H)}$.[79]

3.2.1. Electronic communication

An important characteristic of the different linker units is the efficacy of electronic communication within the carbon scaffold ("through-bond") and the bridgehead-bridgehead carbons ("through-space"). A highly effective approach to investigate those influences is the acidity of linear-substituted carboxylic acids (Table 4). The acidity of BCP acid **46a** (pK_a = 5.63) and cubane acid **49a** (pK_a = 5.94) is significantly higher compared to unstrained BCO acid **47a** (pK_a = 6.54), as a result of the increased electronegativity (s-character) of the exocyclic carbon bonding orbitals relative to BCO.[88] In addition, there is a clear correlation of bridgehead–bridgehead distance and the influence of the substituent. The short bridgehead–bridgehead distance within the BCP derivatives leads to a strong influence of the substituent.

Table 4. Acidity of linear-substituted hydrocarbons.[a]

Linker				
pK_a for X	**46**	**47**	**48**	**49**
a	H 5.63	H 6.54	H 5.20	H 5.94
b	F 4.84	CH_3 6.50	CH_3 5.23	CO_2H 5.43
c	Cl 4.69	Cl 5.72	Cl 4.67	CO_2Me 5.40
d	CF_3 4.75	CF_3 5.79	Br 4.67	Br 5.32

[a] Values were determined in EtOH/H_2O *v/v* (1:1).[88–90]

This effect can be further demonstrated by the position of the substituent: 3-substituted BCO acids show less influence compared to 4-substituted ones, since the effect of the bridgehead–bridgehead interaction is missing.[91] Wiberg could show that the effects of the different substituents for bicyclic carboxylic acids result from a field effect.[91] This inductive/field effect was shown to have a linear-dependence on the acidity of the compound and the C–X dipole. The electronic effects in 4-substituted cubane carboxylic acids can even be utilized to illustrate substituent effects in cyclobutanes, which are otherwise too weak to be detected.[92] Irngartinger et al. could determine the different carbon–carbon bond lengths within the cubane

skeleton, depending on the substituent present in the 4-position.[93] Again, a closer look into the strong 1,3-nonbonding interactions between bridgehead carbon atoms is necessary for the BCP cage system. As mentioned above, the short interbridgehead distance (1.80–1.98 Å) leads to repulsion of the back lobes of the exocyclic hybrid orbitals, and is considered to be a main contributor to the overall strain energy of the system.[12,14]

A very valuable method to illustrate the effects of electronic communication between two separated electronic systems is photoelectron spectroscopy (PE). According to Koopman's theorem the first ionization energy of a molecular system is equal to the negative energy of the HOMO.[94] The effects of direct interactions (through-space) and mediated interactions via the σ-skeleton (through-bond) can be directly observed in the PE spectra. The assignment of the absorption energies to the according molecular orbitals (MO) can be quite challenging, due to different effects (Jahn–Teller effect, spin-orbit coupling for heavy heteroatoms, vibrational fine structure, etc.). However, semiempirical models for molecules consisting of the first and second row atoms have been used with great success and are a helpful tool within the assignment of the MOs. The corresponding splitting of the ionization energies with the assigned MOs (ΔI_n) represents the degree of interaction. Initial studies on cubane,[95] cubane derivatives,[96] and BCO derivatives[97] showed only very small splitting, characteristics for only a very feeble interaction of the linked systems. A different picture was observed for BCP derivatives. Here a rather strong splitting of linked systems occurs (Figure 7).[98]

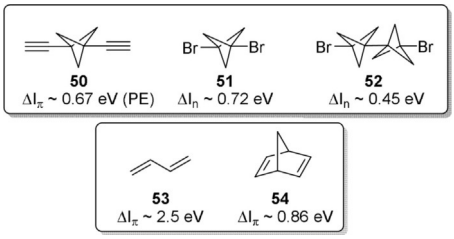

Figure 7. Orbital energy splitting.[98]

The π-MOs of 1,3-diethynylbicyclo[1.1.1]pentane **50** showed a remarkable split of about 0.67 eV and similar effects occurred for the 1,3-dibromo[1.1.1]pentane **51** (0.72 eV) and the extended 3,3′-dibromo-1,1′-bis(BCP) **52** (0.45 eV). These effects are not as strong as the conjugation effect for butadiene **53** (2.5 eV) or the homoconjugation effect of norbornadiene **54** (0.86 eV), but still show the good relay effect. Recent measurements and calculations even showed the possibility to tweak the orbital-splitting energy with additional substituents on the carbon cage, for example, hexafluorination led to further enhancement.[99] Quantum chemical calculations for diethynyl[*n*]staffanes, with $1 \leq n \leq 5$, predict a long-range interaction of 0.04 eV over a distance of 18 Å for the longest staffane ($n = 5$).[100] A further hint for the strong through bond-coupling within the BCP-skeleton is shown by electron transmission spectroscopy (ETS) studies done by Schafer et al.[101] They determined the π*-splitting of the acetylenic π*-orbitals in 1,3-diethynylbicyclo[1.1.1]pentane **50** to be 1.1 eV. This results complement the findings of Gleiter et al.,[98] showing a strong through-bond coupling of the π*-orbitals, facilitated by the σ/σ*-skeleton of the linker.

In conclusion, both spectroscopic methods, PE and ETS, classified the BCP bridging unit as an excellent mediator for electron transfer, not only for radical cations (PE) but also for radical anions (ETS). On the other hand, cubanes and BCO would be prime linkers in terms or electronic resistors, since little communication occurs via the σ-skeleton. Recent literature offers detailed theoretical studies,[102] discussing influences and consequences of electron-transfer systems containing nonconjugated hydrocarbon linkers, but little experimental data.

3.2.2. Ring strain

Unusual bonding situations are exemplified by the strain energy of the particular systems. Usually the overall ring strain is a combination of various parameters: 1) Baeyer strain[103] or angle strain (deformation of bond angle); 2) Pitzer strain[104] or conformational strain (torsional eclipsing interactions); 3) Prelog strain[105] or transannular strain (van der Waals interactions of transannular atoms). For example, the angle strain, the deviation from the tetrahedral angle of 109.5°, is higher in cyclopropane than that in cyclobutane (Table 5). The strain

Table 5. Heat of combustion and strain energy of cycloalkanes.

Compound	Heat of combustion ΔH_c [kcal mol^{-1}]	Heat of formation ΔH_f [kcal mol^{-1}]	Strain energy[15] [kcal mol^{-1}]	Strain energy per C–C bond [kcal mol^{-1}]
cyclopropane (C_3H_6)	505.8[106]	12.7[106]	27.7[15]	9.1
cyclobutane (C_4H_8)	656.0[92]	6.8[107]	26.3[15]	6.6
cyclohexane (C_6H_{12})	943.8[108]	29.8[108]	0.4[15]	0.1
BCP (C_5H_8)	N/D[a]	51 (calcd)[109]	68.0[15]	11.3
cubane (C_8H_8)	1155.2[67]	142.7[67]	161.5[68]	13.5
BCO (C_8H_{14})	1195.5[110]	23.6[110]	7.4	0.8
triptycene	2409.1[111]	76.8[111]	7.0[111]	0.8

[a] N/D = not determined.

energy of cubane is about six times the amount of cyclobutane, which represents the sum of the six "cyclobutane faces of the cube". But compared to the ring strain per carbon–carbon bond, cubane has double the amount of cyclobutane. The deviation is even higher when the strain energy is calculated per number of carbon atoms (cubane ≈20.2 kcal vs. butane ≈6.6 kcal). However, one should be aware, that the concept of ring strain has its intrinsic limitations, for example, in terms of chemical stability. The less-strained isomer is not always the most stable one. In addition, cubane and BCP are relatively stable compounds, even though highly strained. But nevertheless, the concept of ring strain is still very valuable and can be applied for a better interpretation of chemical reactivity.[112] An interesting example is the correlation of ring strain with the ability of the molecule to act as a hydrogen bond donor; the higher the strain, the more acidic the C–H bond.[113] While many of these strained hydrocarbons are thermodynamically unstable, due to their deviation from standard sp^3 geometry, they possess remarkable kinetic stability. For example, cubane is thermodynamically unstable ($\Delta H_f = 144$ kcal mol^{-1}), and highly strained (SE = 161.5 kcal mol^{-1}), but it is capable of withstanding temperatures of up to 220 °C (Table 5).[66] BCP also contains notable kinetic stability, as it is shown to withstand temperatures greater than 280 °C.[21] BCO and triptycene are notably less strained (SE = 7.4 and 7, respectively) with heats of formation of 23.6 and 76.8 kcal mol^{-1}.

3.3. Bridgehead cations, anions, radicals and radical-cations

In terms of chemical reactivity and stability other important factors have to be considered. How does the rigid scaffold behave in reactive intermediates? How stable are the according bridgehead cations or anions? Is the homolysis of the carbon–hydrogen bond possible, and how stable is the corresponding bridgehead radical? Which intermediates will break the rigid cage-like structure and rearrange to more stable products? In this chapter those questions will be answered from a rather physical point of view; examples concerning the actual reactivity and chemistry will be discussed in detail in Chapter 4.

3.3.1. Bridgehead cations

The short nonbonding contact in BCP allows for the fast solvolysis of halosubstituted BCP, despite the expected high strain of the resulting carbocation intermediates (Figure 8).[114] Generally the positive charge of carbocations is stabilized in planar geometries, but this cannot occur at the pyramidalized bridgehead positions of BCP.[115] Due to the close nonbonding contact, a rather strong transannular stabilization of the developing BCP cation can be observed.[116] The fast solvolysis rate of BCP also enables relief from ring strain, which can be observed by the presence of solely the rearranged substituted-cyclobutane products.[117]

The cubane cage, on the other hand, is very stable toward skeletal rearrangement and the solvolysis rate is about 10^{15} times faster than originally calculated, even though the cubyl

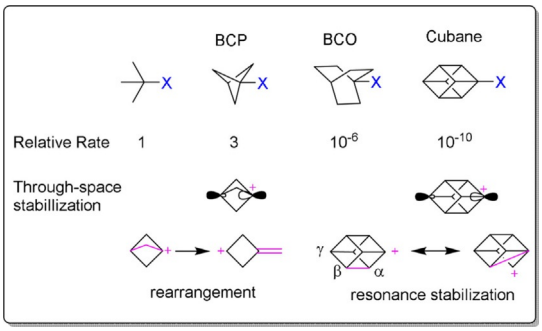

Figure 8. Approximate solvolysis rate of brominated bridgeheads and cation stabilization effect.

cation formed seems to neglect all known cation-rationales, such as the geometry is far from flat and hyperconjugation would result in a very strained cubenelike structure, an extreme example of a pyramidalized olefin.[118–121] This remarkable effect can be explained by additional stabilization through delocalization of the positive charge along the surrounding carbon–carbon bonds (resonance stabilization). In addition, further hyperconjugation, vicinal through bond $\sigma_{C\alpha C\beta} \rightarrow p^*$ could be the reason for the notable stability of the cubane cation.[122] Furthermore, Eaton et al. pointed out another consideration: the internuclear line between the individual carbon bonds represents a false picture of the actually bent bond ("banana bond"),[123] since the endocyclic interorbital angle is rather 101–104° than 90°,[124] reducing the actual pyramidalization angle.[122] Further influences on the solvolysis rate are reported for substituted cubanes. While electron-withdrawing groups at the γ-position slow down solvolysis, electron-donors at the β-position accelerate it.[116,120,125] So far no skeletal rearrangement is observed for the cubane cation, and only recent calculations showed a possible pathway for the cage-opening via the cuneyl cation. The rate-determining barrier for ring opening of 25.3 kcal mol^{-1} highlights the kinetic persistence of this unusual cation.[126]

Originally the first synthesis of triptycene by Bartlett et al. was conducted to compare the stabilizing effect of benzene rings on the rigid, tied-back orientation in triptycene with the triptycenyl cation.[39,40,41] In triptycene, the π-system is fixed in an orthogonal orientation relative to the developing p-orbital; therefore, no overlap/stabilization is possible. Leaving groups at the bridgehead position do not show the usual substitution chemistry since it cannot be flattened and as the backside is shielded by the other bridgehead carbon atom.[127] Shielding even occurs at the front side of the molecule, and for the triple benzylic-like position in 9-bromomethyltriptycene, due to the *peri*-type steric hindrance of the cationic center and the adjacent aromatic hydrogen atoms (Figure 9).[128]

Another unique property of the cubane core is the instability of the cubylcarbinyl cation, as the positive charge next to the cubane skeleton usually leads to rapid rearrangement to the homocubyl derivatives, as was observed for cubylmethyl alcohols **55**. Originally described by T. W. Cole in his Ph.D. dissertation with Eaton 1966 (Scheme 12),[129] modern calculations sug-

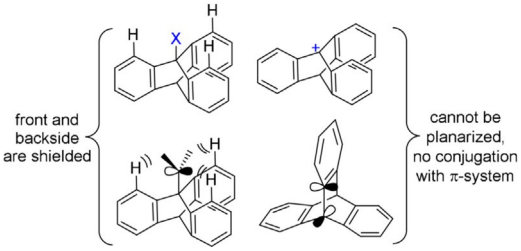

Figure 9. Nucleophilic substitution on 9-substituted triptycenes.

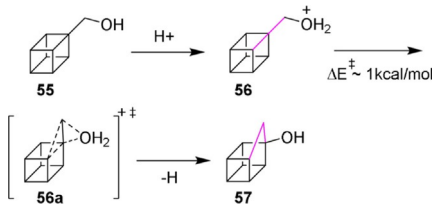

Scheme 12. Cubylcarbinyl cation rearrangement.

gest a mechanism via the homocubyloxonium ion **56a**, for the Wagner–Meerwein-type rearrangement.[130]

3.3.2. Bridgehead anions

Ample research has been conducted to determine the stability of the highly basic hydrocarbon anions.[131] A general method is the preparation in the gas phase in the presence of fluoride anions (DePuy reaction).[132,133] The kinetic acidity can be determined by mass spectrometry (flowing afterglow[134] or ion cyclotron resonance[135]) with a method developed by DePuy et al.[136] The thermodynamic relationship of the homolytic bond dissociation energy (BDE), gas-phase acidities (ΔH_a), the ionization energy of hydrogen (IE(*H*) = 313.6 kcal mol^{-1}),[137] and the electron affinity (EA) is given by the following equation, representing the thermodynamic cycle [Eq. (1)].[138]

$$\mathrm{BDE(R\text{-}H)} = \Delta H_a(\mathrm{RH}) - \mathrm{IE}(\mathrm{H}^{\bullet}) + \mathrm{EA}(\mathrm{R}^{\bullet}) \qquad (1)$$

Strictly speaking, Equation (1) is only valid for localized anions and radicals, and resonance delocalization only plays a minor role in stabilizing these intermediates.[139] In general, the acidities and bond dissociation energies of hydrocarbons are influenced by the hybridization of the according orbital. The higher the s-character, or the $J_{(C-H)}$, the higher the kinetic acidity of the hydrocarbon (low values of ΔH_a) (Figure 10).

This can be seen in the high kinetic acidities of BCP **60** and cubane **37**. The high s-character increases the acidity, as seen when compared to BCO **10**, CP **58**, and *t*Bu **59**. But due to the higher transannular interaction between the back lobes of the bridgehead carbon orbitals, the effect for BCP is partly mitigated. This effect can be illustrated by adding an electronegative substituent, for example, chlorine, at position 3 of BCP. The energetically low-lying σ* orbitals of the halogen–carbon bonds can be populated, leading to a longer carbon–halogen

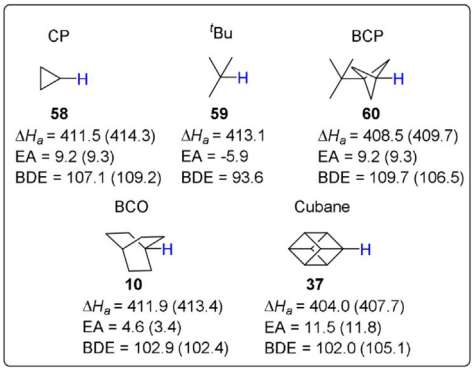

Figure 10. Experimental gas-phase acidities (ΔH_a), electron affinities (EA), and bond dissociation energy (BDE). All values in kcal mol^{-1}; parenthetical values are results of G3 computations.[132,137,140]

bond.[141] The homolytic bond dissociation energy (BDE), reflecting the stability and the ease of formation of the alkyl radical, follows the predicted order for the stability of the radicals. The anionic intermediates are of greater importance for the functionalization than the cationic counterparts. This is especially due to the wide variety of organometallic coupling and exchange reactions.

3.3.3. Bridgehead radicals

As for the bridgehead carbocations, the geometry for bridgehead radicals is quite different from other more flexible systems. The rigid core results in a permanent pyramidal conformation, far from the favored planar conformation. Also, in comparison to the planar *tert*-butyl radical, which shows rapid inversion, the conformation is locked within the inflexible cage structure. The orientation of the SOMO and the tied back carbon atoms result in less distinctive stabilization effects (Figure 11). Hyperconjugative delocalization or β-scission of

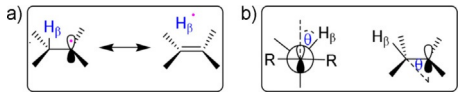

Figure 11. a) Hyperconjugative delocalization; b) definition of dihedral angle Θ.

bridgehead carbon atoms lead to high-energy bridgehead alkenes (anti-Bredt[142] alkenes). Consequently, the reduced steric shielding of the exposed bridgehead radicals, in combination with the alleviated hyperconjugation, results in a much higher reactivity in comparison to "normal" tertiary carbon radicals.[143] But despite their high reactivity, the half-lives for all bridgehead-radicals are long enough to study their properties with spectroscopic methods.

The highest hyperconjugation of the β-hydrogen atoms is observed for a parallel orientation to the SOMO (dihedral angle $\Theta = 0°$). The strength of this effect can be seen in EPR spectra in the hyperfine splitting (hfs) (Figure 12). A significant

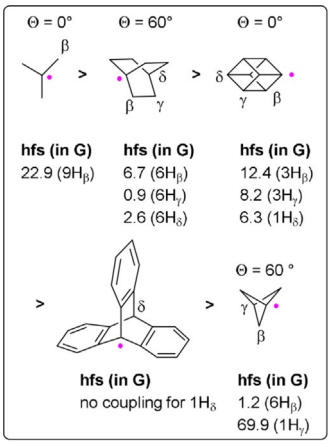

Figure 12. Rate of formation and EPR data.[144,146,149,150]

factor of the stabilization within the *tert*-butyl radical comes from the hyperconjugation with the β-hydrogens (hfs = 22.9 G). Within the bridgehead-systems only cubane shows a minor contribution of the β-hydrogens (hfs = 12.4 G),[144] which is attributed to the optimum overlap with a dihedral angle of $\Theta = 0°$.[145] Remarkable for the BCP-radical is the unusual strong coupling with the γ-hydrogen atoms (hfs = 69.9 G).[146] Again, this effect is owed to the very small bridgehead–bridgehead distance within the BCP-radical of only 1.74 Å,[147] reflecting a large through-space contribution; this is a notable difference in length when compared to the neutral BCP-species of 1.845 Å. In addition, three identical pathways through the carbon–skeleton with an ideal *trans*-arrangement are available for an enhanced through-bond communication.[148]

The triptycene radical on the other hand shows no interaction with the opposite bridgehead substituent. Even if a fluorine atom is placed on the other bridgehead carbon atom, no measurable coupling is observed between the radical and the opposite atom. This indicates that the actual through-space coupling for BCO[150] and cubane, which share similar bridgehead–bridgehead distances (2.60 and 2.72 Å, respectively), is an insignificant effect. Further investigation on related systems confirmed that a through-space coupling mechanism is only valid for distances below 2.1 Å.[151] The strong hyperfine splitting in the BCO and cubane systems is, therefore, only attributed to the through-bond interactions.[149] Even though bridgehead radicals are highly reactive, ring opening via β-scission was only observed for the BCP-radical at elevated temperatures and is, therefore, regarded as kinetically disfavored. The kinetic barrier was determined to be higher than 26 kcal mol^{-1} (Scheme 13).[146] In terms of reactivity and stabilization the radical approach is one of the most reliable approaches for the further functionalization of those strained hydrocarbons. The utility of radical intermediates is discussed in detail below.

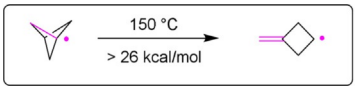

Scheme 13. Allowed radical rearrangement of BCP.

3.3.4. Bridgehead radical cations

Examples of radical cations for the rigid hydrocarbons currently under review, in the literature are limited. Although, one prominent example from the work of the Schreiner group with the cubane radical cation **37**$^{\bullet+}$ should be noted (Scheme 14).[152]

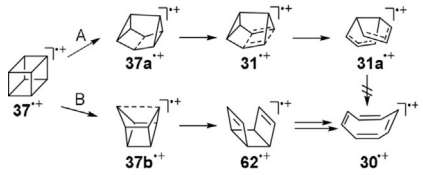

Scheme 14. The two rearrangement pathways for the cubane radical cation.

Both experimental ((photo)chemical oxidation of cubane **37**$^{\bullet+}$ in acetonitrile) and computational (DFT and MP2) techniques were employed to investigate the rearrangement of the cubane radical cation **37**$^{\bullet+}$. Two rearrangement pathways are possible for this radical cation. While the barriers are almost equivalent for the isomerization of **37**$^{\bullet+}$ to the cuneane radical cation **37a**$^{\bullet+}$ (pathway A) and for the C–C bond fragmentation to the secocubane-4,7-diyl radical cation **37b**$^{\bullet+}$ (pathway B) ($\Delta H_0^{\neq} = 7.8$ and 7.9 kcal mol^{-1}, respectively), pathway B is favored, as the rearrangement of **37b**$^{\bullet+}$ to the more stable *syn*-tricyclooctadiene radical cation **62**$^{\bullet+}$ has a low-energy barrier and terminates with the cyclooctatetraene radical cation **30**$^{\bullet+}$. In contrast, cuneane **37a**$^{\bullet+}$ is oxidized exclusively to semibullvalene **31a**$^{\bullet+}$, as a barrier of 35.7 kcal mol^{-1} prohibits the expansion of **31a**$^{\bullet+}$ to **30**$^{\bullet+}$.

4. Reactivity and Manipulation of the Bridgehead Carbon Center

4.1. Limitations of the carbon skeleton–stability and rearrangements of cubane and BCP

The carbon-skeleton of triptycene and BCO—both unstrained linker systems—are nearly indestructible under normal reaction conditions. However, BCP and cubane bear a vast amount of strain energy in their cage structure. Certain reaction conditions are able to crack the kinetically stable skeleton and lead to thermodynamically more stable products. Due to the high activation energy (E_a) the thermal stability of BCP is remarkably high so that the isomerization to 1,4-pentadiene **61** only takes places at elevated temperatures (Scheme 15).[7,21] Similarly in cubane, the activation energy ($E_a = 43$ kcal mol^{-1}) of the rate-

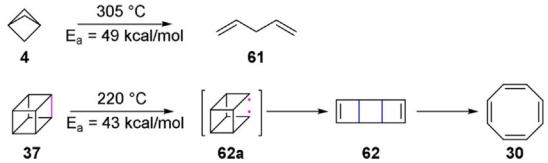

Scheme 15. Thermal isomerization of BCP and cubane.

determining step for a homolytical C–C-bond cleavage, during the rearrangement to cyclooctatetraene **30** provides only limited relief in the overall strain, hence the thermal ring opening only occurs at higher temperatures.[153]

Another option to release some strain energy is a metal-catalyzed σ-bond rearrangement. In the presence of Ag^{I} or Pd^{II}, insertion into the carbon–carbon bond of cubane occurs (Scheme 16a).[154] A rearrangement of the cubane skeleton

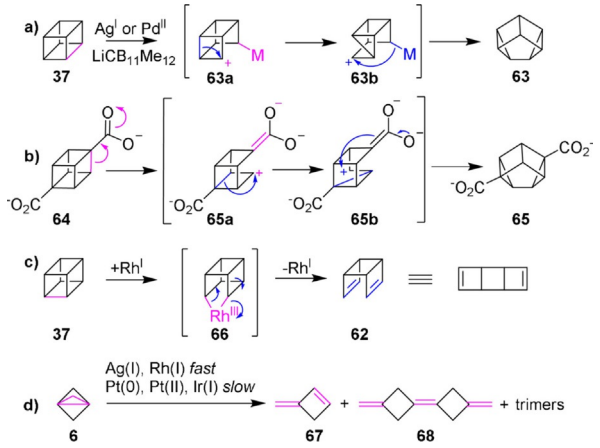

Scheme 16. Rearrangement of cubane (a,b,c) and [1.1.1]propellane (d) skeletons.

yields the stable cuneane **63** (lat. *cuneus* = wedge). A similar rearrangement is observed in the presence of Li cations or protons (Scheme 16b).[155] Rhodium(I) complexes rapidly insert into the carbon–carbon bond of cubanes in an oxidative addition style. The intermediate five-membered metallacycle **66** is rearranged to the more staple tricyclodiene **62** (Scheme 16c).[156] The corresponding BCP-skeleton shows no related reactivity. Only in the case of the very strained bridged [1.1.1]propellane, a comparable ring opening in the presence of transition metals occurs (Scheme 16d).[157]

Despite the stability of the cubane radical, different effects are observed for radicals adjacent to the caged ring system. The cubylcarbinyl radical **69**, generated by the photolysis of the corresponding *N*-hydroxy-2-pyridinethione ester **70** ("Barton ester"),[158] does not show the 1,2-shift to homocubyl radical **71**, which was found for the analogous cubylcarbinyl cation (Scheme 17).[159,160] Instead a very fast ring opening occurs ($k_R = 2 \times 10^{10}\ s^{-1}$). From there different isomers **73a**, **73b,** and the mixture of diastereomeric trienes **74a** and **74b** are isolated with a distribution correlated to their rate formation. Due to the low lifetimes (10–35 ps), rearrangement processes are predominant over diffusion-controlled bimolecular trapping within the cubane system. Again a similar process is observed for BCP-carbinyl radical **76a**. Even at low temperatures, the radical readily rearranges by a β-scission.[161] In presence of a PhSH as a hydrogen donor the photochemical decomposition of the BCP-Barton ester **75** yields a product ratio of about 3 to 1 **76**/**77** (Scheme 18).[151]

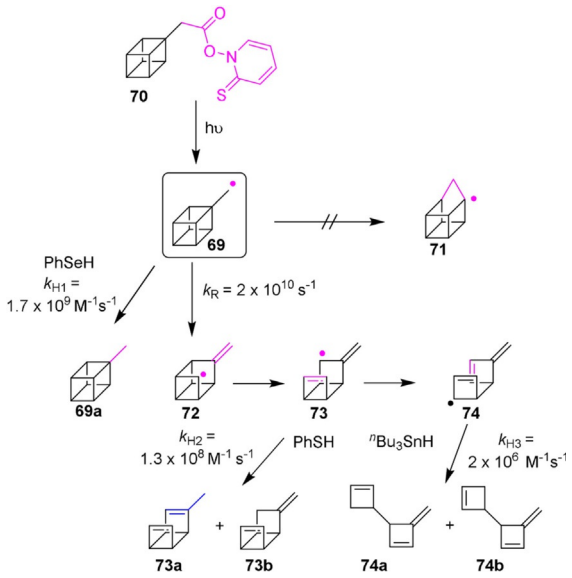

Scheme 17. Kinetics of cubylcarbinyl radical **67**.

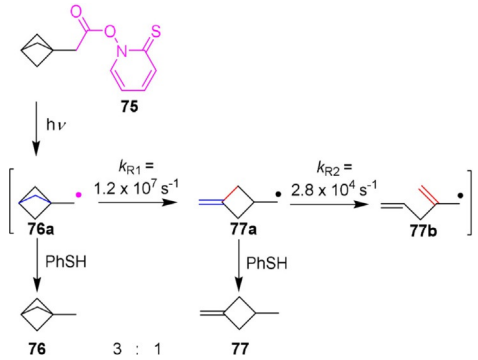

Scheme 18. Kinetics of BCP-carbinyl radical.

Further release of ring strain can be induced by ring expansion. Carbene generation adjacent to the ring skeleton leads to remarkable anti-Bredt olefins. The BCP(phenyl)ketone was used to generate the carbene from the according diazo compound **78**. After refluxing, the existence of the very strained bridgehead olefin **80** was verified with the addition product of ethanol (Scheme 19).[157] For cubane the situation is even more exceptional; the corresponding homocubene **84**, generated from the adjacent carbene **83**, is regarded as one of the most twisted anti-Bredt olefins up to date.[162] The existence of the homocubene **84** was confirmed by trapping experiments.[163] Later,

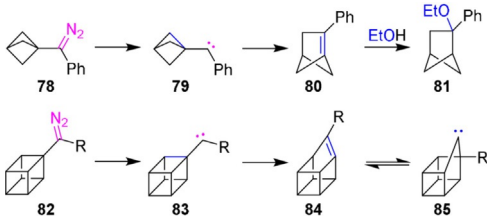

Scheme 19. Ring expansion via carbene insertion.

even more remarkably, Eaton et al. could show with ^{13}C-labeling that the homocubene **84** rearranges reversibly to the homocubylidene **85**.[164] Further studies on the equilibrium between the homocubene and the homocubylidene were conducted by Chen et al. and the equilibrium constant was assigned to be close to unity at room temperature.[165]

Certain other reaction conditions are able to crack the kinetically stable cubane framework. In the presence of palladium-on-charcoal Stober et al. observed a stepwise hydrogenation of the strained skeleton.[166] The scission of the first ring leads to the secocubane **86**. Every further hydrogenation step, from secocubane to nortwistbrendane **87** and from nortwistbrendane to BCO **10**, releases about 50 kcal mol^{-1} of strain energy (Scheme 20).[167] The order of hydrogenation proceeds as expected; the least stable/the longest bond is hydrogenated first.

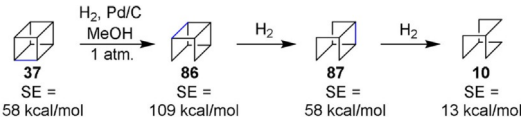

Scheme 20. Stepwise hydrogenation of cubane.

The presence of an anionic charge at the carbon atom vicinal to the cubane skeleton **89** leads to degradation of the ring system **90**. Deprotonation at the α-position of an acceptor system **88a** or **88b** results in the two diene products **92** and **93** (Scheme 21).[168] A similar instability is observed for cubylmethyl alcohol **94**. Slight acidic conditions induce a homoketonization reaction yielding cyclobutene **96** (Scheme 22).[159]

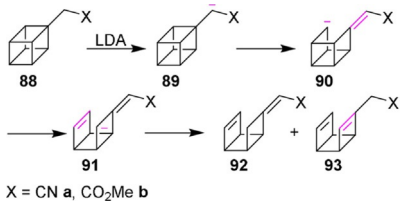

Scheme 21. Cubane skeleton decomposition in the presence of lithium diisopropylamide (LDA).

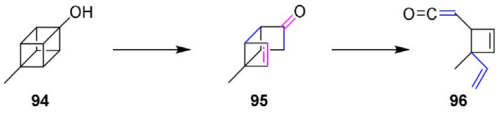

Scheme 22. Ring opening of cubylmethyl alcohol in slightly acidic conditions.

A very interesting ring-opening mechanism of the cubane core was observed during the attempts to polymerize the iodo-vinyl cubane **97**.[169] The partial positive charge in the vicinal position **98** leads to a sequence of skeletal bond migrations (Scheme 23). A similar mechanism was observed under pure thermal conditions and at elevated temperatures during Grubbs-metathesis.[170] The final product after a cascade of cycloreversions and cycloadditions is the stable 4-vinyl-*trans*-β-iodostyrene **103**.

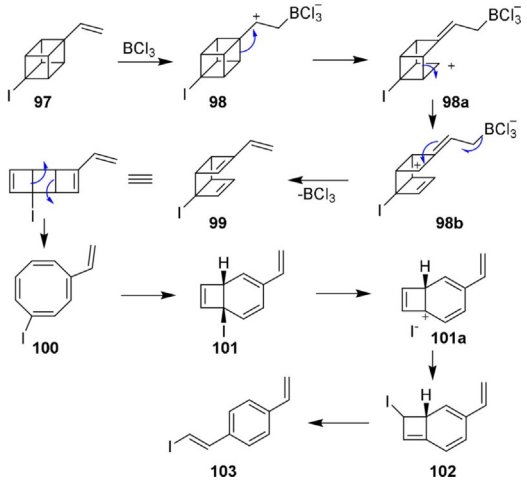

Scheme 23. Ring opening of cubanyl **97** to 4-vinyl-*trans*-β-iodostyrene **103**.

4.2. Functionalization of bridgehead linkers

4.2.1. BCP chemistry

A general approach for the functionalization of BCP utilizes the reactivity of the internal bond in [1.1.1]propellanes **6**. This bond can be opened either by an anionic, radical, or a cationic pathway. Generally the cationic pathway leads to ring opening of the BCP scaffold (Scheme 24), while in the case of cubane,[59–61] BCO,[26] and triptycene no chemistry of the internal bond is utilized.

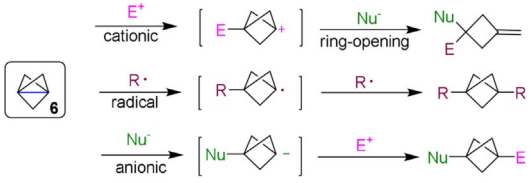

Scheme 24. Functionalization of [1.1.1]propellane.

The polymerization of a [1.1.1]propellane derivative **104** was first achieved through the anion-induced ring opening of BCP with lithium–organic initiators such as *tert*-butyllithium and phenyllithium.[171] The central sigma bond is opened leading to a rigid rod structure **105** with a degree of polymerization greater than 20 units (Scheme 25).

Conversely, nonpolymeric reactions can be carried out with **6**, such as the radical addition of different thiols to the strained carbon–carbon bond of **6** to form BCP-thioether compounds **106**.[172] This reaction proceeds by a radical chain process with high functional group tolerance and few byproducts in yields

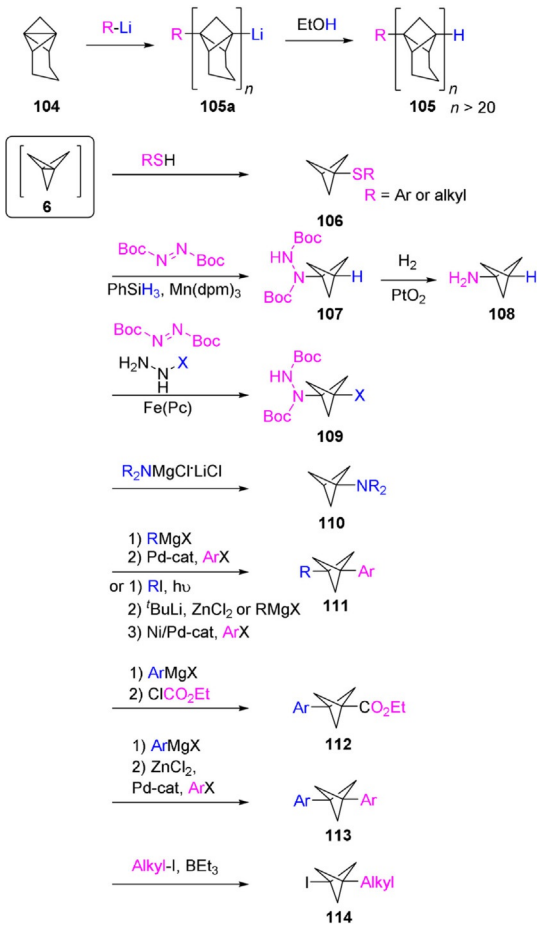

Scheme 25. Poly[1.1.1]propellane, addition of a Grignard reagent to [1.1.1]propellane and radical carboamination of [1.1.1]propellane.

between 16 and 90%. All reactions were performed at room temperature in the absence of any catalysts and with short reaction times of 15 min.

Carboamination was also achieved by reaction with **6**. Di-*tert*-butyl-1-(BCP)hydrazine-1,2-dicarboxylate **107** was synthesized through the reaction of **6** with di-*tert*-butyl azodicarboxylate and phenylsilane in the presence of tris(2,2,6,6-tetramethyl-3,5-heptanedionato)manganese(III) [$Mn(dpm)_3$].[173] It had been previously shown that [1.1.1]propellane can have a similar reactivity profile to that of olefins.[8] Furthermore, it was demonstrated that H–N can be added across olefins by a free-radical mechanism in manganese-catalyzed hydrohydrazination reactions.[174] Coupling these results together enabled the development of this reaction that traps the 1-BCP radical, under similar conditions with an azodicarboxylate. 1-BCP-amine **108** was then accessed through BOC deprotection to give 1-BCP-hydrazine that was then reduced to the product. This synthetic route proved to be superior in terms of scalability, yield, safety, and cost when compared with previously reported routes in the syntheses of 1-bicyclo[1.1.1]pentylamine.[175]

Following this, a one-pot radical carboamination of **6** was developed under mild conditions to afford multifunctionalized BCP derivatives **109** in gram-scale quantities.[176] Notably, the synthetically useful 3-substituted BCP-amines can be accessed with this method. The multicomponent reaction involves a concerted mechanism starting with a radical addition, followed by cleavage of the central bond then radical trapping, allowing the C–C bond to form simultaneously with the C–N bond on the BCP scaffold. Methyl carbazate was used as a methoxycarbonyl radical precursor, while di-*tert*-butyl azodicarboxylate was utilized as the radical acceptor for the intermediary 3-substituted BCP-radical, this radical intermediate is kinetically stable allowing the formation of the C–N bond over BCP oligomerization. The optimized conditions for this reaction were found to be a combination of *tert*-butyl hydroperoxide (TBHP) and (phthalocyaninato)iron(II) (Fe(Pc)) (cat.) with the inorganic base Cs_2CO_3 in MeCN at $-20\,^{\circ}C$ for 1 h.

As has been observed and noted before, the most strained C–C bond present in **6** is the central C–C bond that has a bond energy of $\approx 60\ kcal\,mol^{-1}$. The energy of the "spring-loaded" C–C and C–N bonds was harnessed to develop a synthetic route to BCP amines **110**.[177] The turboamide ($Bn_2NMgCl{\cdot}LiCl$) was reacted with propellane on a >100 g scale to afford the amine in a 54% yield over two steps. Inert conditions are required while the reaction is run from 0 to $60\,^{\circ}C$ and allowed to react for 16 h. The HCl salt was then precipitated once the dibenzyl group was removed. A large number of BCP amines were synthesized through this method.

A significant body of work has also been carried out with the reaction of various Grignard reagents and **6** to form 1,3-difunctionalized BCP products.[178] This was first seen with work performed by the Szeimies group in which various 1,3-bisaryl/alkylarylBCP compounds **111** were synthesized through the reaction of **6** with different Grignard reagents to form alkyl/aryl magnesium halides. These intermediates could then undergo coupling reactions with bromoarenes in the presence of [$PdCl_2$(dppf)] to form the 1,3-difunctionalized products in modest yields between 21–49%, with minimum reaction times of 48 h.[76] Following on from this, 1,3-disubstituted BCP derivatives were synthesized from **6** by an alternative route. Organyl iodides were reacted with **6** by radical addition reactions; then a halogen–lithium exchange was performed followed by either transmetallation with zinc chloride or the addition of a Grignard reagent to open up access to a variety of 3-substituted BCP-1-magnesium and -zinc derivatives. The zinc derivative was then used in coupling reactions with various alkenyl, aryl, and biaryl halides and triflates using either [$NiCl_2$(dppe)], [$Pd(PPh_3)_4$], or [$PdCl_2$(dppf)] catalysts to give a number of 1,3-disubstituted BCP derivatives **111**. Moderate yields were obtained and long reaction times of three to seven days were required for the corresponding BCP magnesium species.

Similarly, arylmagnesium halides were again reacted with **6** and the resulting BCP magnesium intermediates were quenched with ethyl chloroformate to give the corresponding ethyl esters **112** in 60–92% yields.[179] Yields were significantly higher for the arylmagnesium halides that had electron-donating groups (EDG) (74–92%) than those with electron-withdrawing groups (EWG) (47–61%). This result is logical due to the increased nucleophilicity of the EDG Grignard reagents. The optimum reaction conditions for the first step involved two equivalents of the Grignard reagent, heating to $100\,^{\circ}C$ with **6** for

45 min to 3 h. The reaction was then quenched with four equivalents of ethyl chloroformate at −78 °C. Alternatively as seen before, the BCP magnesium intermediates undergo a transmetallation reaction with $ZnCl_2$ that then allowed for Negishi cross-coupling with various aryl or heteroaryl halides (Ar'X) to give 1,3-bisarylated BCP derivatives **113** in good yields. Negishi cross-coupling conditions were carried out with the catalyst $[PdCl_2(dppf)]\cdot CH_2Cl_2$; only a 40 °C temperature was required for coupling with aryl iodides, whereas a higher temperature of 65 °C was necessary to access coupling with heteroaryl bromides and chlorides as electrophiles to provide BCPs bearing various heterocyclic ring systems in 49–91% yields. More sensitive groups such as a nitriles or esters are tolerated under these conditions.

Recent work has also shown the applicability of alkyl iodide substitution with **6** to form iodoalkyl BCP products **114**.[180] These compounds are achieved under mild conditions using 10 mol% of the Lewis acid triethylborane at room temperature and the reaction is often completed within 15 min. Importantly, in the absence of triethylborane, no product formation was observed in the dark or light, highlighting its necessity. Also noteworthy was the absence of any staffane byproducts from the reaction.

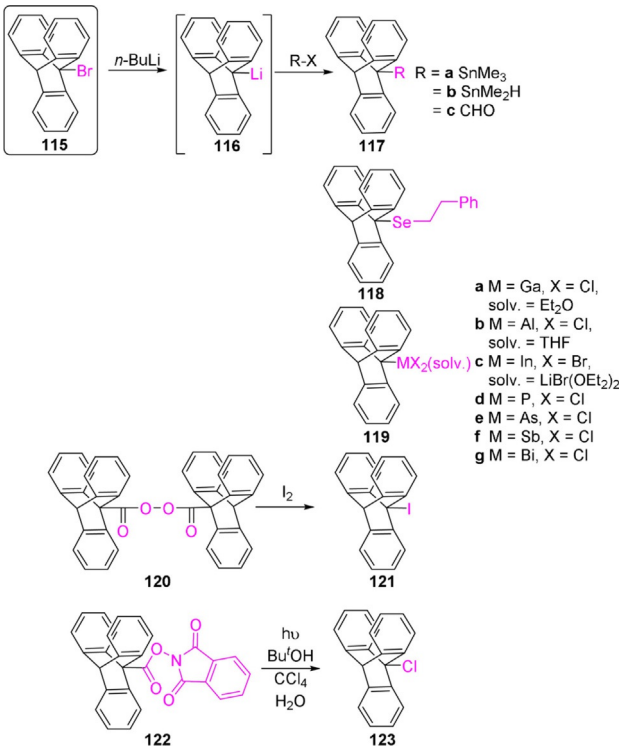

Scheme 26. Functionalization of the bridgehead carbon in triptycenes; solv. = solvent.

4.2.2. Triptycene chemistry

9-Bromotriptycene **115** has been utilized by many groups to further functionalize triptycene at the 9-position. This is most commonly executed through halogen–lithium exchange reactions (Scheme 26). This was first carried out in the 1970s, when trimethyl-9-triptycenyl tin **117a** was synthesized by quenching the 9-lithiotriptycene intermediate **116** with trimethyltinchloride.[181] Following this trimethyl-9-triptycenyl tin **117a** was utilized to access dimethyl-9-triptycenyl tin hydride **117b**. This was achieved by a bromination reaction followed by the reduction of tin with $LiAlH_4$.[182] Additionally, when 9-lithiotriptycene was quenched with formaldehyde, the triptycene carbaldehyde **117c** was formed.[183] 9-Triptycene phenethyl selenide **118** was prepared from 9-bromotriptycene again through the use of a lithium–halogen exchange reaction and quenched with diphenyl diselenide to form the product in a 75% yield.[184,185] Moreover, 9-lithiotriptycene **116** was reacted with a series of metals such as $GaCl_3$, $AlCl_3$, and $InBr_3$ to form the complexes, [(tript)$GaCl_2$(THF)] **119a**, [(tript)$AlCl_2(OEt_2)$] **119b**, and [(tript)$InBr(\mu\text{-}Br)_2Li(OEt_2)_2$] **119c**, in which tript = 9-triptycenyl.[186]

Iodine and chlorine were also introduced at the 9-position of triptycene. Iodination was achieved by Bartlett by the radical-induced decomposition of ditriptycenoyl peroxide **120** at 80 °C in the presence of I_2 to give compound **121**.[187] Chlorination was observed when 9-*N*-(acyloxy)phthalimide triptycene **122** and 1,4-diazaBCO (DABCO) were irradiated for 3 h with a 100 W high pressure Hg lamp in a solution of [*t*BuOH-CCl_4-H_2O (53:42:5, v/v)] resulting in the decarboxylated chloride product **123** in 59%.[188]

4.2.3. Functionalization of the BCO scaffold

A wide variety of chemistry is available for the functionalization of the BCO scaffold. For example, 1,4-dibromoBCO **125a** can be accessed from the conversion of two carboxylic acid groups in **124** by the radical Hunsdiecker reaction (Scheme 27).[189,190] Here the silver salts of the carboxylic acids react with the organic halide, and decarboxylation followed by the radical re-

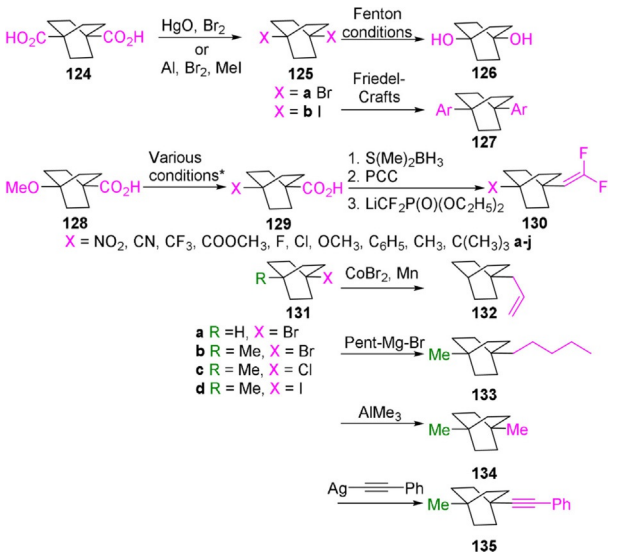

Scheme 27. BCO chemistry at the bridgehead position. PCC = pyridinium chlorochromate. See ref. [192] for further information.

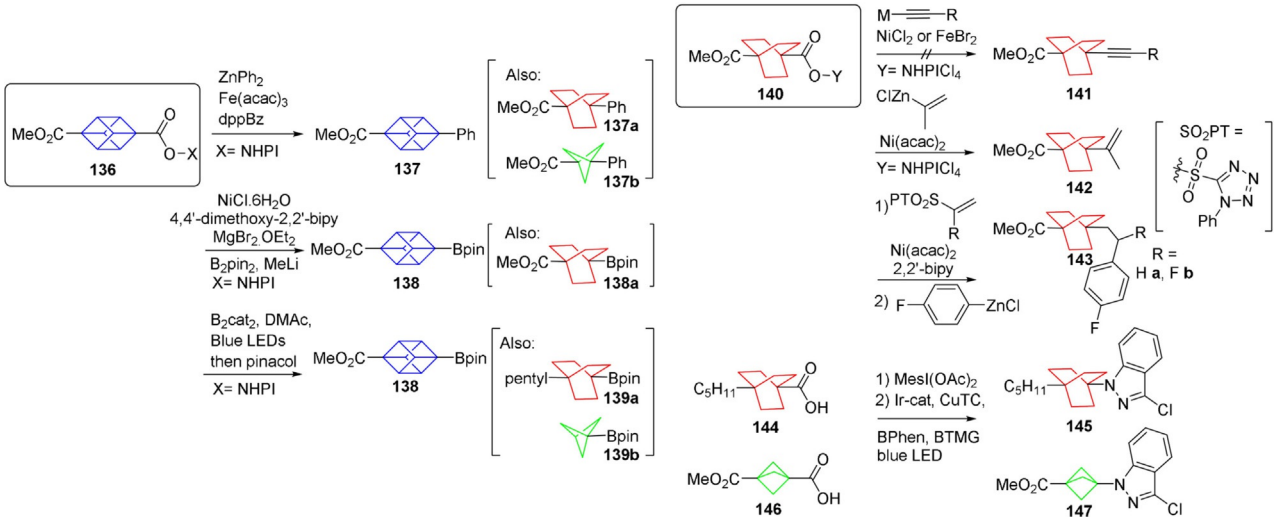

Scheme 28. Redox-active ester chemistry. DMAc = dimethylacetamide; BTMG = 2-*tert*-butyl-1,1,3,3-tetramethylguanidine.

combination of BCO• and Br• results in the desired product. Moreover, the use of aluminum foil and a catalytic amount of bromine in methyl iodide allows for the efficient conversion to 1,4-diiodoBCO **125 b**, whereas Fenton conditions enable the FGI to the 1,4-dihydroBCO species **126**. Friedel–Crafts arylation reactions have also be utilized to access 1,4-diaryl BCO **127** compounds from 1,4-dibromo BCO **125** through the use of $AlCl_3$ and the chlorinated aryl group.[191]

4-Methoxy BCO-1-carboxylic acid **128** was utilized to access a series of difluoroethylene BCOs **130 a–j**.[192] Several different functional-group interconversion reactions were performed at the bridgehead carbon atom of BCO to access groups, such as NO_2, CN, CF_3, $COOCH_3$, F, Cl, OCH_3, C_6H_5, CH_3, and $C(CH_3)_3$ **129 a–j**. Following this the carboxylic acid moiety, at the opposite bridgehead carbon atom, was reduced and subsequently oxidized to the corresponding aldehyde to allow for the final reaction with $LiCF_2P(O)(OC_2H_5)_2$ thus enabling access to a series of 1,1-difluoro-2-(4-substituted-bicyclo[2.2.2]oct-1-yl)ethenes **130 a–j**.

Another example of BCO chemistry uses 1-bromoBCO **131 a** in direct reductive cross-coupling reactions with allylic acetates through the use of a $CoBr_2$/Mn catalyst system and an acetonitrile/pyridine solvent mixture. A variety of compounds including 1-allyl BCO **132** were synthesized through this method in reasonable yields within 4–6 h.[193] The BCO scaffold was successfully alkylated from 1-bromo-4-methyl BCO **131 b** by using the corresponding Grignard reagent to synthesize 1-methyl-4-pent-1-yl BCO **133**.[194] Similarly, Friedel–Crafts alkylation was also employed to alkylate 1-chloro-4-methylBCO **131 c** by using $AlMe_3$ to form 1,4-dimethyl BCO **134**.[192] 4-Methyl-1-(2-phenylethynyl) BCO **135** was synthesized from 1-iodo-4-methylBCO **131 d** through reaction with silver(I) phenylacetylide in anhydrous pyridine under argon at 150 °C in 31 % yield. However, these reaction conditions were only successful for this compound, as attempts to react silver(I) phenylacetylide with 1,4-diiodoBCO and methyl 4-iodoBCO-1-carboxylate failed.[195]

A popular and versatile method has arisen that allows for the attachment of a variety of different functional groups directly to many of the bulky alkyl groups of interest in this review, that is, BCP, BCO, and cubane. These methods, as developed by Baran's group involve the cross-coupling of redox-active esters, derived from alkyl carboxylic acids, with organometallic species and employ single-electron transfer to achieve the desired coupled compounds (Scheme 28). The mechanism for the majority of these reactions involves a single-electron-transfer (SET) mechanism, which circumvents the need for oxidative addition of a transition-metal into the carbon–halogen bond, which can often be detrimental for the stability of the strained alkyl groups under discussion.

The alkyl redox-active ester **136** has been shown to successfully couple with organozinc and organomagnesium species using an Fe-based catalyst system, such as $[Fe(acac)_3]$ (acac = acetylacetone) and the dppBz ligand to attach phenyl groups to cubane **137**, BCO **137 a**, and BCP **137 b**;[196] while the formation of alkyl boronic acids and esters can also be achieved through the use of the alkyl redox-active esters. The catalytic system of $NiCl{\cdot}6H_2O$ and $MgBr_2{\cdot}OEt_2$ is employed to couple the redox-active ester with lithiated bis(pinacolato)diboron.[197] The boronic acid can then be accessed by reacting the ester product with boron trichloride. This method was successfully applied to synthesize methyl 4-(pinacolboron)cubane-1-carboxylate **138** and methyl 4-(pinacolboron)BCO-1-carboxylate **138 a**.

On the other hand, alkyl boronic acids and esters can also be produced through photoinduced decarboxylative borylation of carboxylic acids as developed by Aggarwal and coworkers.[198] This method does not use transition-metal catalysis but instead utilizes light to initiate the radical combination of the *N*-hydroxyphthalimide ester derivative with the diboron reagent bis(catecholato)diboron. This reaction was used with both cubane, BCO, and BCP scaffolds **138**, **139 a**,and **139 b**, respectively, to form their boronic ester derivatives, in moderate to good yields.

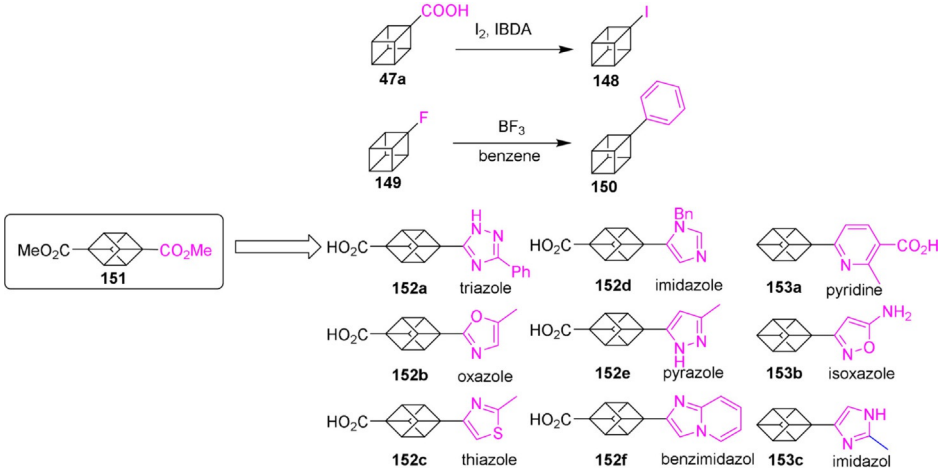

Scheme 29. Examples of organic transformations with cubane and classic cubane carbonyl chemistry. IBDA = iodobenzene I,I-diacetate.

A method for decarboxylative alkynylation was the target of further investigations. Again a redox-active alkyl ester was utilized to react with either an alkynyl Grignard reagent using an iron catalyst or a lithiated-alkynylzinc species with a nickel catalyst. Unfortunately, this approach was not successful for any of the tertiary bulky cagelike alkyl groups **141** in this Review, that is, those derived from BCP, BCO, and cubane.[199] In addition, decarboxylative alkenylation of a variety of groups can be used as well. Here, a redox-active alkyl ester is coupled with an alkenylzinc reagent in the presence of $[Ni(acac)_2]$ and a bipyridine ligand. Methyl 4-(propen-2-yl)BCO-1-carboxylate **142** was prepared in a 42% yield through this method.[200]

Most recently, redox active esters have been employed to synthesize sp^3-rich(fluoro)alkylated scaffolds.[201] This is made possible through modular radical cross-coupling with sulfones in the presence of $[Ni(acac)_2]$ followed by the reaction with (4-fluorophenyl)zinc chloride. This method was shown to be applicable with the BCO scaffold **143**. Copper catalysis and photoredox catalysis were coupled together to develop a new method to incorporate alkyl substrates by sp^3 C–N bond formation.[202] This strategy involves the reaction between alkyl carboxylic acids, such as BCO **144** and BCP **145** (via in situ iodonium activation) and *N*-nucleophiles. *N*-BCO and *N*-BCP products, **146** and **147**, respectively, can be achieved in high yields at room temperature from 5 to 60 min when irradiated with light while activated by an iridium catalyst and in the presence of copper. The reaction proceeds via single-electron transfer pathways and opens a new avenue to C–N bond formations that uses alkyl carboxylic acids over alkyl halides as the coupling partner. Further details of these types of reactions can be found in the recent review entitled "Decarboxylation as the key step in C–C bond-forming reactions".[203]

4.2.4. Cubane chemistry

Cubanyl chemistry has evolved over the years to increase its applicability in modern day synthesis. Work in the 80s showed how a cubanyl carboxylic acid group **47a** could be transformed to an iodide **148** by a hypervalent iodine oxidative decarboxylation mechanism (Scheme 29).[204] This was achieved through the use of hypervalent $PhI(OAc)_2$-CCl_4-I_2 and with irradiation of the compound. The iodocubane products were achieved in 80–90% yields. Phenylcubane **150** was first obtained from the transformation of fluorocubane **149**, when it is reacted with benzene and boron trifluoride in toluene in a Friedel–Crafts type reaction.[205] After 30 min, a 40% yield of phenylcubane was achieved as the sole product.

Much chemistry has been reported based on work with carbonyl cubanes. Dimethyl cubane-1,4-dicarboxylate **151** was transformed into a variety of different functional groups from reactions with the ester functional group. Triazole **152a**, oxazole **152b**, thiazole **152c**, imidazole **152d**, pyrazole **152e**, benzimidazol **152f**, pyridine **153a**, isoxazole **153b**, and imidazole **153c** functionalities were all introduced through classic carbonyl transformations.[206]

To access cubane for use in palladium cross-coupling reactions a series of chemically distinct, highly strained, activated cubane scaffolds were synthesized (Scheme 30). This was achieved by using iodinated cubane derivatives **154** to optimize lithium–halogen exchange reactions.[207] Boron **155a**, phosphorus **155b**, tin **155c**, silicon **155d**, sulfur **155e,** and alkyl **155f** groups were attached to the cubane scaffold with this method. The optimum conditions found for the metal–halogen exchange reaction allowed for the generation of the lithiated intermediate through the reaction of cubanyl iodide **154** with two equivalents of *t*BuLi at −78 °C in THF for 1 h. The reaction mixture was then allowed to warm to room temperature after two equivalents of the relevant R–X reagent were added. These electrophilic cubanes were then investigated for their use in Suzuki–Miyaura, Negishi, and Stille cross-coupling reactions with various halogenated phenyl groups, but all coupling reactions proved unsuccessful.

To avoid transition-metal-facilitated oxidative addition directly onto the cubane core an ethynyl bond was introduced. Sonogashira cross-coupling reactions with ethynylcubane **156** and different halogenated aromatic groups proved successful due to the presence of this spacer. As a result, a variety of ethynyl-linked cubane products were obtained, showing the

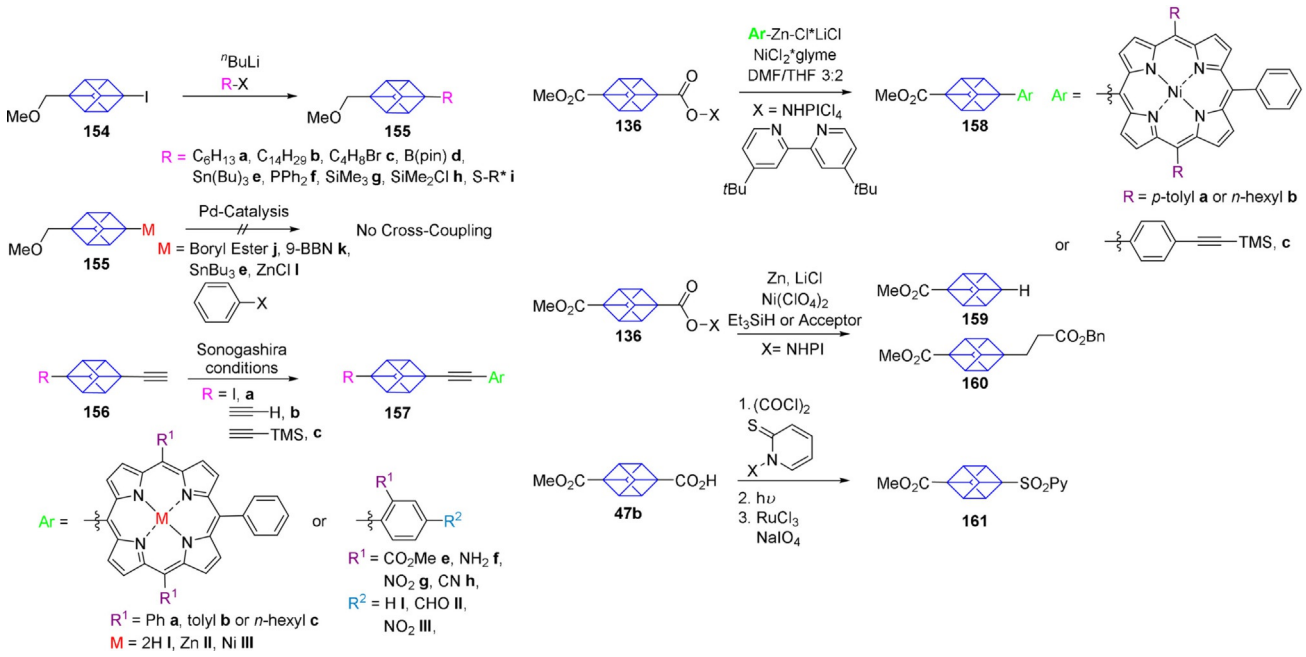

Scheme 30. Expanded cubane chemistry. 9-BBN = 9-borabicyclo[3.3.1]nonane.

first example of cubane stability in the presence of palladium catalysts.[208] Conditions for this reaction were optimized for the coupling of 1-iodo-4-ethynylcubane **156a** with various halogenated substituted aryl groups. These conditions involve the reaction of a 0.1 M concentration of cubane **156a** with three equivalents of the aryl halide, in the presence of $[Pd(PPh_3)_4]$ (10 mol%) and CuI (30 mol%) in NEt_3 under argon for 16 h. The highest yield observed was 90% when cubane **156a** was coupled with ethyl 4-iodobenzoate. Also, the first ever example of a porphyrin attached to a cubane was achieved with this method under copper-free Sonogashira conditions in a 51% yield. Sonogashira conditions were also employed for coupling reactions of 1,4-diethynylcubane with various porphyrins. Monosubstituted products were achieved in yields up to 83%.

The direct attachment of aryl groups, namely porphyrins onto the cubane core was still a synthetic target for us, so a different approach was sought to achieve this as palladium-catalyzed cross-coupling chemistry failed due to the instability of the cubane core in presence of palladium. A single-electron-transfer mechanism was chosen, as it circumvents the requirement for the oxidative addition of the transition metal onto the cubane core by instead utilizing the cubyl radical which is rather stable. Moreover, the versatility of redox-active esters used for decarboxylative cubane-aryl cross-coupling had been seen by work performed by the Baran group, which supported SET as a viable method for cubanyl porphyrin coupling. Firstly, optimization of the nickel-catalyzed cubane-aryl coupling was carried out by looking at five major contributing factors: 1) solvent, 2) temperature, 3) concentration, 4) Ni source, and 5) ligand. The ligand was identified as the main contributing parameter and results showed that the very electron-deficient 4,4′-functionalized bipyridines, especially the rigid phenanthroline derivative provided the best results.[208] It was hypothesized that the ligand affects the rate-determining step of the catalytic cycle, that is, the reductive elimination of the cubane and aryl residue from the nickel center. Yields were achieved of over 50% with this method with very electron-rich aryl moieties and unfunctionalized aryl groups that could be coupled smoothly. This is a two-fold increase over previously reported yield of 25% for the iron-catalyzed coupling.[196] But most excitingly, the first example of a directly coupled cubanyl porphyrin was obtained.

Additional chemistry with cubane can be observed such as the nickel-catalyzed Barton decarboxylation and Giese radical conjugate addition reactions.[209] These reactions were reinvestigated to simplify the required conditions and widen the scope of the reactions. In each case *N*-hydroxyphthalimide (NHPI) based redox-active esters were utilized and a thermally initiated Ni-catalyzed radical formation was carried out. Subsequent trapping with either a hydrogen atom source ($PhSiH_3$) or an electron-deficient olefin in the case of **159** and **160**, respectively, led to the two products of interest. The former route resulted in the decarboxylated cubane product in 77% yield while the latter route gave the alkylated cubanyl product in 56% yield. Additionally, an interrupted Barton decarboxylation reaction can be used to synthesize simple sulfinate salts **161** from readily available carboxylic acids **47b**.[210] The carboxylic acid is transformed to acyl chloride, then reacted with 1-hydroxypyridine-2-thione, followed by illumination with light, then exposure to ruthenium trichloride and sodium periodate to form the sulfone product. Addition of sodium ethoxide allows for the conversion to the sulfinate salt. The cubanyl sulfone product was achieved in 42% and the salt in 95%.

5. Applications of Rigid-Linear Linkers in Electron-Transfer Systems

There is an increasing need to discover more efficient methods to harvest energy and, as is often the case, we can look to nature as the supreme example of how to maximize this process. As a result many artificial molecular devices have been made for solar energy conversion by acting as photosynthetic mimics.[211] During photosynthesis, in order to absorb and transfer solar energy effectively the antenna chlorophylls in photosynthetic bacteria are organized as noncovalent macrorings in a spatially defined manner (Figure 13).[212] Therefore,

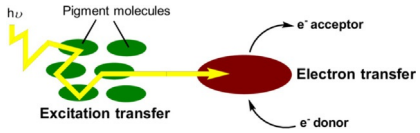

Figure 13. Basic overview of the electron-transfer mechanism occurring in photosystems during photosynthesis.

for electron-transfer systems, it is crucial to have the correct geometry, conformation and spatial arrangement of the molecular building blocks in these photochemical systems.[212c–f] In order to achieve this, rigid-linear isolating linkers (among others) are required to provide defined structures and fixed regiochemical arrangements similar to those seen in nature.

Work began in this area as early as the 1980s with small organic chromophores, and has progressed to larger multiporphyrin complexes.[213] The majority of systems seen in literature are linked with either BCO, triptycene or BCP. Synthetic methods employed to achieve these complexes ranges from substitution reactions to transition-metal-catalyzed cross-coupling methodologies such as Suzuki, Sonogashira, and Stille reactions.

5.1. Small-organic acceptor–donor systems

One of the first examples of an electron-transfer system, modeled with a linear-rigid linker was seen in the 1980s which utilized BCO as the linker.[213] The [2.2.2] rods consisted of one or two BCO moieties with different chromophores attached to the bridgehead carbon atoms. α-Naphthyl **162** and β-naphthyl **163** were used as the donor groups while the energy acceptor units consisted of acetyl, benzoyl, or cyclohexanecarbonyl moieties (Figure 14).

Emission was observed by both the donor and the acceptor moieties upon excitation of the donor chromophore, with the ratio depending on the system. The rates of intramolecular energy transfer and the decay exhibited by the bridgehead groups were determined using single-photon counting. The most rapid transmission was seen with **163 b**, in which the β-naphthyl group was the donor group while benzoyl was the most efficient acceptor. Additionally, the shorter rod length showed quicker transmission, due to the simple dipole–dipole coupling that is aided by excitation transmission through the

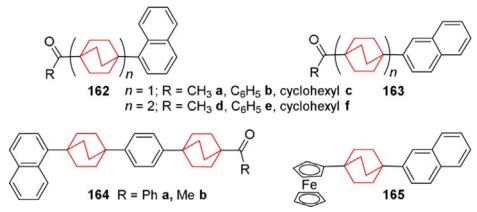

Figure 14. Naphthalene systems with various small molecule chromophores and BCO linkers.

molecule, thus indicating a correlation between distance and transmission. The molecules were synthesized over a series of steps starting from 1,4-dichloroBCO; the two chromophores were attached sequentially, the donor moiety by an aromatic alkylation and, more challengingly, the acceptor units by lithium–halogen exchange reactions.

Following the successful identification of the most efficient donor and acceptor moieties in the rigid linker system seen in **163 b**, the effect of inserting an aromatic ring in between two BCO scaffolds was investigated.[214] α-Substituted naphthalene was implemented as the donor group and an acetyl or benzoyl group acted as the acceptor groups in the phenylene-bridged system **164**. Results showed that transmission of singlet excitation proved to be less efficient compared to the previously studied rods. Δ-Density determinations were employed to describe the distribution of electronic excitation in these systems and to see what was controlling energy transmission. These determinations showed that while most of the excitation energy is located in the terminal chromophores, some is distributed in the BCO units, indicating the presence of through-bond energy transfer. Evidence also showed that energy transfer is mainly through-bond for the short rods but when the rod is lengthened Förster through-space transfer can be observed.

In 1995, the Langmuir–Blodgett technique was used to advance research into artificial molecular devices for solar energy conversion.[215] The BCO linker was utilized for its ability to arrange the functional moieties in a controlled manner across the films in the molecular device and to separate the chromophores at a fixed distance. β-Substituted naphthalene was used as the sensitizer (S) and ferrocene as the electron-donor (D) **165**. Both moieties were attached to the BCO scaffold via Friedel–Crafts alkylation. Further studies into the dynamics of the S–D dyads have yet to be published.

Förster resonance energy transfer (FRET) is used to indicate the molecular proximity of light-absorbing and fluorescent structures.[216] FRET was utilized to investigate if energy transfer occurs when chromophores are arranged orthogonally to one another. The BCO scaffold was chosen to allow for this specific arrangement and the chromophore selected was perylene bisimide **166** (Figure 15). Pump-probe spectroscopy, chemical variation, and calculations were executed, which unexpectedly showed energy transfer in the dyad with near-unit quantum efficiency. However, further experimentation showed that this was due to a break in the orthogonal arrangement, owing to thermally populated ground-state vibrations that allow for

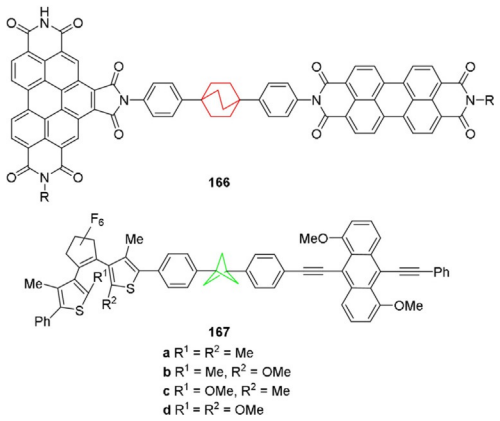

Figure 15. Photochromic systems to investigate Förster resonance energy transfer (FRET).

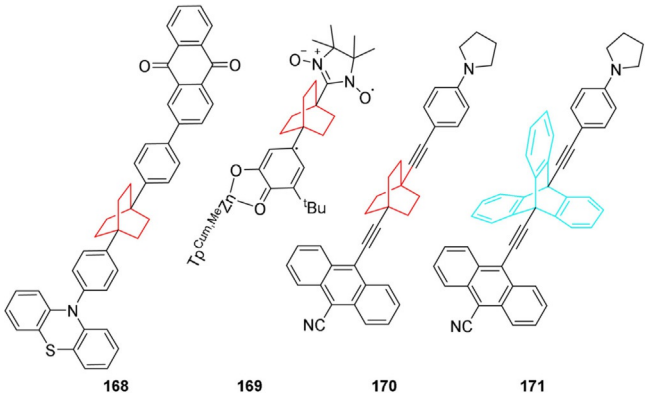

Figure 16. Small molecule chromophores for electron-transfer studies.

multiple transition dipole moment orientations showing the pivotal role vibrational motion plays in energy transfer processes. Further investigations with the transition density cube approach indicated that while chromophores are orthogonally arranged Coulombic interactions do not contribute to electronic coupling. The perylene bisimide was attached to the BCO linker via an amide condensation reaction.

BCP was also utilized as a rigid linker to study FRET between the fluorophore 1,5-dimethoxy-9,10-di(phenylethynyl)anthracene (donor) and different substituted thiophene acceptor units **167**.[3,217] Its short C^1–C^3 distance makes it a unique linker, allowing two conjugated chromophores to be in close proximity while not allowing any significant π-conjugation. A suggested application for the BCP dyad is use in (rewritable) data storage media, where fluorescence can be reversibly switched "on" and "off", depending on the state of the photochromic part. Encouragingly, results showed quantitative resonance energy transfer between the excited state of the fluorophore and the closed form of the photochromic units. However, when the photochromic units were substituted with methoxy groups their photostability is reduced compared to methyl groups, which may limit their use in fatigue-resistant optical switches. To synthesize these compounds Sonogashira methodologies were followed to introduce the anthracene fluorophore to the BCP linker and a lithium reaction was employed to attach the photochromic units.

The efficient conversion of light to storable electric or chemical energy was investigated with a phenothiazineanthraquinone dyad **168**, connected via BCO (Figure 16).[218] The photoinduced charge separation of the dyad was determined through the use of picosecond and nanosecond transient absorption and time-resolved ESR spectroscopies. A long-lived charge separated (CS) state was observed in the dyad upon excitation of the anthraquinone (AQ) donor chromophore, as AQ acts as a triplet photosensitizer. Time constants of 1.3 ns and 1.0 μs were found of the formation and the decay of the CS state, respectively. Owing to the formation of the CS state via the triplet mechanism, time-resolved ESR showed spin polarization for all the emission signals. The dyad was synthesized via Pd cross-coupling methodologies.

p-Phenylene, methyl-substituted *p*-phenylene and BCO were employed as linkers to determine the torsional dependence of donor–acceptor systems when they are mediated by the σ/π-systems of a bridging linker.[219] BCO, which possesses the "Aviram–Ratner" diode bridge, can be used to evaluate J_σ and H_σ explicitly in the absence of any π-contributions to the exchange and electronic coupling. A semiquinone (Zn-SQ) donor and a nitronylnitroxide (NN) acceptor **169** were used in the D–B–A system. CASSCF calculations gave results consistent with that of the exchange coupling parameter, showing that the σ-superexchange, mediated by a saturated BCO bridge, is equivalent to the predicted σ-superexchange through a p-phenylene ring perpendicular to both SQ and NN. Furthermore, there is no measurable hybridization-dependent difference in the magnitude of the σ-contribution to the superexchange, as the carbon atoms are sp^2 for the phenylene ring and sp^3 for the BCO bridge. Additionally, no measurable difference is observed owing to the three $-CH_2CH_2-$ σ-pathways for BCO, compared to *para*-phenylene's two pathways.

The effect of sequential addition of π-bridges in the form of benzene rings to the BCO scaffold (to eventually form triptycene **171** was investigated with respect to the electron transfer rates.[220] A 4-(pyrrolidin-1-yl)phenyl electron donor and 10-cyanoanthracen-9-yl electron acceptor were attached via alkyne linkages to the scaffold and used as the model system **170**. Previous studies have proven the existence of the Marcus inverted region through the use of saturated spacer groups, whereas the advantage of π-bridges are that they maintain closer energetic resonance between the π-systems of the D and A group conveying electronic communication. But surprisingly, it was shown, by Natural Bond Orbital (NBO) analysis, that the additional π-pathways played no role in the electron transfer. Furthermore, no effect was seen from the changes in the σ-system because of shifting hybridization, despite the predictions of photoelectron spectra.

1,4-Bis(*p*-cyanophenyl)BCO **172** and 1-benzoyl-4-(α-naphthyl)BCO **162b**, amongst other compounds, were synthesized for energy and electron-transfer studies,[221] to investigate whether electrons can be transferred, upon electron excitation, through a saturated hydrocarbon insulator (Figure 17). BCO was selected for the scaffold as it provides a symmetrical and

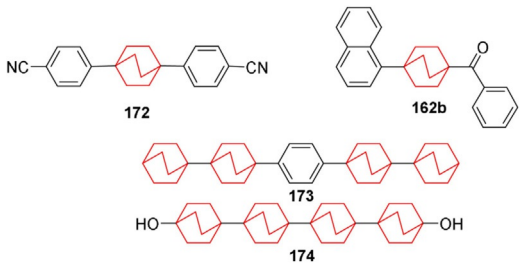

Figure 17. Electric rods linked by BCO units.

accessible framework dissuading the approach of orbitals from separate π-systems.[222] The introduction of a single electron into one aromatic ring of the symmetrical diaryl derivatives led to radical anions in which the odd electron was localized in one of the two aromatic rings. This result was hypothesized to be due to a tunneling problem from a single potential energy barrier in the bicyclic ring structure. In contrast, singlet energy transfer was observed from the naphthyl to the benzoyl moiety in compound **162b**, and triplet transfer from benzoyl to naphthyl. A dipole–dipole mechanism is involved in the singlet transfer, while the triplet–triplet transfer suggests that a close approach may not be necessary. A sodium–potassium alloy was used to introduce the electron and ESR spectroscopy of monoradical anions was used to determine whether the electron was delocalized over one or both rings.

Following this, rodlike linear units consisting of four BCO units (**173** and **174**) were synthesized and a series of excitation and electron-transfer studies were carried out.[223] The reason for the longer rods was to investigate "through-space" electron transfer as the previous rods all showed only singlet and triplet "through-bond" transfers. Results showed that both singlet and triplet through-bond energy transfer were occurring. To synthesize the longer rods a new synthetic approach was required. Sodium–potassium coupling was implemented to achieve these systems by radical dimerization of the bridgehead free radicals.

To investigate the decay constant of *p*-phenylene, oligophenylene molecular rods bearing the BCO moiety were synthesized with two nitronyl nitroxide radicals **175** (Figure 18).[191] Owing to its rigid π-conjugated structure, oligo(*p*-phenylene) can be used to query molecular conductance. The decay constant has been obtained for molecular conductance,[224] the rate of electron transfer,[225] and the magnitude of exchange interaction,[226] and all were shown to decay exponentially with molecular length. To measure the decay constant of the exchange, the effect of the magnetic field on the electron transfer and the splitting of the molecular orbital was studied. Different rod lengths were used with the nitroxide biradicals and the complexes were measured through the simulation of the ESR spectra. Results showed that the exchange interaction decreased with the decay constant, indicating that the spin–spin exchange interaction between neutral radicals has a decay constant similar to the molecular conductance. The diradicals were synthesized using 1,4-dibromoBCO as an intermediate. A series of steps afforded diformyl intermediates that enabled access to the desired nitronyl nitroxide derivatives following reaction with 2,3-bis(hydroxyamino)-2,3-dimethylbutane sulfate and oxidation by sodium periodate.

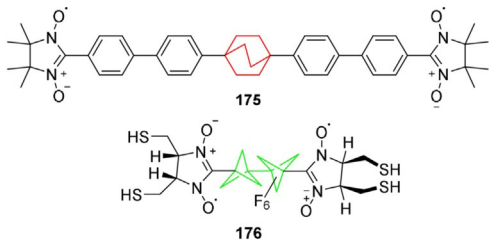

Figure 18. Nitroxide biradicals for the theoretical investigation of decay constants and use in light-induced spin-pump devices.

Calculations were used to determine the suitability of organic molecular systems in a single molecular spin-pump device.[227] As they are well spaced and energetically separated, biradicals with triplet state singly occupied molecular orbitals (SOMOs) are proposed for such devices. Different candidates were designed and computationally studied through density functional theory, all of which employed bis(nitronyl nitroxide) based biradicals, including a complex with two fused propellane units **176** (a purely theoretical compound) as the bridging unit. It was estimated that the proposed molecular structures will operate as spin-pumps using harmonic magnetic fields in the MHz regime and optical fields in the IR to visible light regime.

To effectively study electron transfer, practical devices require vectorial energy or electron transfer over long distances. Moreover, the geometry of the system must be rigidly defined to compare with the predictions made for energy and electron transfer.[228] A novel bridging ligand 1,4-bis[2-(2,2′-bipyridine-5-yl)ethynyl]BCO **177** (b-Z-b) was synthesized with two bipyridine units (b) that are separated by the rigid 1,4-diethynylBCO (Z) spacer. The ligands were then employed to construct mono- and dinuclear complexes of Ru^{II} and Os^{II} and investigated for electron-transfer studies (Figure 19).[229] Light excitation of the Ru-based unit followed by a very efficient (>90%) energy transfer to the sensitized Os-based unit was observed in the heterometallic $[(bpy)_2Ru(b\text{-}Z\text{-}b)Os(bpy)_2]^{4+}$ complex, overcoming the long metal–metal distance. The key step in the synthesis of the **177** complex connected the diformylBCO to the dipyridyl units via a Wadsworth–Emmons reaction giving the (*E,E*) dimer.

Low temperatures are a hindrance in the utilization of electron transfer for practical applications, as the process is blocked when the solvent freezes. It can be seen that in the rodlike dinuclear complex {(ttp)Ru(tpy-ph-BCO-ph-tpy)Os(ttp)}$^{4+}$(RuOs) **178** an electron-transfer process occurs that is independent of temperature and the state of the solvent (ttp = *p*-tolyl-tpy, tpy = terpyridine, ph = 1,4-phenylene).[230] The RuOs complex **178** is a rigid-rodlike linear species owing to the ph-BCO-ph spacer. At high temperatures, the luminescent excited-state lifetime is the same for RuOs as Ru, showing that the dinuclear complex energy transfer is too slow to compete with intrinsic Ru-based deactivation. At low temperatures

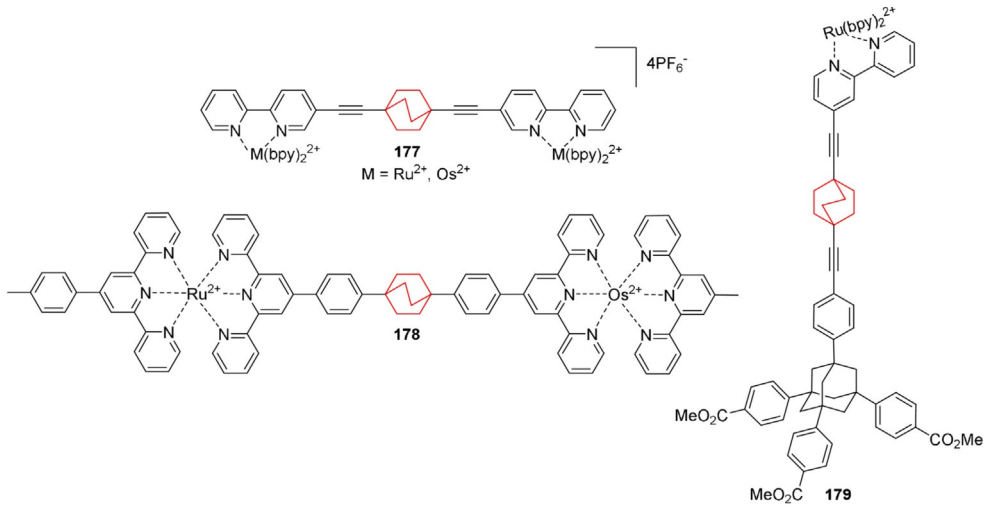

Figure 19. Ru^{2+} complexes linked by BCO that were used to investigate long-range energy transfer.

energy transfer occurs from the Ru center to the Os center, shown through observations in which the Ru luminescence is quenched while sensitization of the Os- based luminescence occurs. In the RuOs complex, the critical temperature for when the energy-transfer rates for Ru-based intrinsic deactivation and Ru→Os are identical is 184 K. It was found that over the temperature range 90–200 K, the Ru→Os energy transfer rate in $\{(ttp)Ru(tpy\text{-}ph\text{-}bco\text{-}ph\text{-}tpy)Os(ttp)\}^{4+}$ is $5.2\times10^6\ s^{-1}$ (20%). Therefore, energy transfer is neither affected by temperature changes nor by the state of the solvent, which is fluid at $T>$ 110 K and frozen below that temperature.

To study long-range electron transfer in TiO_2 semiconductor nanoparticle thin films, a tripodal Ru^{II}–polypyridyl complex **179** was synthesized with a BCO bridge.[231] The BCO moiety was chosen to investigate the role of conjugation in the bridge. 1,3,5,7-Tetraphenyladamantane derivatives, containing three CO_2Me anchoring groups, were used to anchor the molecule to the TiO_2 film while the Ru complex with bpy ligands was employed as the sensitizer. Sonogashira methodologies were utilized to attach the different moieties to the BCO bridge.

Through the use of theoretical calculations the role of BCO as an electronic insulator was evaluated by a comparison of the electronic coupling parameter (V_{ab}) of 1,4-bis(ferrocenyl)-benzene and 1,4-bis(ferrocenyl)BCO **180**. DFT was used to optimize geometries and extended Hückel calculations were employed to calculate V_{ab} by the dimer splitting method. Results of the calculations showed a 12-fold decrease in electronic coupling with the BCO derivative (Figure 20).[232]

Following this, a potential star-shaped molecular motor **181** was synthesized that incorporates the BCO fragment.[233] The molecule is based on a ruthenium complex that bears a tripodal stator functionalized with ester groups to be anchored onto oxide surfaces. These motors contain ferrocenyl electroactive groups and the cyclopentadienyl (Cp) rotor connected through the insulating spacer BCO. The known 1,4-disubstituted BCO is a good candidate, as it has a rigid saturated backbone enabling it to maintain linearity and rigidity in the arms of the motor. This is an example of an electrically fueled, single molecular rotary motor. This concept is based on the transport of electrons between two electrodes by electroactive groups attached to a central rotatable core.[234] The ultimate goal is to study the molecule between the two electrodes of a nanojunction to test its applicability as a molecular machine.

In light-harvesting systems, amongst other electron-transfer processes, $M(N\text{-}N)_2^{n+}$ complexes have become an area of much interest, in which M is a second or third transition-row metal ion such as Ru^{II}, Re^{I}, or Os^{II}.[235] Ru^{II} and Re^{I} act as photosensitizers and are modulated by the donor- or acceptor groups of the coordinated *N*-N ligands, such as 2,2′-bipyridine (bpy) or 1,10-phenanthroline (phen) (Figure 20).

Different triptycene spacers of varying oxidation states were employed to make Ru^{2+} and Os^{2+} complexes **182**–**184**, allowing the spacer to act as a redox-active switching unit and enabling the quinone spacer to potentially control energy and electron-transfer reactions in between two complexed metal centers.[236] Key steps in the synthesis of these complexes were the Diels–Alder reactions to form the triptycene scaffold and the lithium–halogen exchange reactions used to connect the Ru^{II} moieties to the diformyltriptycene. The ratio between the relative emission of (Ru-bmb-Ru), (Ru-btb-Ru), and (Ru-bqb-Ru) was found to be 3.7:2:1. The highest emission was found for the bmb ligand due to the donor effect of the methoxy-substituents, whereas the lowest emission was seen for the bqb system as the emission is strongly quenched by the quinone moiety. Owing to the quinones redox active properties emission tuning can be obtained. The electronic energy level is positive enough for the quinone moiety, in the metal complex Ru–bqb–Os, to act as a quencher for the Ru-based ^3CT excited state as is shown by the lack of phosphorescence seen from the Os-based ^3CT level.

5.2. Porphyrin systems

Porphyrins have been employed as more accurate photosynthetic mimics due to their similarity in structure and electronics with the chlorophyll pigments in plants[212] and due to the

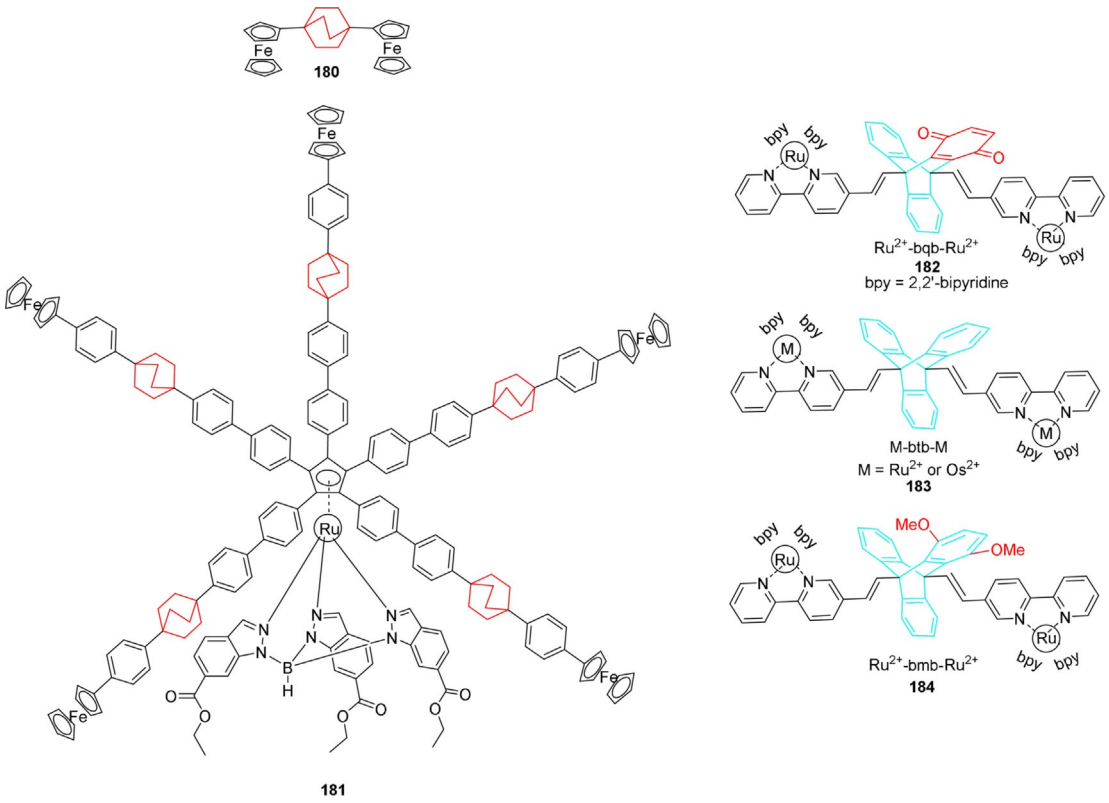

Figure 20. Star-shaped molecular motor and triptycene-linked electron-transfer systems.

many advances in their synthesis, structural understanding, and functionalization.[237] In 1984, the first porphyrin photosynthetic model with a linear-rigid linker was published. The link between electron tunneling and distance was investigated by extending the length between two chromophores with additional BCO linkers (Figure 21).[238] Due to the employment of the rigid BCO linker, the dependence of variables such as distance, orientation, and the energy gap between donor and acceptor molecules in electron-transfer processes can be more effectively studied. The electronic energy for photosynthetic model compounds, linked by BCO, containing a porphyrin and quinone unit in **185** and **186**, was calculated through the use of a semiempirical method. The edge to edge distances of the BCO and biBCO systems **185** and **186** were found to be 10 and 14 Å, respectively. It was predicted in these systems that hole transfer would dominate, resulting in a significant difference between the rate of decay for the forward electron transfer compared with that of the reverse electron transfer over distance. Results indicate that the symmetry of the donor and acceptor orbitals relative to the BCO linker orbitals determines the energy dependence on it to mediate the donor–acceptor interactions. Also, for every additional BCO unit added it was expected that the forward rate from the singlet excited state will slow by a factor of 1500, whereas the reverse rate will only decrease by a factor of 60.

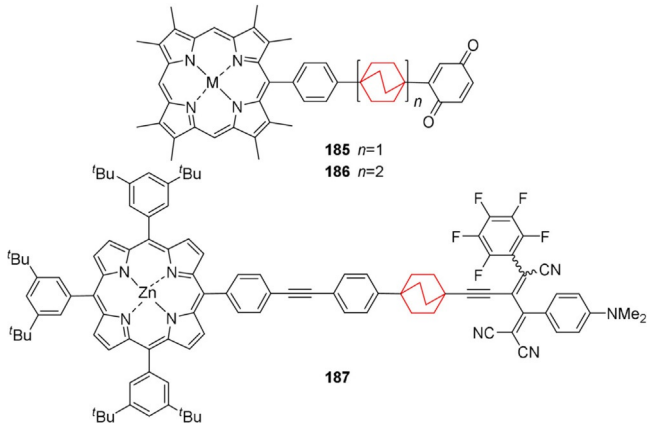

Figure 21. Monoporphyrin BCO-linked systems as photosynthetic mimics.

To effectively mimic photosynthesis, the ability to control the ratio of the rates for charge separation and recombination is key in creating long-lived charge separated states, which is necessary for efficient electron-transfer processes. Marcus theory was used to further understand these rates in electron-transfer reactions on a series of electron donor–acceptor systems with push–pull chromophores as electron acceptors.[239] A zinc(II) porphyrin (ZnP) electron donor connected via a rigid phenylene–ethynylene–phenylene (PEP)BCO linker to different anilino-substituted multicyanobutadienes or extended tetracyanoquinodimethane analogues **187** was synthesized (Figure 21). First reduction potentials were obtained, and coupled with other results, showed that the extent of ZnP fluorescence quenching correlates with the strength of the electron acceptor. This finding indicates that a rational tuning of the photophysical properties by the push–pull chromophores as

electron acceptors is possible. The computed Marcus curves showed that the charge-recombination kinetics in the inverted region was greatly affected by enhancing the electron-vibration couplings, due to the conformationally highly fixed push–pull acceptor chromophores. X-ray crystal structure data showed well-defined systems holding the acceptor and donor moieties at fixed distances with edge-to-edge distances of around 17 Å with little spectral overlap between the porphyrin and acceptor moieties. It can be deduced from this data that if electron transfer is occurring by a through-bond mechanism the likelihood of Förster resonance energy transfer is greatly reduced.

It is of great interest to generate long-lived ion pair (IP) states via singlet radical ion pair states to effectively mimic efficient charge separation (CS) in a photosynthetic reaction center (RC). Strategies based on multicomponent donor–acceptor systems that require multistep electron-transfers offer great possibilities in achieving this goal. With this in mind, conformationally constrained triads **188** were synthesized consisting of a metal-free porphyrin (H_2P), a zinc porphyrin (ZnP) and 1,4:5,8-naphthalenetetracarboximide (NIm) (Figure 23).[240] The porphyrin moieties are bridged by four different aromatic spacers one of which is BCO-1,4-diylbis(1,4-phenylene). Picosecond excited-state dynamics were studied with these systems using picosecond time-resolved transient absorption spectroscopy. Results showed that long-lived ion pair states of the triads $(ZnP)^+$-(H_2P)-$(NIm)^-$ were observed upon photo-excitation by charge separation between the (H_2P)* and NIm followed by a hole-transfer reaction from the $(H_2P)^+$ to the ZnP. The rates of this hole transfer were used to determine quantum yields of the formation of long lived ion-pair states (Figure 22).

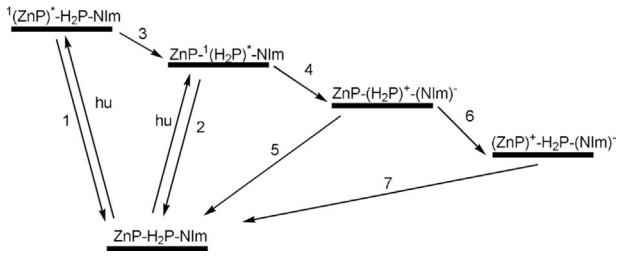

Figure 22. Energy-level diagram of artificial photosynthetic-bisporphyrin model **188** (ZnP = zinc(II) porphyrin, H_2P = free base porphyrin, NIm = 1,4:5,8-naphthalenetetracarboximide; cf. Figure 23).

To further understand the factors that control the dependence of ET rates on the distance between the electron-donor and the -acceptor, a series of (Zn^{II}–Fe^{III}) 5,10,15,20-tetraarylmetalloporphyrin dimers **189**, with a variety of different linkers, including BCO, were synthesized and the kinetics of their PET reactivity were measured.[241] Through the use of fluorescence lifetime measurements, the electronically excited states of the zinc porphyrin to the bis(imidazole)iron porphyrin cation could be determined. Results showed that when the distance was increased by 13 Å the rate of electron-transfer only decreased by a factor of 165 indicating a small reduction of the electronic coupling with distance. Selective nucleophilic aromatic substitution of the *para*-fluorine atoms in tetra-arylporphyrins was employed in the synthesis of the molecular building blocks. This method allowed for a wide variety of systematic modifications such as type and length of spacer, metal center, and redox-potential difference between donor and acceptor. A single zinc(II) or one iron(III) atom can be inserted after the synthesis of the symmetrical porphyrin dimer (Figure 23).

Further studies involving porphyrin-based donor–bridge–acceptor (D–B–A) systems aimed to find the triplet excited-state deactivation of a gold porphyrin (AuP) (Figure 24).[242] 1,4-Diethynyl-BCO was utilized as a saturated linker to explore whether electrons/electron holes can be transferred within the dimer **190** between AuP and ZnP. As a comparison, 1,4-diethynylbenzene (BB) and 1,4-diethynylnaphthalene (NB) were derived as conjugated linkers. The porphyrins are separated by 19 Å, edge-to-edge, so a direct (through-space) exchange mechanism was not predicted. Results showed no quenching of AuP that is, no hole transfer, when the conjugation in the system is broken due to the BCO linker. While long-range hole transfer from AuP to ZnP occurs on the nanosecond time scale at room temperature in the dimers connected by fully-conjugated bridging chromophores (NB and BB).

A similar porphyrin scaffold was used to investigate effects on the photophysical processes in the donor–bridge–acceptor (D–B–A) systems through studies of the acceptor spin state.[243] Again, 1,4-diethynyl-BCO, -BB and -NB were the linkers investigated. In this system **191**, FeP acts as the acceptor while ZnP acts as the donor. FeP is modulated from iron(II) to low-spin iron(III) by the coordination of an imidazole ligand. In previous such systems, the high-spin $Fe^{III}P$ significantly enhances the intersystem crossing in the ZnP, as the dominating deactivation pathway for the singlet excited zinc porphyrin. But this process is only a minor contribution to the quenching of the low-spin

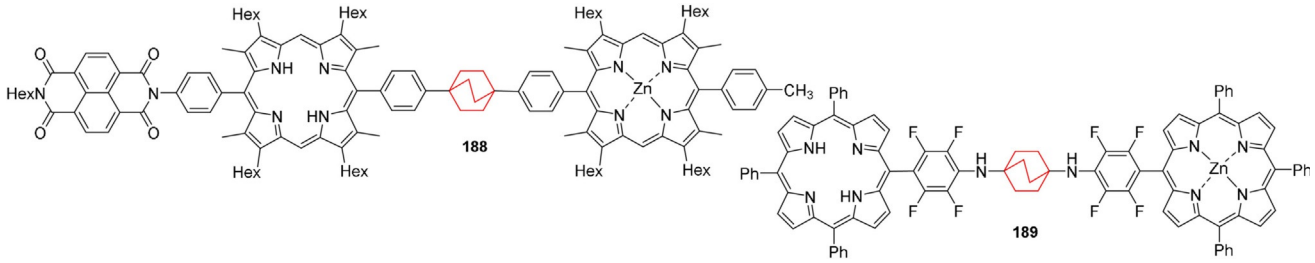

Figure 23. BCO-linked porphyrin dimers.

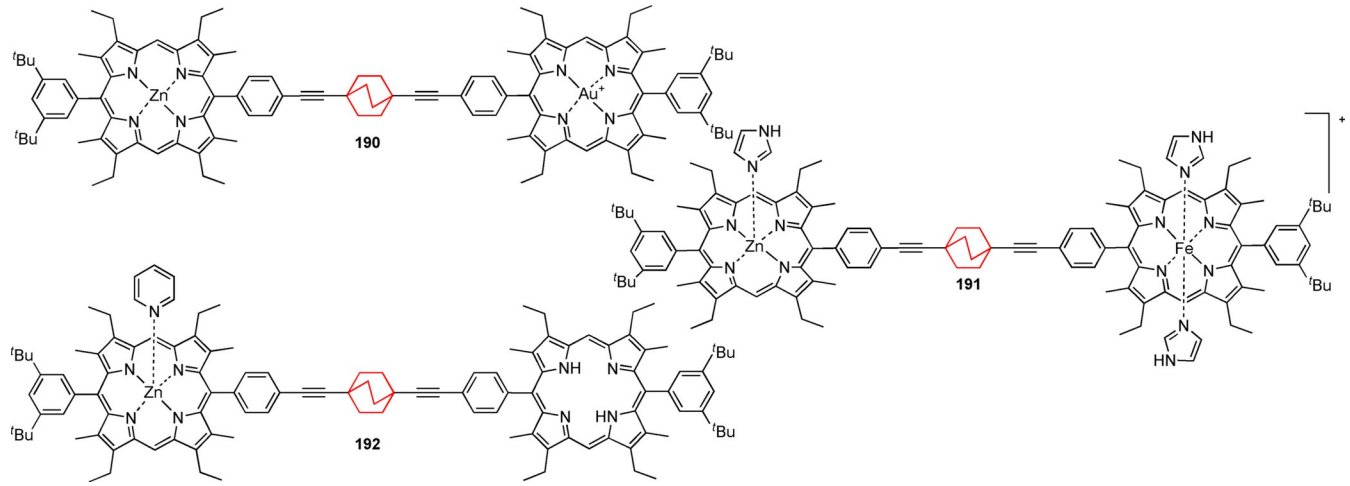

Figure 24. BCO-linked bisporphyrin systems as photosynthetic mimics.

iron(III); instead the major photophysical process that is occurring is a long-range electron transfer on the picosecond timescale allowing intersystem crossing to occur at its "normal" rate. EPR and UV/Vis measurements were used to prove the change from iron's high-spin state to low-spin state upon imidazole coordination. Steady-state and time-resolved fluorescence measurements were used to measure total quenching efficiencies for the excited states of the zinc porphyrin donors.

Again an analogous porphyrin-based donor–bridge–acceptor (D-B-A) system **192** with a 1,4-diethynyl-BCO spacer was investigated, this time to find out the contributions towards singlet energy transfer from Förster and Dexter mechanisms.[244] A clear distinction between the two mechanisms can be seen when the inert BCO-linker is used. This so-called superexchange mechanism for singlet energy transfer has been shown to make a significant contribution to the energy transfer rates in several D–B–A systems and its D–A distance as well as D–B energy gap dependencies have been studied. In each system, the acceptor is a free base porphyrin and the donor consists of a zinc porphyrin with/without a coordinated pyridine ligand. Complementary results were obtained for the energy-transfer processes in these BCO-bridged porphyrin D–B–A systems with both experimental and theoretical methods. Results highlighted that the singlet energy transfer contribution is relatively similar from both Coulombic (Förster) and through-bond superexchange mechanisms and that the relative contributions do not vary with the D–A distance. The distance-dependence was shown to be approximately exponential for through-bond coupling for singlet energy transfer.

6. Applications of Rigid-Linear Linkers in Molecular Rods and Rotors

Aliphatic rigid linkers are seen throughout material chemistry, from areas such as molecular rods and rotors to metal organic frameworks (MOFs). Molecular rods first became of interest due to their applications in electron and energy transfer studies, their use in liquid crystals and polymer chemistry, as well as for the construction of supramolecular assemblies and giant molecules. Furthermore, in the last decade, the mechanical properties of wheels, vehicles, rotors, and motors have been vigorously studied. Molecular machines and rotors are seen in all living organisms and possess vital roles in many biological processes from cell division, motility and muscle contraction to supporting cellular metabolism, vesicle and neuronal transport, as well as signaling and energy processing in cellular membranes.[245] As a result of the impressive flexibility and efficiency observed in these biological nanomachines, much experimental effort has been invested to develop artificial molecular devices that can be used in areas such as medicine, nanotechnology and material science.

6.1. Rods

6.1.1. Liquid crystals

Liquid crystals (LCs) are largely known for their use in LCDs, namely liquid-crystal displays that are incorporated into many everyday electronic devices such as electric wrist-watches. A nematic LC is a transparent liquid that can cause the polarization of light due to its crystal-like organization, and how much the light is polarized can in turn be modulated through the application of electric current. LCDs are made from nematic, smectic A or C materials. The LC phases are usually comprised of molecules containing a rigid core with flexible substituents to for an extended rod. The mesogenic rigid cores provide the anisotropic interactions, required to form the LC state and are thought to modulate the properties of the materials while the substituents lower the melting point of the molecule.[246]

It is rare that thermotropic LC phases are found in single-ring compounds as they often crystallize before forming a mesophase. But these compounds, especially with simple alkyl substituents, are desirable for their potential to reduce the viscosity of nematic mixtures while not affecting the devices operating range.[247] Additionally, studies with these simplified structures reduce the number of variables so the actual ring effect on mesogenic behavior can be assessed. Simple nonpo-

lar compounds with homostructural cores were employed using the BCO moiety.[246] Previous studies with two-ringed structures showed inconsistencies in their structure–property relationship and it was thought to be due to conformational preferences and intramolecular dynamics of the two-ring compounds taking precedence over the relative sizes of the cores rings.

The dipentyl- and diheptyl-BCO derivatives **193** and **194** were synthesized and studied in the pure state and in binary mixtures with a nematic host and they were found to exhibit a monotropic nematic phase (Figure 25).[246] This the first example of a single-ring hydrocarbon and opens up possibilities to find low-temperature thermotropic phases for other single-ring structures. A comparison of single- and two- ring structures showed that ring stereochemistry might be influencing the stability of the liquid crystals, but further studies are necessary with larger rods to confirm this. 4-pentyl-BCO-1-carboxylic acid was utilized to synthesize these compounds, firstly a lithium–halogen exchange reaction was employed to form the butyl ketone, followed by a reduction to form the desired alkylated product **193**.

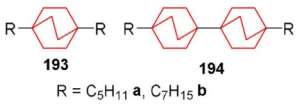

Figure 25. BCO-based liquid crystals.

Previous nematic materials used for LCDs have several undesirable properties associated with them such as coloration and chemical and/or photochemical instability, which are attributed to the central linking unit between the two benzene rings in the compounds, such as cyano-substituted stilbenes and Schiff's bases, azo and azoxy compounds. The removal of these aromatic linking through the replacement of a benzene ring by a cyclohexane ring not only allowed for mesogens with lower melting points, but often they had higher clearing points too.[248] While these results provided a range of stable nematogens of high positive dielectric anisotropy, ever increasing demands require LCs capable of wider ranges in function.[249]

The BCO scaffold had previously been shown to be detrimental to the LC properties.[189] However, a series of mono- and diester BCO molecules displayed higher nematic to isotropic liquid transition temperatures than analogous materials such as phenylene rings and cyclohexane rings (Figure 26).[250] 1,4-Disubstituted-BCOs **195**–**200** were synthesized with three types of ester from BCO carboxylic acids and phenols. This series of LCs provided a new range of colorless, chemically and photochemically stable compounds that consisted of nematic phases with low birefringence and high positive dielectric anisotropy. Friedel–Crafts alkylation reactions were employed to attach the aromatic units to the brominated BCO moiety, followed by a functional interconversion on the brominated aromatic for a cyano group.[251]

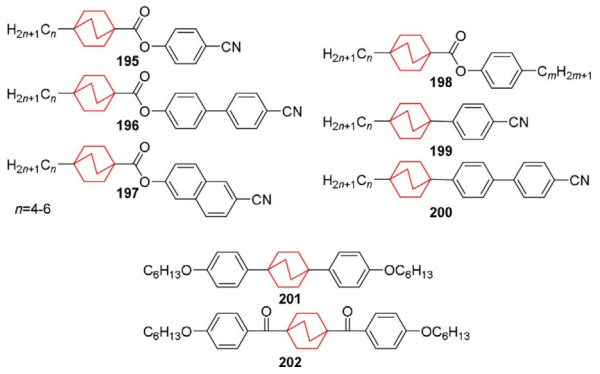

Figure 26. Various BCO-based liquid crystals exhibiting wide-range nematic phases.

A group of 33 4-*n*-alkylphenyl-4-*n*-alkyl-BCO-1-carboxylates **201**–**202** were synthesized and were shown to possess many nematic phases that exist up to high temperatures and have higher clearing points when compared with cyclohexane and benzyl derivatives.[252] Moreover, they exhibited moderate viscosity, low birefringence, and low dielectric anisotropy in the nematic phase. But the most significant features of these ester mixtures with cyanobiphenyls is the sharpness, and low temperature dependence of the threshold voltage, and the low tendency for injected smectic properties. For all BCO derivatives, although the nematic-isotropic transition temperatures (TN-1) may vary for different functional groups, what remains constant is the higher TN-1 values obtained for BCO compared with cyclohexane and benzene analogues.[253]

The relationship between LC stability and molecular conformational effects has been show through empirical data.[254] The data suggests the increased flexibly in the molecule leads to decreased phase stability owing to a lower dynamic aspect ratio and lower packing density in the liquid crystalline phase. These trends can be observed in homologous series, where increased chain length results in decreased clearing temperature for high-temperature materials.[255] A series of isostructural compounds containing *p*-carborane, BCO and benzene were synthesized to investigate the effect that different phenyl/alkyl connecting groups have on the mesogenic properties of LCs using thermal and optical methods.[256] Results showed the order for mesophase stability in the series as (Alk)CH_2CH_2– < (Alk)OOC– < (Alk)CH_2O– < (Alk)COO–. Different tests aimed to distinguish what factor caused the impact of the structural elements BCO, benzene etc. on phase stabilization but none could be identified. Instead, it is proposed that a combination of conformational properties of structural elements, such as their relative sizes, and electronic properties of the benzene ring bearing the substituent, dictate mesogenic properties.

A common way to modulate aromatic cores in LC systems is through fluoro substitution. Fluorine substituents can reduce melting without total elimination of liquid crystal phase due to its small atom size and high electronegativity that modulate the physical properties of the molecule.[257] A variety of linearly-BCO-connected LC were synthesized with fluorine-substituted benzenes incorporated in different positions of the meso-

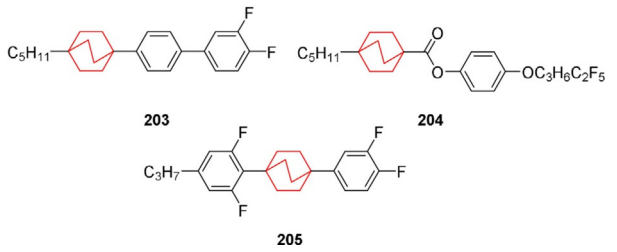

Figure 27. Investigation of the mesogenic and dielectric properties of laterally fluorinated three-ring mesogens.

genic core **203**–**204** (Figure 27).[258–260] Results showed that when fluorine atoms were incorporated at the end or in the middle of the mesogenic core a decrease of melting and clearing point values was observed which either reduced the interval of the mesophase or removed the LC phase completely depending on the location and number of fluorine atoms. Key steps to the synthesis of these compounds involve the reaction of a BCO copper reagent with the iodinated bicyclic aromatic units.

The fluorinated BCO derivative **205** and benzene LCs showed that upon fluorination nematic behavior was eliminated for both compounds while their SmC and SmA phases were enhanced and for the BCO derivative induced SmA, smectic I (SmI) and smectic F (SmF) phases were observed.[258] The key step in the synthesis of compound **205** involved the reaction of the BCO alcohol, 4-(3,4-difluorophenyl)bicyclo[2.2.2]octan-1-ol, with 1,3-difluoro-5-propylbenzene in the presence of H_2SO_4.

The interest to incorporate BCP into LCs first began as it was hypothesized to increase the thermal stability of the mesogen and improve other mechanical properties.[8] Research has shown BCP to contribute to both low- and high-order phases,[261] although in general, thermal stabilities of the liquid-crystalline phases are lower than other analogous compounds. It has also been shown that BCP is far inferior to BCO, benzene and cyclohexane rings at stabilizing nematic phases. This is thought to be due to low rotational barriers and thus high conformational mobility of the bridgehead substituents.[262]

BCP has been attached directly to the other rings such as in **207** and **208**, but also via ester linkages such as in **206** and **209** and ethylene bonds (Figure 28). When directly attached to an aromatic ring BCP compounds behave similarly to BCO analogues albeit with much lower clearing points. Conversely, when connected between two aromatic groups mesophase stability is undermined and only low-transition temperatures are observed.[263] When BCP is connected to the aromatic rings via an ester link the mesogenic properties slightly improves again. On the other hand, when BCP is connected directly to aliphatic substituents **211** or via an ester link **209** relatively high-phase stabilities are observed and almost exclusively in the highly-ordered smectic phases. In order for [*n*]staffanes to exhibit liquid-crystalline phases, a minimum of three BCP units are required,[264] whereas with BCO only one unit is required for the nematic phase and two for the smectic phase[246,265] To further cement BCP unsuitability as a LC component, a comparison between a known polymer was performed with BCP

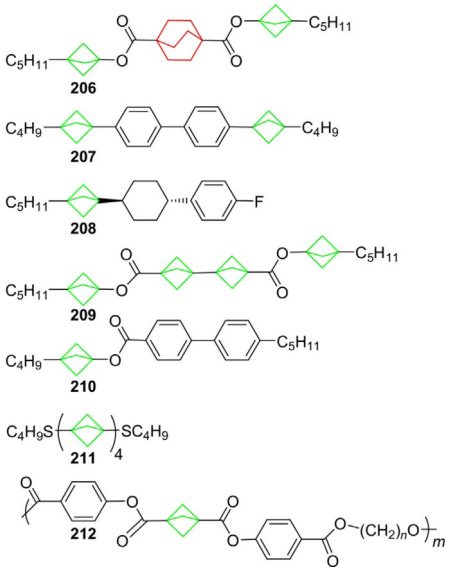

Figure 28. BCP liquid crystals.

212, benzene and cyclohexane derivatives and as expected the BCP analogue showed strong destabilization in the smectic phases and much lower clearing temperatures.[262]

6.1.2. Structural chemistry and crystal engineering

Crystal engineering utilizes intermolecular interactions to construct crystal structures from molecular components into reoccurring patterns; understanding the relationship between molecular structure and crystal structure is imperative for its success. Identification of specific functional groups that allow for predictable and persistent robust synthons is required to reach the target crystal structure. Carboxylic acids are strong donor–acceptor functionalities that allow for hydrogen bonding with other weak donors and acceptor moieties. There are two distinct conformations that occur when carboxylic acid moieties hydrogen bond, notably *syn*-planar or *anti*-planar. As a result of these two conformations, there are four possible ways that functionalities interlink, the most dominant is the *syn-syn* centrosymmetric dimer. The other possible catemers known to form are of the type *syn-syn*, *anti-anti*, and the rare alternating *syn-anti* (Figure 29 a,b).

A series of 4-substituted-1-cubanecarboxylic acids were synthesized with interesting crystallization patterns that indicate their potential for crystal engineering.[266] Within this family of compounds, the unusual catemers of the *syn-anti*-conformation are frequently observed, specifically in the cases for which X = Cl, Br, I, or CO_2Me. The reoccurrence of this rare conformation is attributed to the stabilization between C–H···O and cubanyl C–H bonds caused by the high acidity of the cubanyl protons. In this orientation the halogen atoms can be seen to fill the centrosymmetric voids that are present due to the rest of the packing, thus stabilizing the whole crystal structure. Moreover, when X = CO_2Me cyclic patterns are formed, and in cases for which the substituent is too small that is, X = H, too big, for example, X = Ph, or when it has a specific hydrogen-

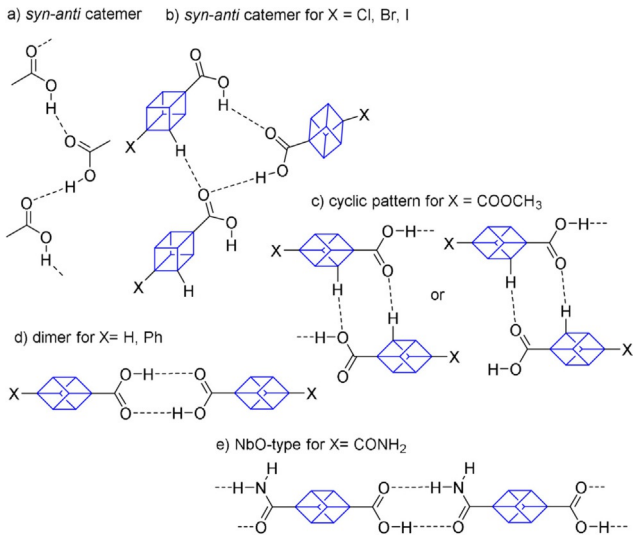

Figure 29. Different hydrogen-bonding interactions for 1,4-substituted cubane carboxylic acids.

bonding preference of its own X = $CONH_2$ the catemer no longer forms and instead dimer formation is seen (Figure 29c–e).

Following this work, an additional study was carried out that further showed how the C–H bond of cubane is activated toward hydrogen-bond formation and its ability to support a crystallographic framework with stabilizing C–H···O bonds.[267] This was demonstrated in an alternative way with a series of primary cubane carboxamides, which investigated the N–H···O hydrogen bonds in amides.[268] The usual motif observed for primary carboxamides is the centrosymmetric dimer with *syn*-oriented N–H groups, similar to the carboxylic acid dimer, while the *anti*-oriented N–H groups form either a linear pattern with or without a glide plane (shallow-glide motif). The motif without the glided plane characteristically has succeeding molecules that are related by 5.1 Å translation (Figure 30a).

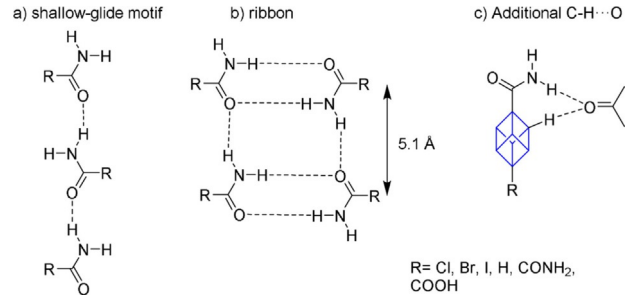

Figure 30. Amide hydrogen-bonding motifs.

When a linear pattern without a glide plan occurs in combination the dimer motif the commonly occurring translational ribbon synthon is formed (Figure 30b). Notably, the primary cubane carboxamides have been shown not to utilize the ribbon motif, because the cubane skeleton is too big for the 5.1 Å translation motif, thus encouraging formation of the less sterically demanding shallow glide conformation. This conformation is further reinforced by the C–H···O hydrogen bond from an acidic cubyl C–H group (Figure 30c). Furthermore, there is an increased ability for cubane to form C–H···H–C bonds, explaining its high melting point. This ability is attributed to the large C–C-H pyramidality angle of the interacting hydrogen atoms present due to the tertiary and restricted nature of the carbon atoms.[269]

Remarkable not only because of its aesthetic curiosity, the structure of fullerene-cubane heteromolecular crystals with C_{60} and C_{70} fullerenes were shown to form high-symmetry molecular crystals with cubane due to the topological molecular recognition that occurs between the complementary surfaces of the fullerene and cubane molecules (Figure 31).[270] These compounds were prepared by evaporating a 1:1 mixture of fullerenes and cubanes. In these crystals static cubane acts as a bearing between the rotating fullerene molecules by occupying the octahedral voids of the face-centered-cubic (*fcc*) structures. The rotation of fullerenes around the static cubane occurs by a "rotor-stator"-phase between 140 and 470 K, whereas below 140 K a phase transition to orthorhombic oriented phase occurs.[271]

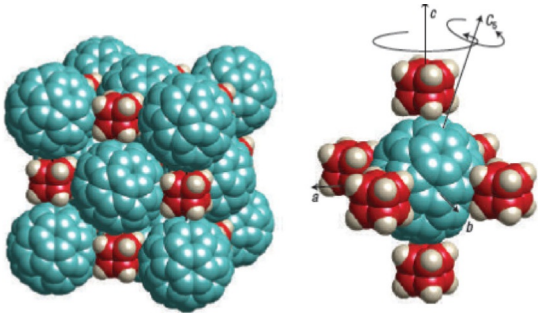

Figure 31. Fullerene–cubane heteromolecular crystals Reproduced with permission from ref. [270]. Copyright Nature Springer 2005.

6.1.3. Other rods

Polymerization of BCP enables access to rigid molecular rods that show restricted rotation along the rod axis. BCP polymers **213–216** can be synthesized using either radical[272,273] or anionic initiators,[274] but also from the unsubstituted [1.1.1]propellane which polymerizes spontaneously. Additionally, Grignard reagents can be coupled via palladium catalysis to produce symmetrically disubstituted [2]staffanes **217**. The success of this homocoupling hinges on the presence of bromomethane, a byproduct from the first step of the BCP synthesis, as it enables the oxidation of Pd to Pd^{II}.[3,275] Another series of different [*n*]staffanes were synthesized with combinations of BCP with BCO **218** and cubane **219** moieties (Figure 32). Substituents were added at the end of the oligomers, such as $-CO_2CH_3$, $-n\text{-}C_4H_9$, $-C_6Hs$, –Br, –I, and $-SCOCH_3$.[273] A comparison was made of these straight rods and spool-like connectors as a molecular-size civil engineering equivalent to a child's

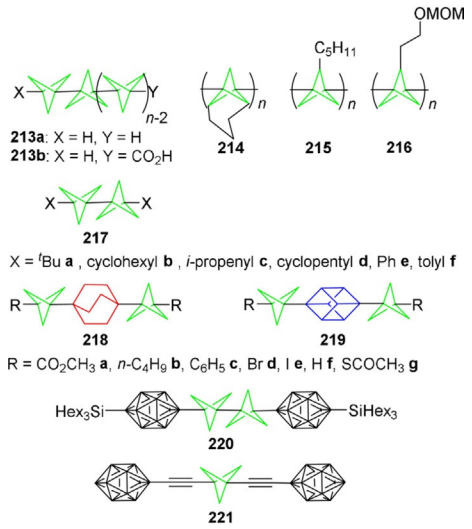

Figure 32. Molecular rods that exhibit restricted rotation along the rod axis.

"Tinkertoy" play set which is essentially a toy construction set. These "mixed" staffanes have approximately equal separations, as BCO and cubane have similar lengths. The use of these moieties in rod structures also enables a 2 Å increment relative to a parent [*n*]staffane so they can also be utilized for rod extension applications. Synthesis of the compounds was initially performed by radical induced oligomerization from the highly reactive tricyclo[1.1.1.0]pentane intermediate with either itself or 1,4-diiodocubane.[60,273] Further methods were developed to symmetrically couple bridgehead-BCP bromides and iodides via the oxidation of bridgehead-cuprates with lithium reagents.[276]

Carborane was also connected to the BCP moiety either directly or via two ethynyl bonds enabling the construction of a new type of rodlike structure **220** and **221**, respectively. Its application as a molecular rotor is also apparent as both cages have free-rotation around the axial-linking bond. Sonogashira methodologies were employed to attach the substituents to 1,3-diethynylBCP to form **221**, overcoming the possible rearrangement of the bicyclopentane cage that occurred in many other cases.[277]

As an expansion of the Tinkertoy tool box, different rods and connectors have been used to construct large molecular structures and connectors. 1,3-diethynyl-BCP has been used to synthesize 1,3,5- and 1,2,4,5-substituted benzene derivatives **222** and **223**, which are linked by BCP to the bipyrimidyl termini, as trigonal or tetragonal connectors for the construction of large molecular structures. Sonogashira methods were employed to link the units in a convergent synthesis (Figure 33).[278]

The synthesis of rodlike molecules was achieved using Kolbe electrolysis enabling a shorter, less labor intensive method to access rigid noncollapsible nanosize spacer units.[279] Kolbe electrolysis works by joining two carboxylic acids bearing alkyl groups in the α-position. Previous examples included only simple alkyl groups, whereas now the method has been expanded to include the highly branched BCO scaffold **224**. Po-

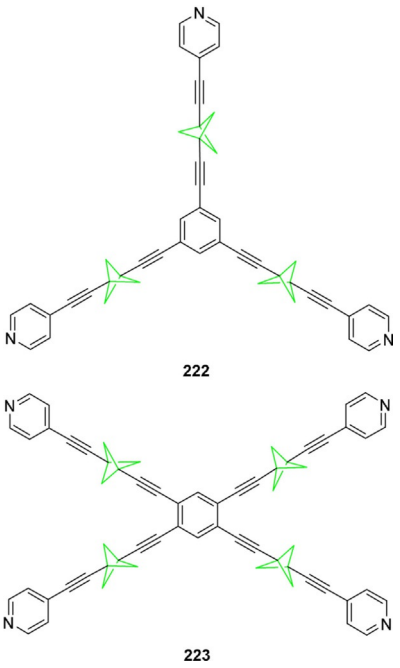

Figure 33. Terminal mono- and bidentate binding sites, star-shaped structures used as trigonal and tetragonal connectors.

tential applications of these rodlike molecules include use as liquid crystals, use in electron-transfer reaction studies, and use as noncollapsible nanosized molecules (Figure 34).

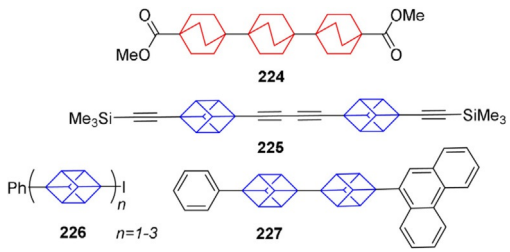

Figure 34. Rodlike molecules with BCO and cubane linkers.

A method for the synthesis of alkynylcubanes was developed to expand currently available nanoarchitectures.[280] Terminal and substituted alkynylcubanes were synthesized through the *n*BuLi-promoted elimination of halogen atoms from 1,1-dibromovinylcubanes followed by quenching with the desired electrophile, while dimerization and cross-coupling reactions of various diethynylcubanes afforded longer rods **225**.

Directly-linked cubane polymers were also synthesized forming rode-like structures with very poor solubility.[62,281] The synthesis was performed with cubyllithium and 1,4-diiodocubane to afford the oligomers **226** through successive halogen-exchange equilibrium reactions. Termination of the reaction occurs with a halogen–metal exchange. The longest rod obtained by this method was 15 Å, in which each cubane contributes ~4.15 Å. The application of this method can be extended by trapping the lithiocubane intermediate with various com-

pounds such as phenanthrene-9,10-epoxide, followed by a dehydration reaction to form the product **227**.

Due it its very rigid 3D structure, cubane offers opportunities to make a variety of new materials, including polymers. The first cubanyl polymer was achieved by the metathesis polymerization of the 1,4-bis(homoallyl)cubane **228**. Addition of Schrock's molybdenum catalyst enabled the production of an oligomer with an average of 6.2 repeat units per chain (Figure 35).[282]

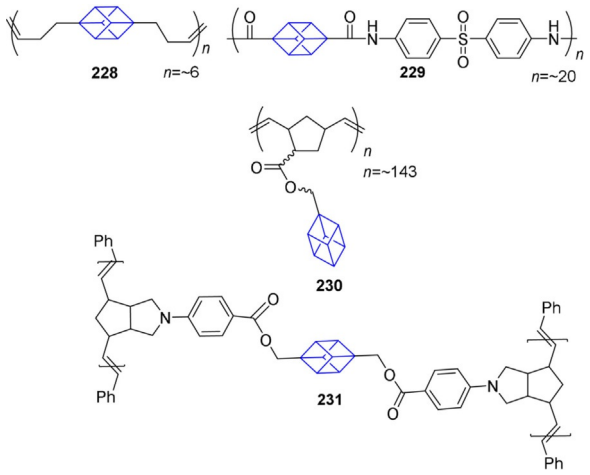

Figure 35. Cubane polymers.

Solubility of these oligomers posed a problem as it inhibited the synthesis of longer length chains. Poor solubility was thought to be due to the hindered free-rotation of the polymer chain because of the steric bulk of cubane, thus leading to the precipitation and premature terminate of the polymerization reaction. Different functionalities were incorporated into the chain to overcome this problem such as amide linkages **229** with aromatic diamines and it was found that chains up to ≈20 units could be obtained.[283] Additionally, tethering cubane to a polymer backbone **230** was carried out to increase its free-rotation and thus increase its entropy and, *in lieu*, its solubility. Ring-opening metathesis polymerization of cubane-tethered norbornene monomers was employed to obtain polymer chains of up to ~143 units.[284]

Polymerization reactions were also employed to synthesize a double-stranded ladderphane **231** containing cubane ester linkers by ring-opening metathesis polymerization (ROMP) of bisnorbornene monomers (Figure 35).[285] The ladderphanes were prepared through self-assembly, forming an ordered pattern similar to that seen in a double-stranded DNA helix.

6.2. Rotors

6.2.1. Molecular rotors

Molecular rotors are described as molecules containing two parts that can easily rotate relative to each other. The parts can either be interlocked such as rotaxanes and catenanes or held together by chemical bonds. The rotator has the smaller moment of inertia while the stator has the largest.

Hexagonal tris(*o*-phenylenedioxy)cyclotriphosphazene (TPP) was employed as a host to investigate the behavior of dipolar rotor assemblies that acted as guests.[286] A variety of different 3,6-disubstituted pyridazines were synthesized including 3,6-bis(3-methylbicyclo[1.1.1]pent-1-yl)-pyridazine **232** (Figure 36). It was seen that the BCP compound formed hexagonal bulk inclusion compounds with TPP and that the in-plane lattice parameters for the hexagonal phases increased with the size of the end group, which in turn controlled the energy barriers for rotation of the pyridazine dipole. Overall it was shown that through a combination of molecular design and optimal positioning of the rotor molecules in the host material, a dramatic lowering of rotational barriers can be achieved. Key steps in the synthesis of **232** included a Grubbs metastasis reaction to connect the two BCP moieties by a double bond. The introduction on the pyridazine ring was achieved by the reaction of hydrazine with the bridging 1,4-diketone moiety, followed by its subsequent aromatization with Pd/C.

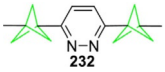

Figure 36. BCP rotor.

Bis{[4-(4-pyridyl)ethynyl]bicyclo[2.2.2]oct-1-yl}buta-1,3-diyne **233** was synthesized containing two 1,4-diethynyl-BCO rotators linked by a diyne fragment (Figure 37). Sonogashira methodologies were employed to link the BCO and pyridine moieties.[287]

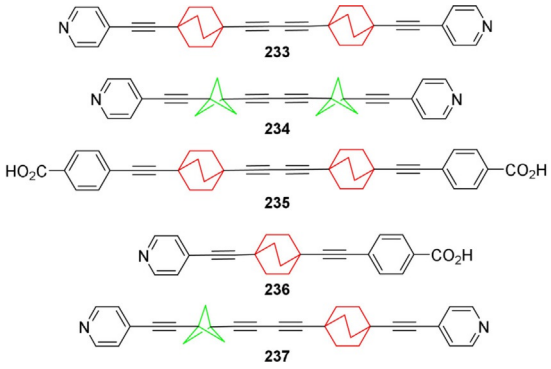

Figure 37. Ethynyl-linked mixed molecular rotors.

Unique features were observed for this compound as it contains two Brownian rotators with different activation energies and as it self assembles into a 1D crystalline array with space inversion symmetry. The dynamic equilibrium of the BCO rotors was investigated and evidence was found showing pairs of adjacent rotors in adjacent molecules rubbing against each other just like two cog wheels that are in direct contact with one another in a microscopic clockwork.

In this polymorph, the motion is highly correlated, whereas, in contrast, another polymorph was observed in which half of the rodlike molecules appear to be shifted with respect to their closest neighbors. This translation disconnects the cog-wheel-like pairs of rotators in the lattice in such a way that

their motion becomes uncorrelated. In both polymorphs, this motion takes place independent of mutations in the preferred rotators and of the "mutamer"-induced second harmonic generation.[288] Remarkably, alternating the speed of crystallization controls which polymorph is formed. Faster recrystallization results in the first polymer while a slower process forms the more thermodynamically stable shifted second polymorph enabling the coglike motion to be switched on and off. A potential application of these molecules includes molecular optomechanical switches.

1,4-Bis{3-[(trimethylsilyl)ethynyl]bicyclo-[1.1.1]pent-1-yl}buta-1,3-diyne **234** was also synthesized in a control experiment utilizing two BCP moieties instead of the two BCO units (Figure 37).[289] The BCP units can rotate but are achiral so produce no second-order optical response. They self-assemble by C–H···N hydrogen bonds in a crystalline array similar to the BCO derivative, but the rotor–rotor interactions are weaker as they do not rub against each other as often so no coglike motion is observed. At thermodynamic equilibrium the same type of correlated gearing motion is occurring for both derivatives, but the BCP derivative has a much smaller difference in energy between the low-energy gearing relaxation process and a higher-energy gear-slipping relaxation process.

As unsymmetric rotators with a 1,4-diethynyl-BCO core are needed for engineering crystalline arrays of functional molecular rotors, new methods to expand and improve the available synthesis with this moiety were investigated.[290] Protecting groups of the acetylene bonds such as carbinol were utilized to give the 2-methyl-3-butyn-2-ol moiety that is desirable for its polar character, ability to sustain orthogonal functionalization and easy removal. This enabled the BCO moiety to be unsymmetrically functionalized to allow for compound **236** and homocoupled by Glaser-coupling methodologies to give compound **235**. Vastly improved yields were obtained with this strategy and a larger diversity of polyrotors has been made available. The mixed rotor **237** was synthesized using Sonogashira methodologies to expand the library of asymmetrically substituted BCO derivatives. The key step to connect the BCP and BCO units employed Cadiot–Chodkiewicz cross-coupling.[291]

Initially bis(9-triptycenyl)X-type molecules were investigated for their use in dynamic gearing. The triptycene moieties are connected by single atoms/groups (X = CH_2, NH, O, SiH_2, Ph, S) producing nonlinear compounds. While these compounds are outside the scope of this review, they are some of the first examples of compounds in this class. It was seen that the barrier heights for gear slipping are dependent on the connecting X group.[292] Following this, the use of three consecutive bonds was investigated to see if the angle and/or distance between the two 9-triptycenyl groups would vary significantly, effecting the tightness of gearing in these systems. A *cis*-vinylene group was employed as the connecting group to synthesize *cis*-1,2-bis(9-triptycenyl)ethylene **239** through the hydrogenation of a ethynyl linker **238** (Figure 38).[293]

Work with molecular machines was first pioneered and developed by Jean-Pierre Sauvage, Sir J. Fraser Stoddart, and Bernard L. Feringa, who were awarded the 2016 Nobel prize *"for the design and synthesis of molecular machines"*.[294] The interest in functional molecular machines first began in the nineties when the real time rotation of an ATP synthase macromolecular motor was observed.[295] The synthetic aim of this field of study involves the synthesis of miniature man-made mechanical devices on the nanoscale. For this to be successful the motions of the molecular machine must be controllable, the surface the molecule is on must be suitable as must the external stimuli that is necessary to provide the energy for movement.[296]

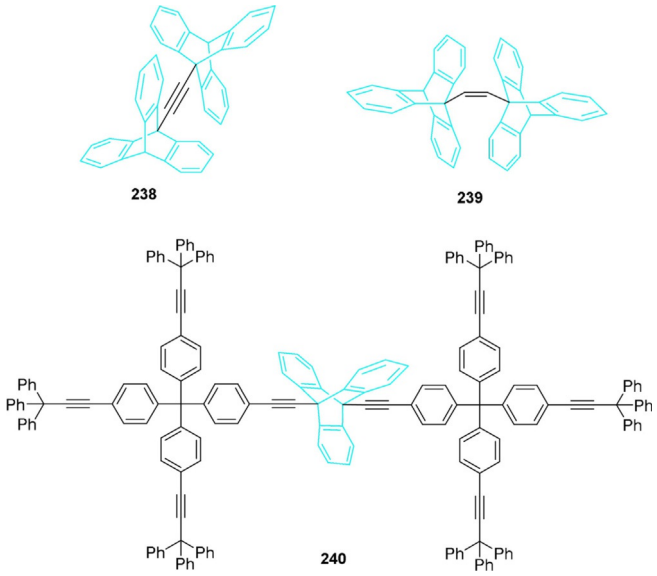

Figure 38. Triptycene rotors.

A solid-state molecular rotor with a large triptycene rotator **240** was synthesized, up to three times larger than previous phenylene rotators (Figure 38).[297] This expanded triptycene rotator was found to be functional due to its volume conserving system. Experiments revealed that mechanical functions in solids can be attained for larger molecules by suitable molecular design. The key step in the synthesis was a Diels–Alder reaction with benzyne and functionalized 9,10-diethynylanthracene to form the triptycene moiety followed by deprotection of the ethynyl protons and Sonogashira reactions to give **240**.

A series of molecular machines have been synthesized that employ triptycene as the molecular wheels with various aromatic and unsaturated backbone connectors, for example, triptycene with a butadiyne linker **241** (Figure 39). A macroscopic wheelbarrow **242** was synthesized with triptycene wheels that theoretically could rotate in the same direction, with a large polycyclic aromatic backbone, two 3,5-di-*tert*-butylphenyl 'legs', and two 4-*tert*-butylphenyl 'handles' that underwent manipulation with the tip of the microscope.[298] Attached to a Cu(100) surface, unfortunately, no lateral motion of the wheelbarrow was observed upon stimulation with the STM tip due to the aromatic rings of triptycene strongly physisorbing by parallelization to the metal surface causing deformation. The synthesis of this molecule involved multiple Knoevenagel-Diels–Alder reaction sequences with an α-diketo fragment to build the dibenzopyracene chassis. The triptycene moieties

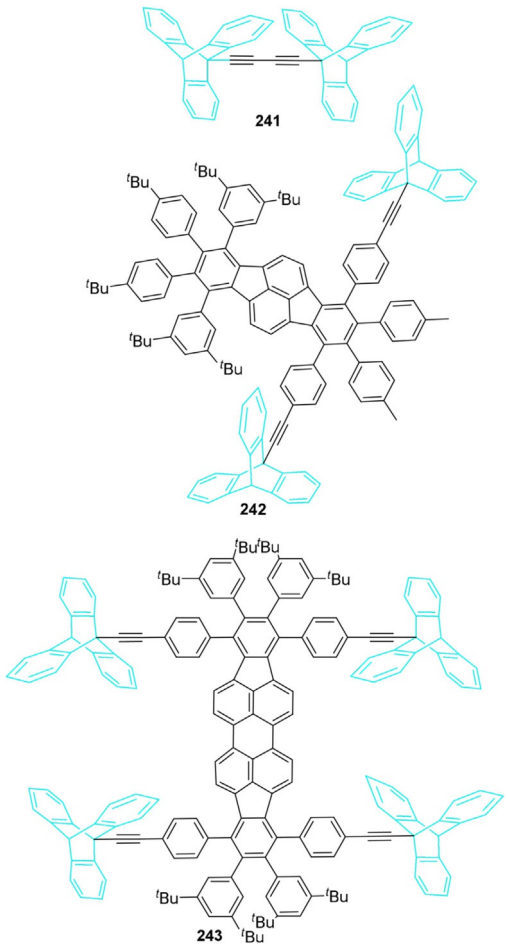

Figure 39. Molecular machines with triptycene wheels.

were attached in the last step using classic Sonogashira conditions.

Triptycene enables the entire functionalized molecule to move easily on the surface by its rolling motion. System **243** was the first ever synthesized nanovehicle, with the two triptycene wheels linked along a butadiyne axel, that enabled the molecule to have almost free-rotation and maintained a linear geometry.[71,300] Synthesized over three steps from 9-bromoanthracene, 9-ethynyltriptycene was then dimerized using Glaser-Hay methods to give the diethynyltriptycene wheel dimer.[299] The molecule was sublimed onto a Cu(110) surface and wheel rotation was induced and observed for the first time using a STM tip. Typically, only one triptycene wheel was observed moving while the other stayed stationary, so further molecules were investigated to see if both wheels could simultaneously be activated.

The molecular rotor **244** was synthesized in crystalline arrays with a 1,4-diethynyl-BCO core that acts as a neutral, soluble spacer for the design of halogen-bonded metallic conductors and superconductors.[301] It was found that the dynamics of the system was affected by the environment it was in, which induced phase transitions (Figure 40). 1,4-Bis[(2,4,6-trifluoro-3,5-diiodophenyl)ethynyl]BCO **244**, synthesized by Sonogashira methodologies, changes back and forth across a reversible

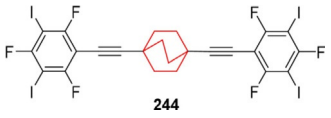

Figure 40. A crystalline rotor.

transition at 145 K. The switching mechanism of the rotational barriers and the frequency of associated rotational motion in this system were investigated through the deliberate use of halogen- and hydrogen-bonding. Observations showed that the reversible change is caused by a squeezing of the rotators' $C–H_{rotator}\cdots I_{stator}$ hydrogen bond cloud across the $C–I_{stator}\cdots I_{stator}–C$ halogen bond. Moreover, second-harmonic generation from this material has been observed, showing the advantages of using polarized light to probe the torsional degree of freedom of chiral helix blades, in addition to symmetry and dimensionality of large collections of chiral rotors in the solid state.

6.2.2. Molecular gyroscopes

There is a growing need for organic materials that have tunable transmittance, refraction, polarization, and color for use in communication technologies. While current research in this area originates from polymer and liquid crystal chemistry, a new concept has emerged in which photonics materials are constructed using dipolar units that can reorient rapidly under the influence of electric, magnetic, and optical stimuli. These new molecular architectures are expected to function similarly to macroscopic compasses and gyroscopes.

A facile synthesis has been developed for molecular rotors made up of ethynyltriptycenes linked together by various aromatic groups such as 1,4-phenylene **245 a**, 1,4-biphenyl **245 b**, 9,10-anthracenylene **245 c**, and 2,7-pyrenylene **245 d** (Figure 41).[302] The dibromoarenes are coupled with ethynyl triptycenes through Sonogashira reactions. Semiempirical calculations were conducted on these materials with the AM1 method and results suggested that an essentially frictionless rotation about triptycene–alkyne and aryl–alkyne single bonds

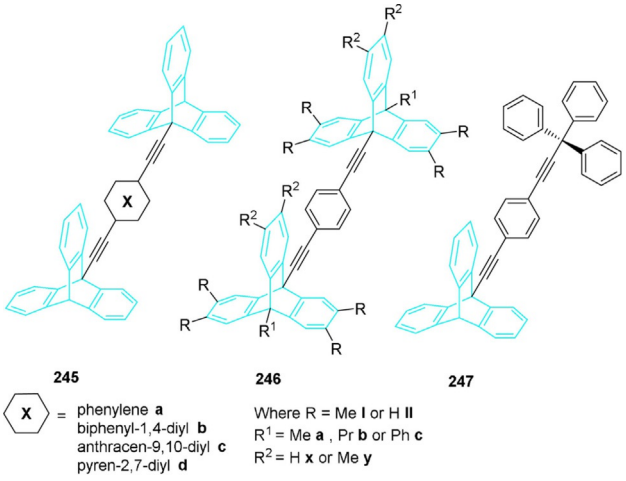

Figure 41. Molecular compasses and gyroscopes.

should be occurring in gas phase. Rapid rotation was also observed also in the solution phase from a dynamically averaged ^{1}H and ^{13}C NMR spectra.

A convergent synthesis was reported to prepare molecular gyroscopes in which *para*-phenylene rotors linked by triple bonds to methyl-substituted triptycenes act as pivots and encapsulating frames. 1,4-Bis[2-(2,3,6,7,12,13-hexamethyl-10-alkyl-9-triptycenyl)ethynyl]benzenes **246** were prepared from 2,3-dimethyl-1,3-butadiene by using Diels–Alder cycloaddition and a Sonogashira reactions to attach the three units. Different triptycenes with methyl, propyl, and benzene substituents at the bridgehead C10-position were employed to synthesize a variety of molecular gyroscopes. The best results were observed with small methyl and propyl electron donating substituents at C10 over the larger benzene group. Also, results suggest for free movement around the phenylene axis to occur as low as 100 K, illustrating a relatively efficient gyroscopic motion.[303] To further improve upon the solubility and dynamic properties of the 1,4-phenylene linked triptycene molecular gyroscopes the unsymmetric triptycenyl-trityl stator **247** was prepared. This compound retains the relatively high melting point of the two symmetric structures, while achieving the other aforementioned properties. The unsymmetric molecule was synthesized again through the use of Pd^{0}-catalyzed cross-coupling with 1,4-diiodobenzene.[304]

The target of amphidynamic crystals (otherwise known as molecular gyroscopes) is to obtain a molecule that rotates close to its moment of inertia. A molecular rotor with a high symmetry order was synthesized with a BCO rotator linked to rigid mestranol fragments.[305,306] The compound was synthesized in a one-pot, three-step coupling reaction between 1,4-diethynyl-BCO and mestrone with perfect diastereoselectivity and good overall yields. Isomorphous crystals were formed with the benzene derivative of **248**, but were not observed for the BCO rotator due to disorder in the packing (Figure 42).

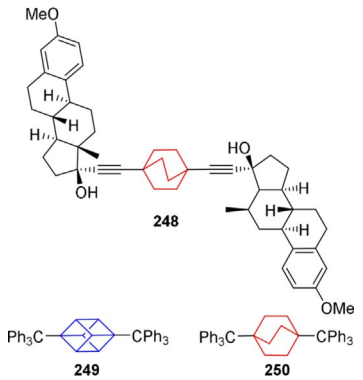

Figure 42. Amphidynamic crystals of molecular rotors.

NMR experiments showed that the BCO has a relatively low activation energy barrier allowing it to achieve a high average site exchange rate at ambient temperatures which is notable due to the large size of BCO. These results suggest the applicability of BCO derivatives in ultrafast responsive materials and molecular machines based on amphidynamic crystals with inertial rotors.

Amphidynamic crystals have strong translational interactions that are separate from internal rotational motions which are thermally activated in the solid-state.[307,308] The role of intramolecular interactions, vibrations, coupling, and flexibility of different segments were investigated using extensive rigid-body molecular dynamics simulations and simple phenomenological arguments. Cubane **249** and BCO **250** analogues with 1,4-trityl substitutions were model systems (Figure 42).[309] Results suggest that the flexibility and size of a molecular rotor, alongside intramolecular interactions within the rotator and stator, strongly affect their crystal packing structure, energies and rotational behavior. Ordered crystalline phases that have specified free volume for rotations of the central group are seen when there are strong interactions are present in the stator segments. Increased flexibility in the stator leads to increased disorder in the system, drastically affecting rotational dynamics due to increased interactions with the local environment. Furthermore, the theoretical results obtained correlate with experimental data that suggested that rotational barriers are generally larger for less symmetric rotator groups and that electrostatic effects might be not very important.

6.2.3. Molecular gears

6.2.3.1. Molecular spur gears

The correlated motion of macroscopic mechanical devices can be mimicked on the microscopic level through designed molecular gears that consist of two or more rotators in one molecule. The most widely synthesized gears are spur gears which hold the two rotors parallel to one another at the axes and have straight-teeth relative to the axes. For a gearing mimic to be successful, it is essential to have the gear axes mounted on a rigid base in the same direction. Triptycene is a popular choice for molecular gearing due to its D_{3h} symmetry, a resemblance to a macroscopic gearwheel.

9-(2-Indenyl)-triptycene was dimerized to investigate whether the free-rotation around the indenyl-triptycene bond that occurs in the monomer could be affected or inhibited.[310] The sterically congested size and shape of the dimer **251** determined the orientation of the triptycene blades (Figure 43). In the solid state, the *C2*-symmetry of the whole molecule is broken due to the intermeshing of the pairs of triple paddlewheels and rotation is restricted. In solution *C2*-symmetry is restored, as seen by the gear-like rapid contra-rotation of the triptycene paddlewheels when it is dissolved. The racemic dimer 2,2′-bis(9-triptycenyl)-1,1′-biindenyl **251** was formed through the lithiation and subsequent oxidation of 9-(2-indenyl)triptycene.

Spur gears were synthesized with either an anthracene **252** or naphthalene **253** base and two triptycene rotors connected by two acetylene shafts to diminish steric interactions between the two moieties. These molecular structures were compared to investigate the orientation of the two gear shafts and the meshing of rotor moieties.[311] Results showed that tuning the orientation of the two rotors was possible by varying the base

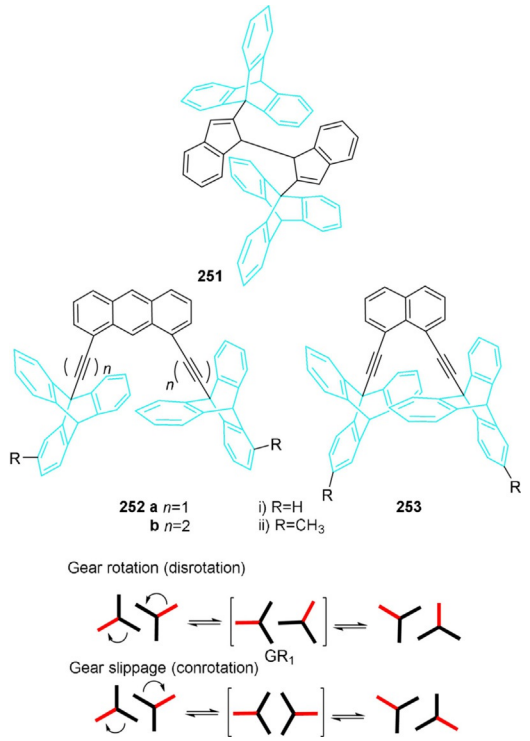

Figure 43. Triptycenyl spur gears.

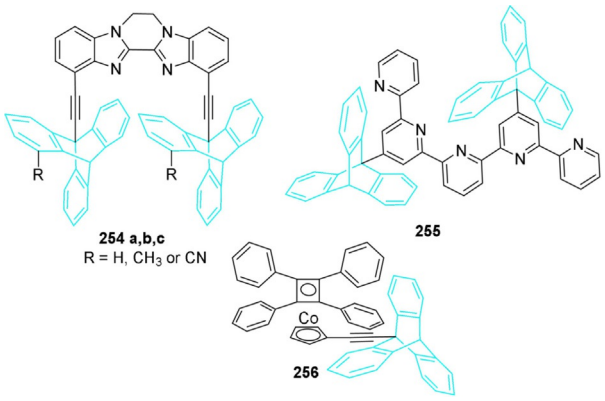

Figure 44. Triptycenyl spur gears with nitrogen-aromatic linkers and a metallocene molecular gear.

component, and that the best system was achieved with the anthracene base **252**. There are two mechanisms of rotation possible when two triptycene rotors are connected in a spur gear. Firstly, the desired gear rotation can occur when the two wheels rotate in opposite directions, causing the "cogs" to turn. In the second mechanism, gear slippage is seen when conrotation is observed, that is, rotation of the wheels in the same direction causing the cogs to not interact. DFT calculations showed that the optimum transition state for geared rotation is structure **GR1** where the barrier to gear slippage is higher making gear rotation the preferred mechanism. Keys steps in the synthesis involved Sonogashira coupling of 9-ethynyltriptycene with the corresponding diiodoacenes.

The gearing behavior of two parallel triptycene groups was further investigated using derivatives of 4,4-bis(triptycen-9-ylethynyl)bisbenzimidazole, including the first desymmetrized spur gear **254** (Figure 44).[312] DFT calculations were employed that showed a preference for geared rotation over gear slippage. Key steps in the synthesis involved a Sonogashira reaction to attach the acetylene triptycenes to 4,4-dibromo-2,2-bisbenzimidazole (BBI) and treatment of the free BBI nitrogen atoms with excess 1-bromo-2-chloroethane to form the six-membered ring.

The linear quinquepyridine (QPY) foldamer was connected to two triptycene molecules at the second and fourth pyridine rings (in order to reversibly control the gearing system) forming a molecular spur gear **255** (Figure 44).[313] Control was established by the complexation and decomplexation of Ag^{I} to the pyridine ligands. Upon complexation with a metal, mononuclear helical complexes are formed preventing the rotation of the triptycene ligands. The linear-to-helical conformational switching, which is triggered by complexation/decomplexation, thus enables reversible control the intermeshed and demeshed states. Key steps in the synthesis include a Diels–Alder reaction with a functionalized anthracene to form the triptycene unit, an aldol condensation to attach an acceptor substituted olefin to the triptycene which was then converted to the final product **255** through reaction with 2,6-diacetylpyridine.

The air-stable (9-triptycenylethynylcyclopentadienyl)(tetraphenylcyclobutadiene)cobalt complex **256** was synthesized as the first example of a metallocene-containing molecular gear, in an effort to expand the number of teeth in the system over the commonly used 3-toothed bitriptycene systems.[314] Additionally, this is an example of a molecular gear employing non-equal gearing ratios. There is a low energy barrier to rotation about the metal fragment in the complex and it is described as analogous to a low friction ball-bearing. ^{1}H NMR studies were carried out on the system and, although independent rotation of the individual triptycene and metallocene rotors cannot be quantifiably ruled out, it is strongly supported due to results from previous studies that show bridgehead-substituted triptycenes to have a very high threefold torsional barrier.[315] Thus, it can be deduced that in order to avoid free-rotation a low energy-correlated gearing mechanism between the two intermeshing cogs of the four and three toothed metallocene gear is occurring. The cobalt complex **256** was synthesized from sodium carbomethoxy-cyclopentadienylide and key steps in the synthesis include a cross-coupling reaction with 9-iodoanthracene and a cycloaddition reaction with benzyne.

6.2.3.2. Molecular multigear systems

A cyclic multigear system **257** was synthesized with four 9,10-triptycene units connected to four 1,2-phenylene units via ethynyl linkers. This macrocycle was achieved through successive Sonogashira reactions with 9,10-diethynyltriptycene derivatives and diiodobenzene. DFT calculations showed the triptycene units to be intermeshed with one another via π···π and CH···π interactions. Despite this, all triptycene units in the tetramer rotated in a correlated and frictionless manner, regardless

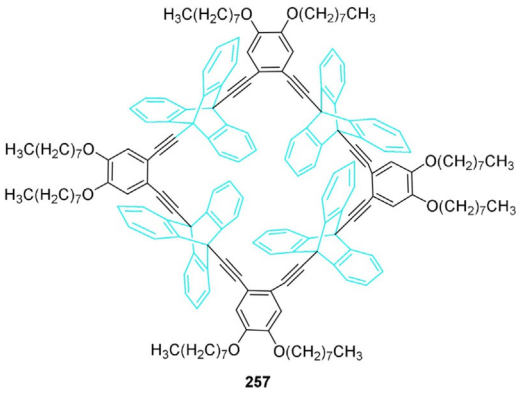

Figure 45. Quadruple triptycene gears.

of the continuous interactions between the gear units. ^{1}H NMR showed rapid rotation of the system, even at low temperatures (Figure 45).[316]

6.2.3.3. Molecular turnstiles

A family of metal-mediated molecular turnstiles **258** was synthesized with various methyl-substituted triptycene rotors connected to two stators with pyridyl binding sites (Figure 46).[317]

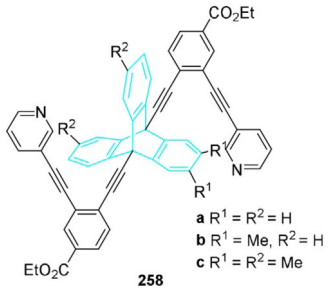

Figure 46. Molecular turnstiles regulated by metal ions.

The methyl groups were introduced into the triptycene rotor to investigate the effect that increased rotor size has on the closed-state formation. In addition, metal-ion coordination was investigated for close-state formation. It was observed that free-rotation occurs in the system at room temperature but in the presence of either Pd^{2+} or Ag^{+} rotation is restricted, by metal coordination at the pyridyl sites. The closed-state of the system is only observed at reduced temperatures upon Ag^{+} coordination showing that it is the binding of metal ions to the pyridyl group that determines the closed-state not the size of the rotor. In this manner the bistability of molecular turnstiles can be regulated allowing for potential applications in the construction of functional molecular devices.

6.2.3.4. Molecular brake and ratchet

The operation of machines is governed mainly by brakes and motors, whether they are man-made, such as vehicles and appliances, or from nature such as muscles and flagellae. For example, in a vehicle the ability to stop by the use of a brake is often as important as acceleration. On the molecular level, spontaneous free-rotation around a single bond is continuous. By reversibly coordinating a metal to a designed compound at a remote site, a conformational change occurs in the molecule restricting movement around the single bond, thus functioning as a molecular brake.

Triptycene has been shown to function as a three-toothed gear in the compound **259** (Figure 47).[318] It spins rapidly around the bridgehead C–C bond that connects it with the dipyridyl moiety. Upon coordination of a Hg^{2+} ion to the dipyridyl moiety, the free-rotation around this bond is inhibited, enabling it to act as a braking system in the molecule **259 a**. The complex was accessed easily through two palladium-catalyzed biaryl coupling reactions, the first to attach the two pyridine moieties and the second a Stille coupling with 9-(Me_3Sn)anthracene. The final reaction to form the triptycene scaffold involved a cycloaddition reaction with benzyne.

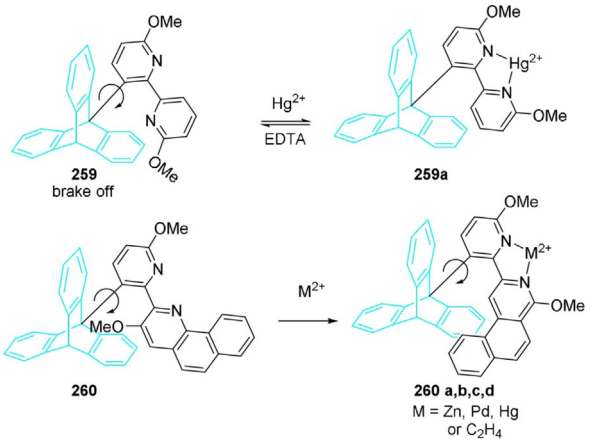

Figure 47. Ion-regulated molecular brake.

The longer triply-fused pyridine arene unit was also investigated for its use as a molecular brake **260**.[319] Observations showed that upon coordination of Hg^{2+}, Zn^{2+}, and Pd^{2+} ions, or even upon covalently bonding the two nitrogen units together by a two-carbon bridge **260 a**–**d**, rotation was still observed in the system, even at temperatures as low as −120 °C. An analogy for what is happening in this system was suggested to be similar to a fastening a playing card to a child's bike and the card becoming continuously dislodged by each passing spoke.

A device that only allows rotation in one direction is commonly known as a ratchet. The most basic components of a ratchet consist of a toothed ratchet wheel, a pawl to enforce unidirectional rotation of the ratchet wheel, and a spring that holds the pawl in place. Triptycene substituted with a helicene such as in **261** was investigated for its use as a molecular ratchet (Figure 48).[320] The triptycene acts as the ratchet wheel while the helicene is used as the pawl and spring. At room temperature rotation is frozen around the triptycene/helicene

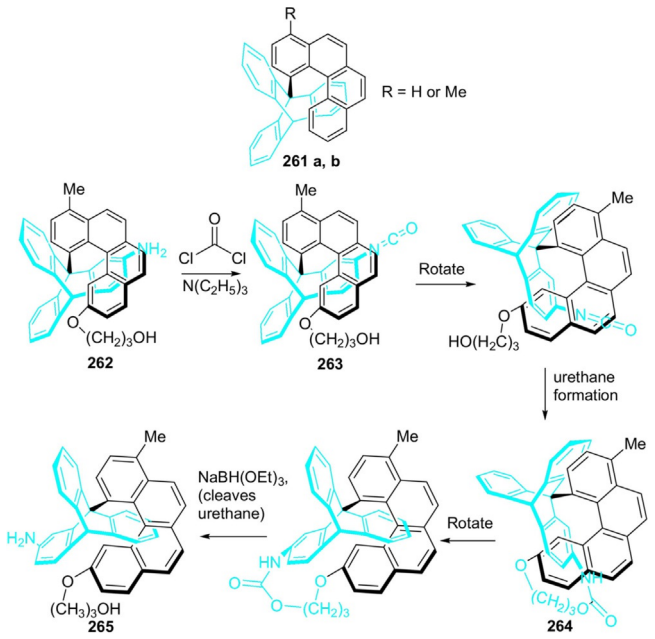

Figure 48. Covalent regulated molecular brake.

single bond. The molecule uses chemical energy to activate rotation and a thermally induced isomerization reaction to achieve unidirectional intramolecular rotary motion. When R = H there is a plane of symmetry in the molecule **261 a**, preventing it to function as a unidirectional ratchet. While when R = Me **261 b** symmetry is broken in the system but NMR studies indicated that the triptycene rotates equally in both directions. The helicene where R = H is more seen as a friction brake that inhibits, but does not completely prevent, spontaneous rotation of the triptycene. Continuing the friction braking action is required to fully prevent anticlockwise rotation.

Theoretically unidirectional motion is achieved by reversibly introducing a tether between the two units to energetically favor one of the two possible rotation directions. To make the triptycene/helicene molecule suitable for use as a molecular ratchet, modifications were made to each unit. An amino group was added to triptycene and an oxypropan-1-ol unit was added to the tip of the helicene unit (Figure 48).[321] When carbonyl dichloride is added to a solution of **262**, the chemical energy provided lowers the energy barrier of clockwise rotation thereby increasing its likelihood of occurring. This unidirectional rotation is ultimately caused by the asymmetric skew of the helicene coupled with monosubstituted triptycene, producing nonidentical energy surfaces for clockwise and anticlockwise rotation. To synthesize **262** palladium cross-coupling was implemented, anthracene was functionalized at the 9-position with a benzaldehyde derivative, a cycloaddition reaction with benzyne and the anthracene produced the triptycene unit, followed by a Horner–Wittig reaction then to afford the "helicene" unit.

Internal rotations can be induced chemically or photochemically resulting in unidirectional rotations and controlled molecular brakes or gyroscopes. This phenomenon can ultimately be utilized for molecular machines or switches. An organometallic molecular brake was designed where protonation of [{η^6-2-(9-triptycenyl)indene}$Cr(CO)_3$] **266 a** notably increased the barrier of rotation of the triptycene paddlewheel by causing a haptotropic migration ($\eta^6 \rightarrow \eta^5$) of the bulky metal carbonyl fragment onto the adjacent five-membered ring (Figure 49).[322] Deprotonation reversed this process. 9-(3-Indenyl)anthracene was synthesized using Heck conditions to couple indene with 9-bromoanthracene; the triptycene product was achieved through a Diels–Alder reaction with benzyne.

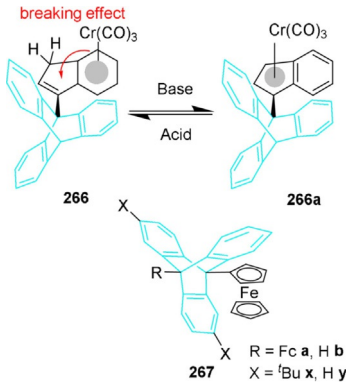

Figure 49. A ferrocenyl kaleidoscope.

An electrochemically driven redox approach was then investigated aiming at more widespread applicability. 9-Ferrocenyltriptycene **267 by** and 9,10-diferrocenyltriptycene **267 ay** were synthesized. Results showed that the diferrocenyl species exists as slowly interconverting *meso* and racemic rotamers that occur in a stepwise manner suggesting its suitability for use as a molecular dial, as they can rotate only one position at a time. The different forms of the rotamer are temperature-independent implying that they are energetically equivalent.[323] To expand upon these results the triptycene moieties were functionalized with di-*tert*-butyl groups affording 2,6-di-*tert*-butyl-9,10-diferrocenyltriptycene **267 ax**, breaking the threefold symmetry of the triptycenyl framework. This was achieved through the cycloaddition of benzyne to 9,10-diferrocenyl-2,6-di-*tert*-butylanthracene. Results showed six slowly interconverting rotamers in solution that are almost equivalent in energy. Steric interactions of the *tert*-butyl groups were shown to control the barriers between rotamers.[324]

6.2.4. Metalorganic frameworks (MOFs)

Metal–organic frameworks (MOFs) have a wide range of applications from gas storage and sensors, to catalysis and medicine. Made from combinations of metallic clusters and organic linkers, MOFs offer tunable pore sizes that can accommodate a range of different-sized molecules, from small molecular hydrogen to larger molecules such as proteins.[325] In particular, MOFs with small pore sizes can incorporate certain molecules without the need for intermolecular interactions between the guest species. In contrast, the majority of MOFs require functional groups capable, mainly, of hydrogen bonding in order

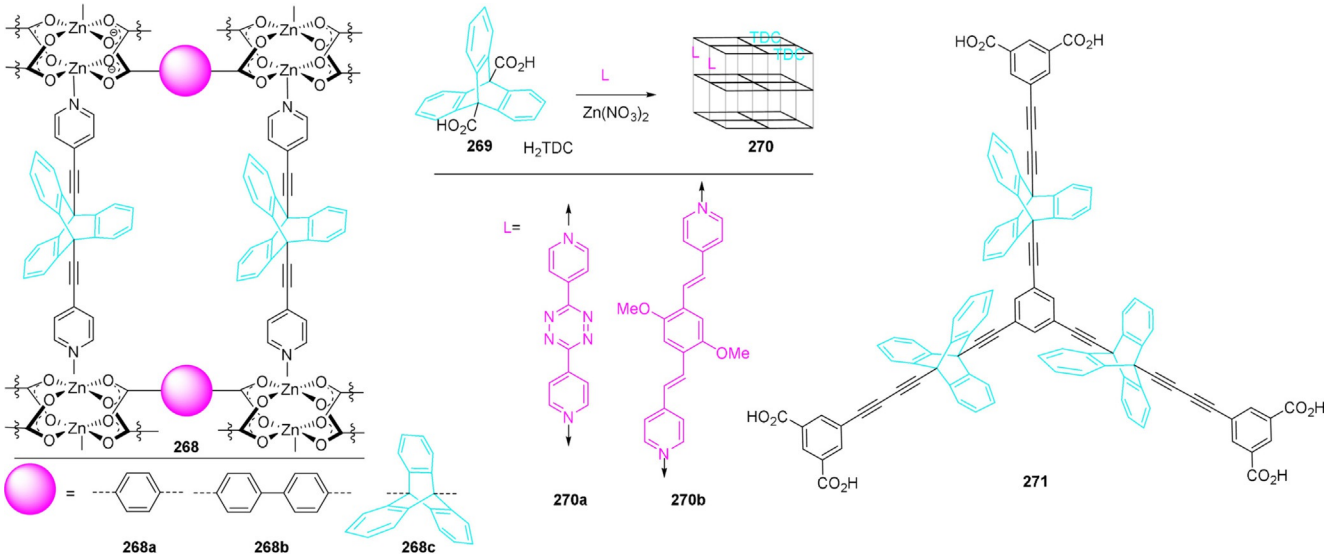

Figure 50. Triptycene-based MOFs.

to encapsulate the desired molecules.[326] Rigid organic ligands, usually those containing aromatic units or spacers, are employed in the construction of MOFs, although, as is outlined in this section, rigid-aliphatic linkers can also be implemented.[327]

MOFs can be utilized in the pursuit of potential artificial molecular machines. A set of pillared paddlewheel MOFs were prepared containing 9,10-bis(4-pyridylethynyl)triptycene with the purpose to act simultaneously as a pillar and molecular rotator **268**, three axially substituted dicarboxylate linkers of varying lengths and steric bulk were also employed (Figure 50).[328] Changing the linker from benzene to a biphenyl and then a triptycene moiety, **268 a**, **268 b**, and **268 c**, showed 2-fold, 4-fold, and no catenation, respectively, when crystalized from DMF, in correlation to the amount of space available in their 2D frames. Tight packing is observed for the two catenated structures while the triptycene derivative shows no contacts between pillars and linkers in the lattice. Rotation is occurring in this compound via a Brownian three-fold jumping mechanism and, as there are no steric interactions in this molecule, it is suggested that the confined DMF molecules in the lattice cause the rotation. A hydrodynamic model was used to estimate a four orders of magnitude greater viscosity of the DMF MOF compared with that of the bulk liquid and this has been compared to the consistency of honey. The viscosity changes allow an opportunity to analyze the dynamics of fluids under tight confinement at variable temperatures.

(Triptycenedicarboxylato)zinc MOFs **270** were prepared and constructed with paddle wheel secondary building units containing different axial ligands.[329] 3D frameworks were made by a pillaring approach as triptycene paddlewheels **269** reliably form layers with zinc nitrate. By employing different ligands, such as bis(4-pyridyl)-*s*-tetrazine **270 a** and bis(4-pyridyl)-dimethoxy-*p*-phenylenedivinylene **270 b**, the functionalities of the MOFs were modified. Guest-exchange behavior, microporosity, luminescence, and stability were investigated for these MOFs. In was seen that the presence of 2D triptycene allowed for the reliable formation of the 3D MOF whereas interpenetrated 3D frameworks have a tendency to form in other rodlike pillaring ligands such as those containing bipyridine in terephthalates.[330] Potential applications of this MOF include uses in the field of sensing and energy transfer on the micro- and nanoscales in fluid media.

A 1,3,5-trisubstituted benzene was coupled with triptycene to incorporate rigid arms with two carboxylic acid moieties at the end of the chain. A MOF **271** was then created by complexing the triptycene system with CuO.[331] This complex was studied computationally to investigate the effect triptycene has on methane adsorption properties. Calculations of methane adsorption properties were performed with Grand Canonical Monte Carlo simulations and showed favorable results when compared to known MOFs of a similar structure and topology. It was showed that the methane adsorption uptake was significantly enhanced on a volumetric basis with this complex **271**.

Terephthalic acid is one of the most commonly reported spacers in MOF constructions, although it has several drawbacks, such as solid-state transparency only between 350 and 800 nm. To extend transparency in the UV domain (below 320 nm) BCO **124** was employed as a terephthalic acid replacement in a MOF construction **272 a** along with Zn^{II} as both are expected to have a higher transparency (Figure 51 i and ii).[327] A classic MOF-5,10 was prepared, with BCO **124** instead of terephthalic acid, and Zn_4O clusters that arranged the moieties into a cubic network with BCO **124** on the edges and the zinc cluster on the vertices. The BCO moiety was found to retain the rigidity of the structure while removing aromaticity, thus increasing transparency, making it highly suitable for the preparation of transparent metal–organic frameworks (TMOFs). The TMOF was synthesized with high reproducibility, a good yield, and was formed by self-assembly.

The density functional based tight-binding method was used to compute the properties of an isoreticular series of

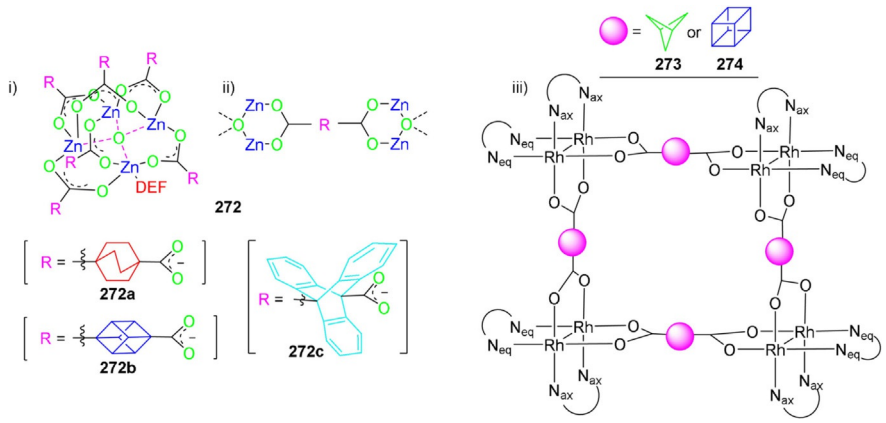

Figure 51. Towards a "transparent MOF" showing, metal-view (i) and ligand-view (ii). DEF = *N*,*N*′-diethylformamide. View of molecular tunnel formation (iii). N_{ax} = axial nitrogen atoms; N_{eq} = equatorial nitrogen atoms.

metal–organic frameworks (IRMOFs).[332] Again, Zn_4O clusters are arranged in a cubic network composed this time of cubane-1,4-dicarboxylic acid **36** or triptycene-9,10-dicarboxylic acid **269** on the edges and the metal cluster on the vertices forming **272b** and **272c** (Figure 51 i and ii). Results showed all MOFs to be energetically stable semiconductors or insulators and that unsymmetric linkers caused marked distortions in the zinc-oxo carboxylato rings while symmetric linkers show little or no influence on the geometry.

Atomic charges with similar values are observed for the free building blocks and the solid MOFs, except those seen with linking oxygen atoms as they change when going from the free linker to the MOF. This knowledge could allow for the creation of materials for hydrogen storage and optical applications amongst other applications.

Layered double hydroxides (LDHs) are a class of claylike anionic nanoscale minerals consisting of $[Mg(OH)_2]$-like layers in which trivalent ions have replaced ordinarily divalent cations to form positively charged sheets.[333] A cubane MOF was constructed when cubane-1,4-dicarboxylate (cubane-dc) anions were incorporated into a Zn_2Al LDH inorganic host. This was achieved through means of the coprecipitation method, with solutions of Zn^{II} and Al^{III} nitrate salts and an alkaline solution of cubane-dc. DOS calculations computed with the DFT method and the molecular orbital models showed a redshift in the spectrum of the large intercalated cubane-dc anions with a subsequent lower band energy gap than that of Zn-Al-NO_3-LDH, which is a much smaller anion.[334]

The singly metal–metal-bonded complex $[Rh_2(cis\text{-}DAniF)_2(CH_3CN_{eq})_4(CH_3CN_{ax})_2](BF_4)_2$ (DAniF = *N*,*N*′-di-*p*-anisylformamidinate) was assembled with $(Et_4N^+)_2(Carb^{2-})$, in which $Carb^{2-}$ is the dicarboxylate anion of BCP and cubane **273** and **274**, respectively, amongst other groups to form square complexes (Figure 51 iii). In crystal form these complexes stack forming infinite tunnels which can be closed to allow for the encapsulation of solvent molecules.[335]

7. Application of Rigid-Linear Linkers in Small Molecule Drugs

Over the years bioisosteres have been implemented in drug design and development to overcome problems associated with potential drug candidates. At the late stage of drug development, the utilization of bioisosteres is often the only viable option. Pharmacokinetic properties (PK) such as bioavailability, solubility, metabolic stability, and toxicity limit a drugs' application even though good potency and selectivity may be observed in vitro. Alternatively, bioisosteres have been employed simply to expand the scope of a family of compounds but also to investigate structure–activity relationships (SAR).

Benzene bioisosteres have been investigated most extensively in the literature, but several examples of bioisosteres for ethynyl, cyclohexane rings, adamantane, and *tert*-butyl and methyl groups have also been reported. Linear-aliphatic-rigid linkers are ideal replacements for these functional groups as they can maintain the structure of the drug that is often crucial to activity, offer metabolic stability when enzymatic action dramatically reduces the half-life of a drug, and increase the lipophilicity of a drug that may be required to cross the blood–brain-barrier. Moreover, BCP has been shown to increase the aqueous solubility of a drug,[336] and, alongside cubane[337] and BCO, has been proven to increase the selectivity and potency for specific receptors.

7.1. Aromatic bioisosteres

A popular option to overcome problems with the design and development of drug candidates is the use of bioisosteres. Due to its ubiquity in most drug molecules benzene is often chosen as a target for bioisosteric manipulation.[338] Chosen for its rigidity, unique electronics and synthetic accessibility, benzene is known to be one of the leading causes for compound attrition in drug discovery (Figure 52).[339]

Figure 52. A visual concept of cubane as a benzene bioisostere.

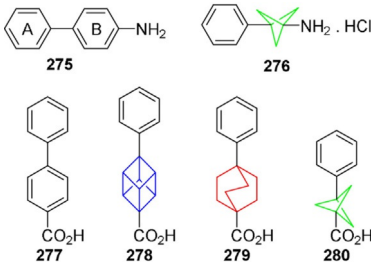

Figure 53. Arylated cubane, BCO, and BCP as *para*-benzene bioisosteres.

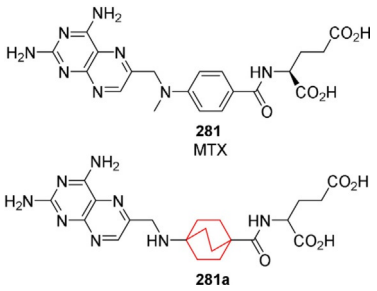

Figure 54. Synthesis and antifolate evaluation of the aminopterin analogue with a BCO ring in place of the benzene ring.

For example, the effect of substitution of the B ring of the diaryl amine system **275** was investigated (Figure 53).[340] Traditional bioisosteres, such as fluorobenzene and pyrimidine were trialed first but seemed to be ineffective at overcoming compound attrition. Following this, the BCP moiety was incorporated to give **276**. This involved a new five-step synthetic route from commercially available starting materials with an overall yield of 32%. This is an improvement over the original seven-step synthesis which had a yield of 14% and incorporated the use of the corrosive hydrazoic acid reagent.[341] The key step involved a novel, potentially versatile method using metal-free homolytic alkylation.

To improve the quality of imaging reagents and modify the physiochemical properties of different drug candidates BCP **280**, BCO **279**, and cubane **278** were utilized as benzene bioisosteres for biarylcarboxy compounds to develop methods for use in more complex systems.[342] The success of a bioisostere is dependent on the role the aromatic group it is replacing has in the overall molecule. If the *para*-substituted arene of the drug molecule influences the conformation of the molecule or has a role in the pharmacophore (e.g., π–π staking)—an aliphatic bioisostere will not be effective. It was shown that BCP improves aqueous solubility by at least 50-fold and markedly decreases nonspecific binding (NSB).[124] On the other hand, BCO increased the lipophilicity of the molecules but did not show the same benefits regarding NSB or solubility. Cubane showed improvements for both parameters. These results confirm the potential advantages of both BCP and cubane motifs as bioisosteric replacements for optimizing *para*-substituted benzene derivatives.

N-(4-{[(2,4-Diamino-6-pteridinyl)methyl]amin}BCO-1-carbonyl)-L-glutamic acid **281 a** was synthesized and tested for antifolate activity (Figure 54).[343] Methotrexate (MTX) is a clinically used antitumor agent and has also seen application against psoriasis and rheumatoid arthritis.[344] MTX acts as a difolate reductase (DHFR) antagonist, inhibiting the production of folic acid in tumor cells that regulates cell division, DNA/RNA synthesis and repair and protein synthesis. The central benzene ring was replaced in **281** by BCO to improve selective uptake and activity in tumor cells. Results showed that although spatial requirements are met a 740-fold reduction in potency was observed. This is one of the few examples of BCO as a benzene bioisostere reported in the literature, suggesting that more desirable effects are observed with BCP and cubane analogues.

While the cause of Alzheimer's disease (AD) is unknown, contributors to the development of the disease have been identified as β-amyloid peptide (Aβ) chains of 40–42 amino acids. Activated by secretases (β and γ), APP (β-amyloid precursor protein) releases β-amyloids into the plasma and the cerebrospinal fluid.[345] It is the aggregation of these peptides into oligomers and plaques that is thought to contribute to the diseases progression. γ-Secretase is an attractive drug target as it regulates the solubility of the AB fragments by controlling their length. The main obstacle drug design must overcome is the selectivity for the APP enzyme over the Notch signaling protein which is involved in the differentiation and proliferation of many different cell types.[346] A previously identified γ-secretase inhibitor (GSIs) BMS-708 **282**, showed excellent antagonist activity.[347] To improve upon the potency of the flurobenzene compound **282**, a BCP derivative **282 a** was made with subnanomolar γ-secretase inhibitory potency in vitro and a robust pharmacological response in vivo. Moreover, the BCP analogue showed increased aqueous solubility, passive permeability, and oral bioavailability in mouse studies (Figure 55).[336a]

Initially a therapeutic target for the treatment of atherosclerosis, Lipoprotein-associated phospholipase A2 ($LpPLA_2$) has also been shown to have a role in Alzheimer's disease.[348] The inhibitor darapladib **283** has been developed to combat the

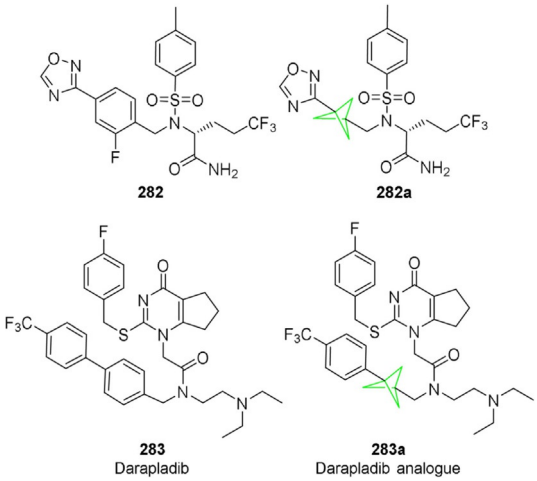

Figure 55. Analogues of the γ-secretase inhibitor smd-1 and the $LpPLA_2$ inhibitor Darapladib.

adverse effects associated with $LpPLA_2$, such as myocardial infarction or ischemic stroke (Figure 55).[349] Darapladib has been shown to have good potency and lipophilicity while maintaining artificial membrane permeability. But, unfortunately, the inhibitor has a suboptimal physicochemical profile, with a high molecular weight, low aqueous solubility, and high property forecast indices (PFI); a risk indicator of developability.[350] But through the substitution of the suboptimal benzene ring with a BCP moiety **283 a**, the PK profile of the drug was improved while maintaining potency.[351] This drug was synthesized over a number of steps, the key transformation involved a dichlorocarbene insertion into a bicyclo[1.1.0]butane system.

Great interest has been shown in resveratrol **284** due to its wide range of therapeutic properties, such as antioxidant, anticancer, antidiabetic, or cardioprotective (Figure 56).[352] Yet, its application is hindered by its poor bioavailability.[353] Studies

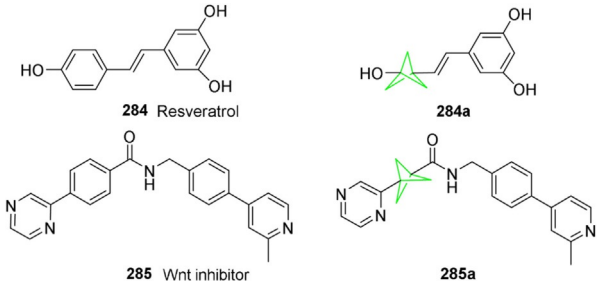

Figure 56. BCP benzene analogues.

have shown this is due to its rapid first-pass metabolism to glucuronide and sulfate conjugates.[354] Routine manipulation of the 4-OH of the phenolic ring would be carried out to overcome this, but previous literature warned against this, as it would be detrimental to activity.[355] As an alternative to overcome these problems the BCP moiety was employed as a bioisostere **284 a** for the phenolic ring.[356] Results showed superior in vivo PK properties over the parent compound and offered reason to proceed with biological testing. Compound **284 a** was synthesized over six steps from the monoester monocarboxylic acid BCP, the key step employing a Wittig reaction to connect the BCP moiety with the benzene diol.

Another benzene bioisostere used was BCP **285 a**, as an alternative to a current Wnt inhibitor **285** (which stops Wnt, a family of proto-oncogenes, encoding secreted signaling proteins that are involved in oncogenesis) (Figure 56).[357] This was done to test and see if the benzene ring is merely a spacer or whether other electronic effects come into play. The synthesis was achieved from commercially available monocarboxylic acid monoesterBCP, attaching the pyridine unit through homolytic alkylation and the second moiety through an amide condensation. Interestingly, biological evaluation showed no inhibitor activity of the BCP derivative in the Wnt-reporter assay indicating that the benzene ring is more than just a spacer and that its unique combination of electronic, stereoelectronic, and steric effects may be crucial for its 1,4-substituents in **285**.

Utilized against a variety of leukemias,[358] commercially available Gleevec, the mesylate salt of Imatinib **286** (Im-1) (Figure 57), is one of the first synthetic tyrosine kinase inhibitors (TKI). Im-1 has a high density of aromatic rings and high

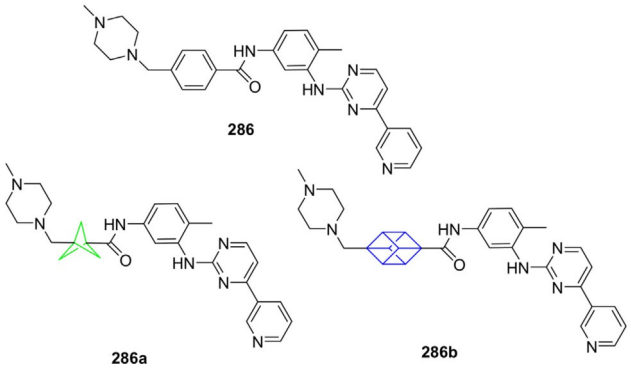

Figure 57. The ABL1 kinase inhibitor Imatinib and its bicyclo[1.1.1]pentyl analogue.

lipophilicity resulting in partial solubility only in neutral aqueous media. The free-base Im-1 was utilized as a model system for evaluating the biopharmaceutical properties (e.g., ABL1 kinase inhibitory activity, cytotoxicity).[336b] Some of the excess aromatic systems were substituted with sp^3 structural motifs, including BCP and cubane moieties, which add increased three-dimensionality and rigidity.

For the BCP analogue **286 a**, an 80-fold increase in aqueous solubility was observed over the parent compound, although there was reduced potency against the target ABL1 kinase and thus therapeutic effects were not conserved. The cubane analogue **286 b** also showed an increased solubility, exhibited the highest inhibitory activity against ABL1 kinase, and the most potent cytotoxicity against cancer cell lines K562 and SUP-B15, but this is still lower than the parent compound. The discrepancy between reduced inhibitory potency of the cubane analogue and the high cytotoxic potency suggests that an additional biological target(s) is being accessed by this molecule. A novel convenient synthesis of Im-1 was described where the bioisosteres were attached through amide condensation reactions.

In the early 90s Eaton postulated that cubane would be an ideal isostere for benzene due to their similarity in size and shape (Figure 52).[62,119] Various molecules were synthesized to test the applicability of this hypothesis with applications in cancer therapeutics, AD medication and pain management.[74] The histone deacetylase inhibitor SAHA **287** (suberanilohydroxamic acid),[359] used for the treatment of cutaneous T-cell lymphoma (CTCL) was the first molecule investigated (Figure 58). Tumor cell line inhibition studies showed both SAHA and the cubane analogue **287 a** had similar potencies in tumor cell inhibition, but SAHA's toxicity was slightly greater towards NFF primary cells.

Previous studies showed significantly increased neurite outgrowth in PC12 neural precursor cells derived from a rat pheochromocytoma upon administration of the neotrophic drug le-

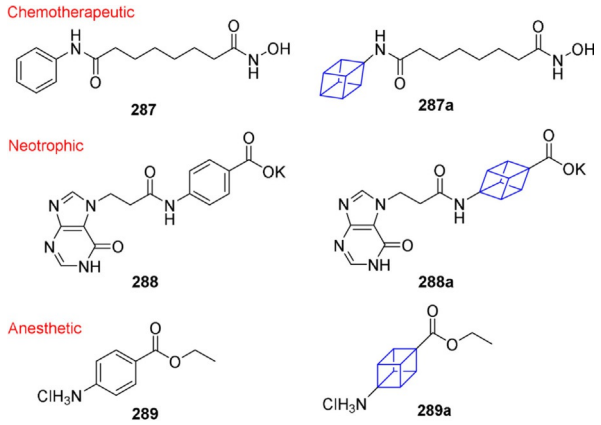

Figure 58. Cubane benzene bioisosteres.

teprinim.[360] The treatment of PC12 cells with either leteprinim **288** or the cubane analogue **288 a** were both ineffective in the absence of nerve growth factor (NGF). But upon administration together the differentiation capacity of the cubane analogue was remarkably better than the parent compound.

The third compound targeted was the nonselective sodium-ion channel blocker benzocaine **289**,[361] a widely used local anesthetic. Adult male rats were used to test the effect of the cubane **289 a** and parent analogues, through injection of the drugs and application of an acute noxious heat stimulus at the source of injection. Results showed the same local anesthetic efficacy of both drugs in this model. Other examples of cubane as a bioisosteres are outlined in the publication.[74] Overall results showed the applicability of cubane as a benzene bioisostere.

7.2. Aliphatic bioisosteres

Alternatively to acting as a benzene bioisosteres, BCP can also be implemented as *tert*-butyl substitute due to its small constrained size. While *tert*-butyl is widely employed as a motif in medicinal chemistry it can affect the properties of the molecule causing drawbacks such as increased lipophilicity and enhanced metabolism rates.[362] From the family of fluoroquinones, Ciprofloxacin **290** is a potent antibacterial drug with

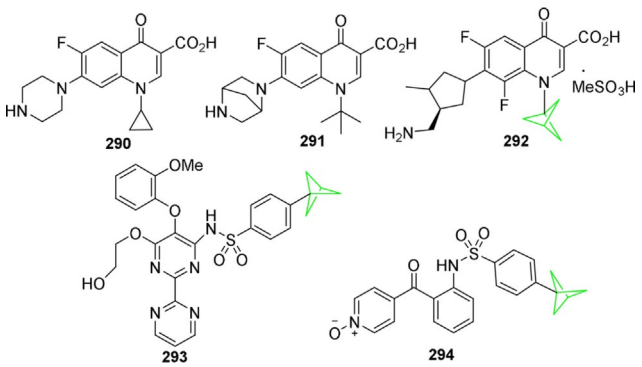

Figure 59. BCP-substituted *tert*-butyl bioisosteres.

broad spectrum activity (Figure 59). However, bacterial resistance is always an ongoing problem. An alternative quinolone analogue **291** was prepared with a *tert*-butyl group at the N-1 position.[363] Following this, a BCP analogue **292** was synthesized, replacing the *tert*-butyl group.[362] This compound showed enhanced activity against gram-positive aerobic bacteria and anaerobic organisms, relative to that of ciprofloxacin. Moreover, time-kill kinetic studies revealed that BCP **292** is extremely potent against ciprofloxacin-resistant *Staphylococcus aureus*.

The *tert*-butyl groups of Bosentan and Vercirnon were also replaced with BCP groups to increase metabolic stability and other physiochemical affects. Bosentan is used for the treatment of pulmonary arterial hypertension[364] while Vercirnon was developed for the treatment of inflammatory bowel disease.[365] Each compound has a *para*-substituted *tert*-butylbenzene sulfonamide unit and straightforward synthesis makes them ideal candidates for *tert*-butyl isostere studies. All the BCP derivatives **293** and **294** were shown to remain biologically active and in the Bosentan series an even higher potency was observed with IC_{50} values compared with that of the parent drug.[366] Additionally, all data on metabolic stability, solubility, logP, p*K*, and permeability showed the applicability of BCP as a viable alternative to *tert*-butyl groups.

To expand the synthetic viability of incorporating BCP into drug molecules a new method involving the reaction of "spring-loaded" strained C–C and C–N molecules with amines was developed, enabling the inclusion of BCP at any point in the synthesis. A series of structurally diverse tertiary BCP-containing amines was synthesized, including derivatized drugs such as maprotiline and amoxapine (Figure 60).[367]

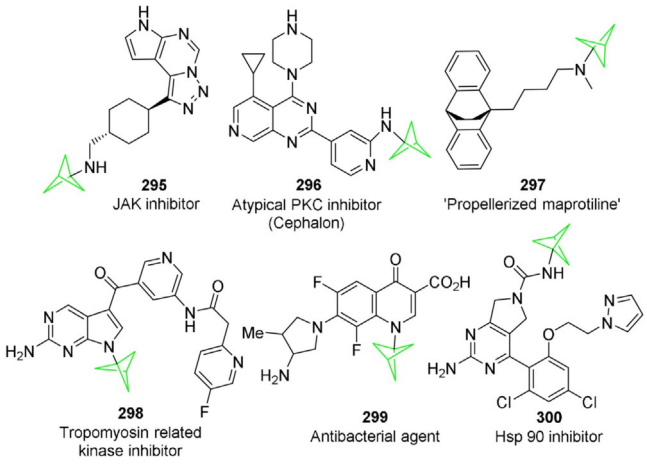

Figure 60. Bioisosteres based on bicyclo[1.1.1]pentan-1-amine.

A novel class of heat shock protein 90 (Hsp90) antagonists was discovered by high-throughput screening and a SAR study was carried out to investigate their properties.[368] Of interest here are the BCP-containing moieties which acted as bulky amide substituents. The BCP-containing compound **300** showed cytochrome P450 inhibition, but unwanted off-target effects were also noted and in animal tumor models potent ef-

ficacy was observed along with other desirable pharmaceutical properties. Likewise, BCP moieties have been installed in several different compounds from a JAK inhibitor **295**, to an atypical PKC inhibitor **296**, a tricyclic antidepressant **297**, a tropomyosin related kinase inhibitor **298**, and an antibacterial agent **299**. These molecules are a part of different series that have been developed by Cephalon, Pfizer, Bristol–Myers–Squibb amongst others as lead compounds in drug trials.[3]

Alternatively to the benzene and *tert*-butyl isosteres already discussed, the ethynyl group was replaced by a BCP unit, as it is closer to BCP in length than the benzene ring. Tazarotene **301** used in the treatment of psoriasis, acne and sun damaged skin and 2-methyl-6-(phenylethynyl)pyridine (MPEP) **302** a mGluR5 antagonist were selected for investigation (Figure 61).[369] The central ethynyl bond in both compounds

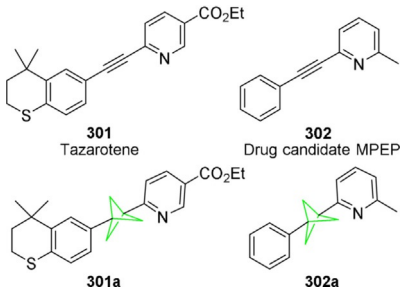

Figure 61. BCP bioisosteres of internal alkynes.

were replaced with a BCP unit so that the pharmacokinetic and physicochemical properties of these analogues could be investigated; but results proved unfavorable.[175] To synthesize these compounds various arylmagnesium halides were employed to ring-open [1.1.1]propellane. The bisarylated BCPs **301 a** and **302 a** were obtained through transmetallation reactions with $ZnCl_2$ and Negishi cross-coupling with aryl and heteroaryl halides.

The opioid activity of morphinoids has been linked to the nature of their nitrogen substituents. Examples in the literature show that the *N*-methyl group in morphine **303** can be replaced by a variety of electron-rich aliphatic compounds to create potent morphine antagonists such as cubylmethylnalorphine, Naloxone, Naltrexone, and Nalbuphine (Figure 62). Inspired by this, cubane was employed as an alternative bioisostere to morphine through the replacement of the methyl group, as it is electronically comparable[370] due to its endocyclic orbitals that are rich in p-character. The *N*-cubylmethyl derivatives of morphine and oxymorphone, *N*-cubylmethylnormorphine **303 a** and *N*-cubylmethylnoroxymorphone **304** were shown to be more potent ligands at the μ and k opioid receptors than morphine and oxymorphone, respectively. However, while compound **303 a** was shown to have moderate narcotic antagonism activity it was much weaker than its *N*-allyl analogue Naloxone. This reduction in potency is hypothesized to be due to the disfavorable steric interactions of the larger cubane scaffold.

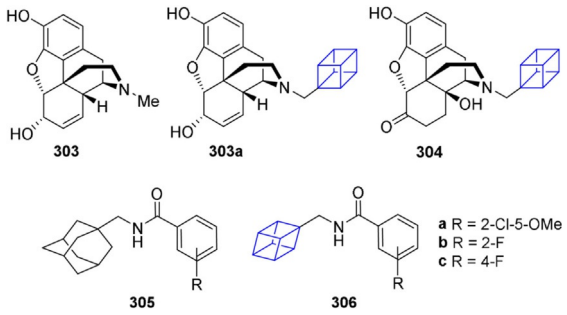

Figure 62. Cubane analogues of *N*-methyl groups and adamantane.

The ATP gated $P2X_7$ receptors ($P2X_7R$) have been indicated to have a role in neurodegenerative diseases[371] and chronic pain modulation.[372] To improve the properties of a current adamantyl benzamide drug **305**, the replacement of the adamantane moiety with cubane **306** was carried out and it was hoped that **306** could be used as a diagnostic probe (when radiolabeled) for in vivo molecular imaging whilst maintaining the activity of the drug.[373] This allowed for the first time to image $P2X_7R$ expression in disease and disease progression. Cubanyl compounds **306 a**–**c** possessed favorable $P2X_7R$ antagonistic properties when tested on rat spinal cord microglia cells. In addition, the cubane analogues **306 a**–**c** showed increased lipophilicity, allowing the drug easier access across the blood–brain barrier to be used as potential PET radioligands. Unfortunately, results of receptor profiling studies indicated that none of the compounds of **306** or **305** exhibited appreciable binding to the many neuroreceptor subtypes assayed. Commercially available dimethyl 1,4-cubanedicarboxylate was utilized to synthesize the product over a series of steps, employing an amide condensation to connect the aryl ring.

Inhibition of DGAT-1 is a popular target for the treatment of obesity and other elements of the metabolic syndrome as it is involved in the final step of triacylglycerol synthesis.[374] A series of pyrazido[4,5-*b*][1,4]oxazine derivatives were published by Japan Tobacco and Tularik companies.[375] Of particular interest was compound **307**, shown to be a potent and selective DGAT-1 inhibitor but with toxic metabolites (Figure 63).[376] Replacement of the cyclohexane ring with sterically bulky, but electronically similar BCO groups **308** was carried out to increase steric crowding around the carboxylic group to limit

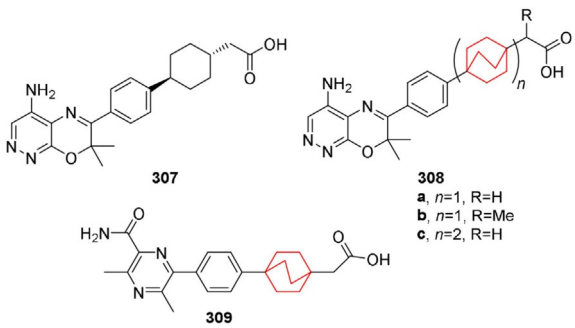

Figure 63. BCO analogues of cyclohexane linkers.

metabolism.[377] Compound **308a** proved to be a potent and selective inhibitor of the enzyme DGAT-1, with a superior PK profiles and a further optimization of **307**, resulted in the formation of BCO **309** with the replacement of bicyclic pyrazido[4,5-*b*][1,4]oxazine with a pyrazine moiety, to give an increased potency at the hDGAT1 receptor amongst other desirable physiochemical properties. The cyclohexane and BCO derivatives were both synthesized, but the former proved most promising as a future drug candidate.[378]

The covalent Bruton's Tyrosine Kinase (BTK) inhibitor Ibrutinib **310** is currently approved for mantle cell lymphoma and chronic lymphocytic leukemia (Figure 64).[379] However, ana-

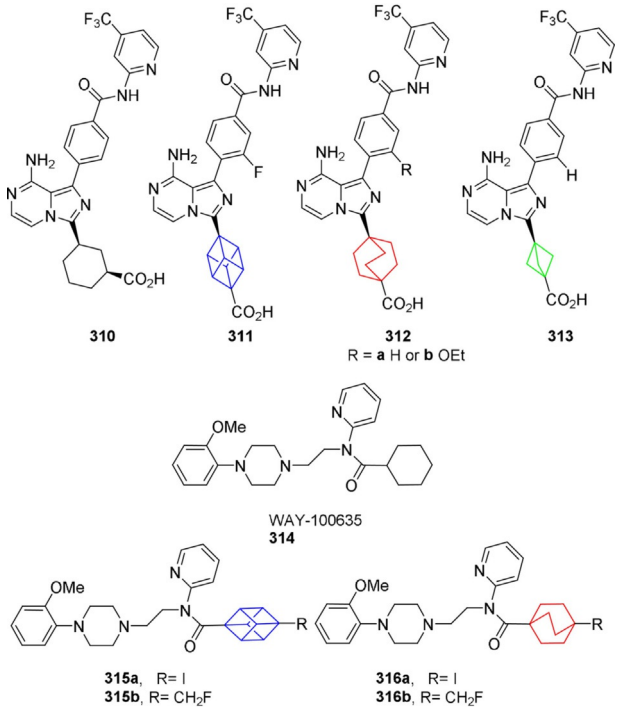

Figure 64. Novel BTK inhibitors and potential SPECT ligands.

logues were shown to inhibit adenosine uptake (AdU) causing undesirable CV effects.[380] To avoid these adverse effects optimization of the drug **310** was carried out by substituting the cyclohexane ring for cubane, BCO, and BCP.[381] The cubane **311** and BCP **313** analogues showed reduced human whole blood (hWB) potency, whereas the BCO **312** analogue exhibited excellent potencies at the desired receptors but was poorly selective for AdU. The addition of an ethoxy group onto the central benzene ring of the compound **312b** resulted in the retention of good potency while reducing adenosine uptake activity. But unfortunately, a high metabolic clearance was observed for this compound making further optimization necessary before it can be effective.

5-HT_{1A} receptor ligands derived from **314** (WAY-100635) were made that replaced the peripheral cyclohexane group of **314** with various halogenated bridge-fused ring systems such as cubane **315** and BCO **316**.[382] The iodinated analogues **315a** and **316a** both showed subnanomolar potency at the 5-HT_{1A} receptor. The C–I bond was found to be stable both in vivo and in vitro. Unfortunately, poor brain uptake of the drugs was observed resulting in low concentrations in the brain, especially in the hippocampus where large volumes of the target receptor are located, making these derivates unsuitable for SPECT. Fluorinated derivatives were also prepared for the cubyl and BCO analogues **315b** and **316b**, respectively.[383] Good potency at the receptor was observed and this time with high selectivity for the 5-HT_{1A} R rich regions of the brain but the major drawback seen with this analogue was the in vivo enzymatic defluorination of the drug, deactivating the radio ligand.

7.3. Additional uses of rigid scaffolds in medicinal chemistry

Collectively the risk factors visceral adiposity, diabetes, dyslipidemia, and hypertension make up the metabolic syndrome and the incidence of cardiovascular disease is greatly increased when they occur together and intracellular cortisol is thought to be the cause.[384] The enzyme 11b-hydroxysteroid dehydrogenase type 1 (11b-HSD1) plays an integral role in the regulation of cortisol activation, thus making it a therapeutic target.[385] Heteroaryl substituted bicyclo[2.2.2]octyltriazoles are potent and selective 11b-HSD1 inhibitors with excellent pharmacokinetic profiles.[386] Owing to this, compound **317** was synthesized and proved to be a very efficient cortisone inhibitor, but with high clearance rate and low bioavailability (Figure 65). The main metabolite was formed as a result of oxi-

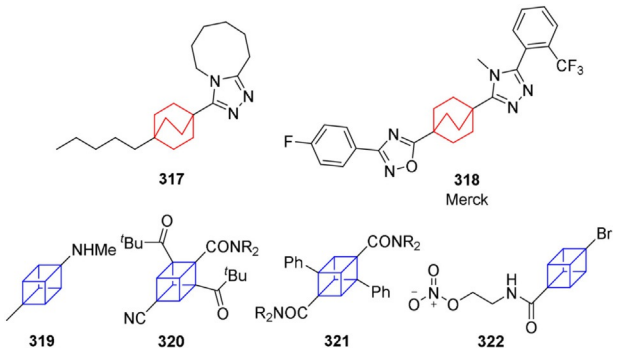

Figure 65. Various rigid linker scaffolds.

dation at the ω-1 position of the 5-carbon alkyl chain. Further experiments were conducted, replacing the chain with various heterocycles, resulting in compound **318** that was shown to have high selectivity of 1800 fold for HSD1 over HSD2, with good cortisone inhibition. Moreover, the compound possesses a very high bioavailability and was selected as a lead compound and patented by Merck.[387]

One of the first examples in medicinal chemistry that employed cubane as a scaffold for medicinal drugs was seen in 1971, when the compound was found to possess antiviral properties, especially towards the influenza virus.[388] Later on, in the 90s Dipivaloylcubane **320** and diphenylcubane **321**

were proposed as cubanyl drugs which displayed moderate antitumor activity and anticancer activity, respectively. In these compounds cubane was shown to increases the lipophilicity of the compound allowing easier movement across cell membranes and to possess minimal toxicity. Additionally, **322** was shown to have applications in aorta relaxation and calcium channel blocking.

7.4. Amino Acids

7.4.1. Glycine and alanine mGluR1 antagonists

Activated by synaptic release of L-glutamic acid **323**, metabotropic glutamate (mGlu) receptors consist of eight (currently known) mGlu receptor subtypes that have been classified into three groups. Group I contains mGlu1 and mGlu5, which are positively coupled to phospholipase C (PLC) and mGlu1 has been linked to the cause and accentuation of post-ischemic neuronal damage.[389] Thus, mGlu1 antagonists are potential therapeutic agents in the treatment of CNS disorders such as ischemia, stroke, head trauma and Alzheimer's disease.[390] Carboxyphenylglycines (CPGs) have been shown to be selective mGlu1 antagonists over glutamate ionotropic receptors[391] and optimizations of this drug category resulted in benzene analogues; *S*-4CPG **323a**, *S*-4C3HPG **323d**, and (+)M4CPG **323g** which have all been shown to inhibit mGlu1 activity, albeit with drawbacks such as low potency and activation of the mGlu2 receptor subtypes (Figure 66).[392] While the coplanarity

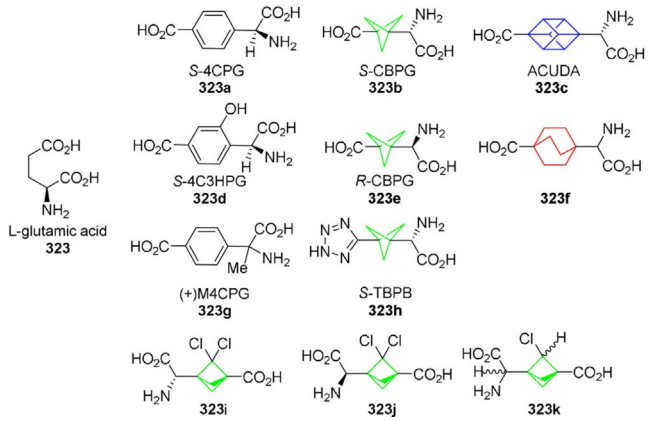

Figure 66. mGluR1 antagonists.

between the α-amino acidic and the ω-carboxy functionalities, introduced by the benzene moiety, is generally accepted to be a crucial feature of the CPG, whether it has other contributions to activity was unknown. SAR studies carried out on the current *S*-4CPG antagonist involved the substitution of the benzene ring with different saturated, rigid hydrocarbons, such as BCP, BCO, and cubane.[393,394]

BCP **323b** was shown to have good potency at the mGlu1 receptor and little activity at the other subtypes in both in vitro and in vivo tests, indicating that the benzene ring is not of importance when linearity and rigidity are maintained. BCP is considerably shorter than an aromatic ring, so further tests are needed to see if its potency was affected. Owing to a more similar size, cubane makes a more suitable bioisostere for benzene, thus ACUDA **323c** was prepared.[395] However, when tested with the mGlu1 ligand **323c** only weak activity was observed and a nine-fold decrease in activity was observed compared to BCP **323b**. This was attributed to the increase in volume of the 3D cube, suggesting that cubane represents the upper limit for the steric accessibility of the mGlu1 binding site. Interestingly, while BCP **323b** has higher activity, ACUDA **323c** was shown to have remarkable selectivity, enabling it to be devoid of any effect at mGluR5, while under the same condition BCP **323b** acts as a partial mGluR5 agonist. A BCO group was also incorporated into CPG framework **323f**, expanding the family of linear-rigid scaffolds employed. Unfortunately though, testing in AV-12 cells showed that the non-natural amino acid was inactive against human mGluR1 and mGluR5.

To further ascertain the influence that the distance between the two pharmacophore groups plays and, additionally, to quantify the importance of the distal carboxylate group, the synthesis of BCP **323h** ((*S*)-TBPG) was carried out, characterized by the tetrazole moiety replacement of the carboxyl group.[396] This substitution compensated for the shorter distance of the BCP-based moiety compared with that of the "standard" *S*-4CPG. A 2.5-fold reduction in potency was observed at mGluR1 when compared with than the parent compound but it was found to be devoid of affinity for the mGluR5 subtype. The reduction in activity was thought to be due to the reduced acidity of the tetrazole ring compared with the carboxylate and/or due to the different hydrogen bonding geometry of the compound. The tetrazole moiety was attached through the cycloaddition of tri-*n*-butyltin azide (nBu$_3$SnN$_3$) with a nitrile group.

Further studies were performed to investigate the influence the introduction of lipophilic moieties in the 2′-position of the core of (*S*)-CBPG **323b** would have on potency and selectivity.[397] Two chloro groups were introduced at the 2′-position of the BCP of both stereoisomers and a racemate of a monochloro BCP group was also synthesized, namely (*R*)-dichloroBCP **323l**, (*S*)-dichloroBCP **323j**, and chloroBCP **323k**. Functional assays showed that all compounds had antagonist activity at group I receptor subtypes but were unselective, working at both mGlu1 and mGlu5 receptors. Docking studies showed that the antagonistic behavior observed was due to the presence of disfavored van der Waals interactions in the binding site which arise because of a different orientation the drugs take compared to the native (*S*)-glutamate.

To obtain a new class of acidic amino acids with specific activities at excitatory amino acid (EAA) receptors, the ω-carboxylate moiety of glutamic acid **323** (L-Glu) was substituted with a ω-phosphonate group. The most potent example of a selective mGluR3 agonist is L-AP4 **324a** (Figure 67).[398] A first-choice strategy to achieve subtype selectivity often is conformational constraining and previous research with 4-PPG **324b** showed it to be a potent group III selective agonist. In search for new group III ligands to enable further characterization of this family of receptors, a BCP bioisosteric replacement approach was employed.[399a] Stereoselective Ugi condensations were

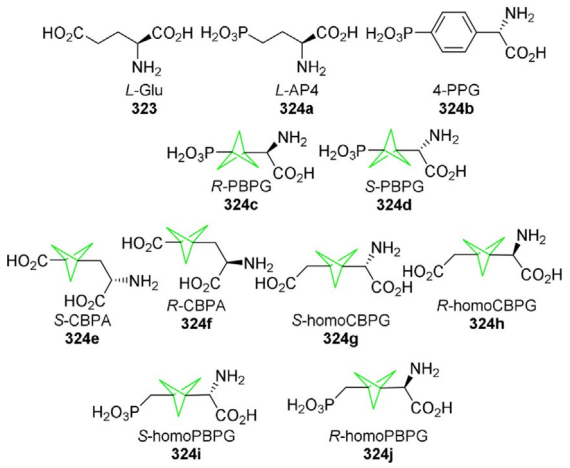

Figure 67. mGlu3 agonists.

employed to synthesize the two isomers (2*R*)- and (2*S*)-phosphono-BCP-glycine **324 c** and **324 d**, which are potent agonists at group III mGluRs, while inactive at mGluR1 receptors and only weakly active at mGluR2. Interestingly, they had opposite effects at mGluR2; the *S*-enantiomer acted as a weak antagonist, whereas (*R*)-PBPG **324 c** was a weak agonist. Within group III receptors (*S*)-PBPG **324 d** exhibited a selective profile for mGluR4, with a 16-fold potency at this receptor subtype over mGluR6, whereas the *R*-enantiomer showed no distinction. Although an increased potency over L-AP4 was not achieved, this increased selectivity will hopefully allow more to be learned about the mGluR4.

Additional BCP amino acid derivatives were synthesized, including (2*S*)- and (2*R*)-carboxyBCPalanines **324 e** and **324 f**, which are elongated versions of (2*S*)- and (2*R*)-CBPG **323 b** and **323 e**, for which the distance between the pharmacophoric groups is increased by homologation of the carbon backbone at the amino functionality. Also (2*S*)- and (2*R*)-carboxymethylBCPglycines **324 g** and **324 h** were prepared, for which the distal carboxylate is the functionality elongated and, finally, (2*S*)- and (2*R*)-phosphonomethylBCPglycines **324 i** and **324 j** were synthesized through the substitution with a ω-phosphonate group of the elongated ω-carboxylate group.[399b]

The biological profiles of the six new compounds were examined at both ionotropic glutamate receptors and recombinant mGluRs subtypes through binding experiments. The most interesting results were obtained for the NMDA receptor. Out of the ω-carboxylate derivatives the (*R*)-enantiomers (*R*)-CBPA **324 f** and (*R*)-homoCBPG **324 h** had the highest potency and good selectivity being completely inactive at the other iGluRs and mGluRs. But the highest affinities for NMDA were observed for the ω-phosphonate derivatives, while still maintaining high degrees of selectivity. (*R*)-homoPBPG **324 j** had the highest potency of them all and has the potential to be a lead compound for the NMDA receptor.

7.4.2. Other natural amino acid derivatives

Fibrinolysis is a natural process that occurs in the body to prevent the build-up and thus harmful effect of blood clots. Primary fibrinolysis involves the normal rate of breakdown for blood clots while the rate of secondary fibrinolysis is excessive, leading to severe bleeding. Previous potential inhibitors are analogous amino acids -aminocaproic acid (EACA), *p*-aminomethylbenzoic acid (PAMBA), and *trans*-4-aminomethylcyclohexanecarboxylic acid.[400] Their proposed mode of action is the inhibition of the proteolytically active enzyme plasmin from plasminogen. These drugs were mostly glycine derivatives and it was thought that the maximum antifibrinolytic activity would be achieved once the optimum distance between amino and carboxyl moieties was obtained. Thus, different rigid spacers, such as cubane and BCO, were investigated to test this theory. The non-natural BCO amino acid **325 b** showed more activity than any molecules previously reported and, in addition, it was shown to be orally available, and without major toxicity (Figure 68). Linearity was also proven to be important as a decrease in activity was seen with

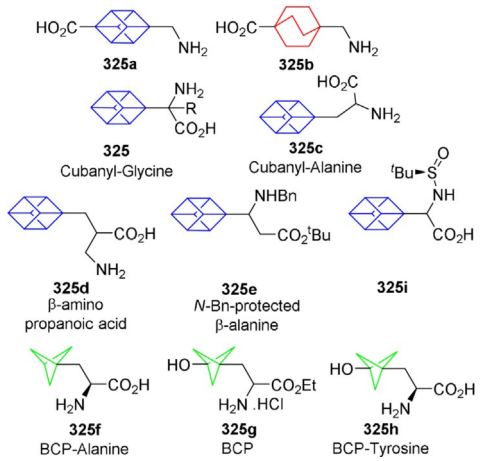

Figure 68. Various amino acid non-natural analogues.

the comparable non-linear bicyclo[3.2.2]nonane analogue. Conversely, the cubane derivative **325 a** did not show superior activity to previous examples, this was thought to be due to the protruding protons from the unoccupied corners of the cube.

In an effort to synthesize pharmaceutically relevant cubane derivatives,[206] a series of novel cubane-containing amino acids were prepared. Initial cubane-containing amino acids synthesized were cubane-containing carboxyglycine **325 a** (R = H)[401] and its derivatives (R = Me, CH_2CHAr_2), accessed by the Strecker method (Figure 68). Reports were also made of the synthesis of the cubane-containing glycine derivative **325 i** using the Ellman method. But cubane-containing glycine **325** itself still remained unreported.[402] The first successful synthesis of cubanyl **325** was finally achieved using readily accessible cubane precursors, while cubane-containing alanine **325 c** could only be prepared after developing conditions for the hydrogenation of the unsaturated precursor. Furthermore, the synthesis of

cubane-containing β-aminopropanoic acid **325 d** and cubane-containing *N*-Bn-protected β-alanine **325 e** was described. These β-amino acids are of interest as previous β-amino acids have shown resistance to proteolysis[403] and form stable and highly structured β-peptides.[404] A Mitsunobu C–C bond-forming reaction was employed to synthesize the β-amino acids and the addition of a lithium amide to an α,β-unsaturated ketone.[401]

A number of different tyrosine **325 h** and phenylalanine **325 g** derivatives have also been reported in the literature.[124,356] BCP analogues of these natural amino acids were made to elucidate conformational and electronic effects in peptides. The BCP-containing glycine derivative was synthesized through the homologation of a carboxylic acid, followed by a Strecker reaction, in eight steps.[124] The BCP-containing tyrosine analogue was accessed from the BCP aldehyde by a Wittig reaction to form an α,β-unsaturated ester, this group was then transformed into a diazo derivative by using hydrohydrazination conditions.[356]

7.4.3. ^{19}F-labeled amino acids

The ^{19}F isotope is of great interest in ^{19}F NMR labeling due to its high sensitivity, its wide range of chemical shifts, the absence of biological background signals, and its strong dipolar interactions.[405] Often in NMR applications fluorine-labeled L-α-amino acids (FAAs) act simply as a qualitative probe to sense changes in the local environment. Only recently, FAAs have been incorporated into membrane-bound peptides to determine the orientational limitations of the peptide and the interatomic distances required between amino acids through the use of solid-state ^{19}F NMR spectroscopy.[406,407] Information can be gained from these studies such as the conformation, alignment, and dynamic behavior in a lipid bilayer under quasi-native conditions of membrane active peptides. In order for the ^{19}F label to be successful strict guidelines must be adhered to. Firstly, the ^{19}F label must be conformationally restrained at a defined position close to the aminocarboxylic moiety. Furthermore, it must be compatible with the synthesis of the peptide and lastly the peptide must not have its structure or its function altered.

To slow down the aggregation of peptides into β-sheeted assemblies, the stereochemistry of a single amino acid can be changed from the D- to the L-enantiomer through substitution. This seemingly simple change can cause significant effects in a system altering its conformational and thus functional and biological properties. The amphiphilic membrane-active model peptide [KIGAKI]$_3$-NH$_2$, is used to investigate this effect of the reversal of an amino acids stereochemistry, as it is known to form amyloid-like fibrils.[408,409] This peptide has been shown to exhibit potent activity against various bacteria compared to that of amphiphilic α-helices.[410] Notably, even with one-third of the amino acids in the form of the D-enantiomer in the KIGAKI sequence a β-sheeted conformation was still predominant.[411] Different functional assays of this peptide have been investigated to deduce whether aggregation plays a role in various biologically relevant functions that involve peptide–lipid interactions. At different hydrophobic positions of the KIGAKI sequence, CF$_3$-Bpg **326** was incorporated either as an L- or a D-enantiomer. The ^{19}F-labeled sequence showed that although D-epimers are known for having higher aggregation thresholds than the L-epimers, aggregation was seen in both (Figure 69).

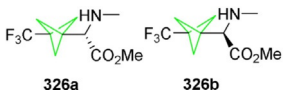

326a **326b**

Figure 69. 3-(Trifluoromethyl)bicyclopent-[1.1.1]-1-yl glycine (CF$_3$-Bpg).

To investigate its use as a synthetic probe, the ^{19}F-labeled amino acid 3-(trifluoromethyl)BCPglycine **327 a** (CF$_3$-Bpg = 3-(trifluoromethyl)bicyclopent-[1.1.1]-1-yl-glycine) was synthesized (Figure 70).[412] The presence of the nonconjugating BCP

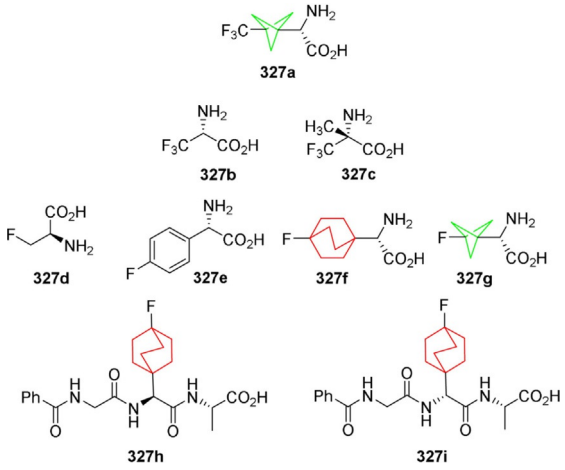

Figure 70. ^{19}F NMR labels for peptide studies.

linker reduced electronic transmission across the amino acid as compared to an aromatic ring, leading to less racemization.[89] Furthermore, the loss of HF is avoided as in the CF$_3$-Ala derivative **327 b**, as is the low reactivity of the aminocarboxylate moiety **327 c** as a result of steric hindrance, under solid-phase peptide synthesis conditions (SPPS). CF$_3$-Bpg **327 a** resembles amino acids Ile and Leu most closely in size and lipophilicity, while it is also suitable as a Met, Phe or Trp isostere in terms of shape and steric volume, although lacking the aromaticity of Trp and Phe. When compared with previously used phenylglycine derivative **327 e**, parameters show that CF$_3$-Bpg is closest to the natural nonpolar amino acids. To confirm the proposed and calculated properties of CF$_3$-Bpg, the new FAA was incorporated in the 21-mer sequence of the antimicrobial peptide PGLa **328**.[406,407] Previous FAA **327 f** racemized completely under the SPPS conditions when used to produce PGLa, while the synthetic peptides containing CF$_3$-Bpg contained only one diastereoisomer, as shown by HPLC/MS. Additionally, the biological activity of these peptides was tested using bacterial-

growth inhibition assays and no change was noted from the activities observed with the wild-type peptide, implying that the introduction of CF_3-Bpg was not detrimental to activity. Moreover, circular dichroism showed that there were no distortions in the peptides that could have been caused by the new unit. The labeled peptides were also arranged mechanically into phospholipid bilayers and behaved compatibly with the known α-helical conformation further showing **327 a** (CF_3-Bpg) suitability as a ^{19}F labeling unit for solid-state ^{19}F NMR spectroscopy.[408,413]

Significant work has been done on CF_3 analogues of various amino acids, whereas monofluorinated labels that allow superior[414] intra- and intermolecular distance measurements have received less attention.[415,416] Previously, examples, such as **327 d** and **327 e** have shown serious drawbacks, these problems also occur in the case of alkyl **327 d**, which has no rigidity in its structure resulting in ambiguous analysis of the NMR data obtained owing to its conformational flexibility. This limitation was overcome with aromatic **327 e** as the position of the ^{19}F atom is fixed, but when replacing aliphatic amino acids (Ala, Val, Ile, Leu) extensive racemization during peptide synthesis is observed. Thus, to overcome these problems, BCO was utilized to synthesize the new aliphatic ^{19}F-substituted amino acid (4-fluoroBCO)glycine **327 f**.[416] Unfortunately, racemization was still observed with the BCO derivative, although only partially, resulting in the two epimeric peptides **327 h**/**327 i** upon synthesis with SPPS. The key transformation in the synthesis of the amino acid **327 f** was a decarboxylative fluorination of an aliphatic carboxylic acid with XeF_2 in C_6F_6.

Following on from this research, an alternative to BCO **327 f** was sought to overcome the reduced reactivity of the amino acid caused by its increased lipophilicity and steric bulk when compared to natural aliphatic amino acids.[416] Hence, 3-fluoro-BCP-glycine (F-Bpg, **327 g**) was prepared, a smaller, while still rigid and nonconjugated core, that allows for an increased activity of the bioisostere in SPPS (Figure 70). The interatomic distances in membrane-active peptides were determined by solid-state ^{19}F NMR spectroscopy, made possible with F-Bpg **327 g** as it avoids the problems associated with the previous FAAs. Calculations showed that the smaller BCP unit was closer in likeness to the natural Leu/Ile than all other ^{19}F labels in terms of size and lipophilicity.

F-Bpg **327 g** was incorporated into the antimicrobial peptide PGLa **328** from the skin of *Xenopus laevis*, to evaluate the potential of the label in detecting the F···F contacts (Figure 71).[417] Manual SPPS was employed to synthesize the polypeptide and encouragingly no degradation, low reactivity, or racemization of F-Bpg was observed.[402] The peptide was reconstituted in 1,2-dimyristoyl-*sn*-glycero-3-phosphocholine (DMPC) bilayers and gave the expected two ^{19}F resonances in the ^{19}F NMR spectrum. CD spectroscopy of the labeled peptide showed slight deviation from the wild-type peptide in its α-helical character, probably caused by the destabilization of the helix near the labeled sites. Overall CD showed the presence of a mostly α-helical-labeled peptide in the membrane mimicking environment and, albeit with reduced activity, the ^{19}F peptide remained antimicrobial. A center band only detection of exchange (CODEX) experiment was used to validate the proposed label for ^{19}F–^{19}F distance measurements.[418] The intramolecular ^{19}F–^{19}F distance was found to be approximately 8 Å, which is much closer in value to the expected distance of 7.5–8.0 Å in an ideal helix than the 6.6 Å value obtained for BCO.[419] The slightly longer distance can be explained by the minor distortion seen of the α-helix in CD, but nevertheless *F*-Bpg **327 g** can still be effectively used as a label to measure interspin distances.

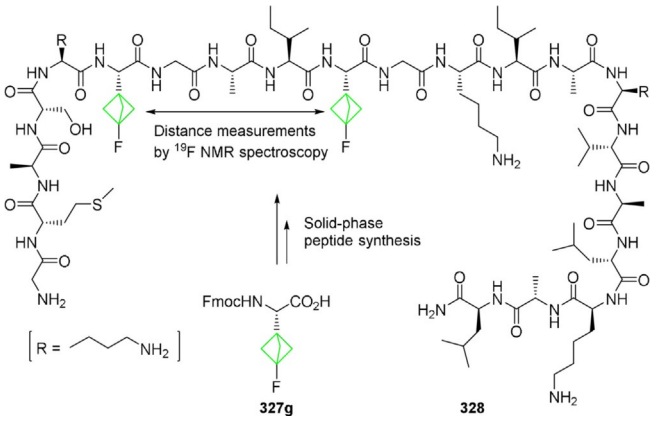

Figure 71. ^{19}F-Labeled peptide.

7.4.4. Non-natural peptides

To increase the metabolic stability and bioavailability of peptides, additional non-natural amino acids have been incorporated into peptides. Adamantane-substituted peptides have been shown to enhance the peptides ability to penetrate biological membranes, and they have been investigated for their anti-tumor[420] and antimicrobial activities.[421] With structural similarities to adamantane, cubane-based derivatives are also a viable option for non-natural amino acids. The first cubane-based amino acid synthesized for its neuroprotective properties was 4-carboxylcubylglycine **325 a**.[394] As unfunctionalized cubane is a closer mimic of hydrophobic amino acids such as leucine, isoleucine, and phenylalanine, cubane derivative **325 i** was synthesized, as were the dipeptide derivatives **329 a**–**c** bearing cubane residues in place of side chains (Figure 72).[402] Due to the high sensitivity of the vinylcubane unit, initial attempts to prepare a cubane-based alanine derivative via the corresponding dehydroalanine were unsuccessful. However, the successful synthesis of a cubane-based glycine derivative and cubane-substituted dipeptides **329 a**–**c** in diastereomerically pure form was achieved upon the addition of lithiated cubane to a (*R*,*S*)-glyoxylate sulfinimine.

C–H activation was utilized to achieve an efficient synthesis of N^{14}-desacetoxytubulysin H (Tb1) and pretubulysin D, alongside the derivatives tubulysin BCP **330 a** and cubane **330 b**.[422] The synthesized compounds were biologically evaluated with an array of cancer cell lines. Notable results included the novel BCP analogue Tb14 **330 a**, which showed high potencies against certain cell lines such as uterine sarcoma and human

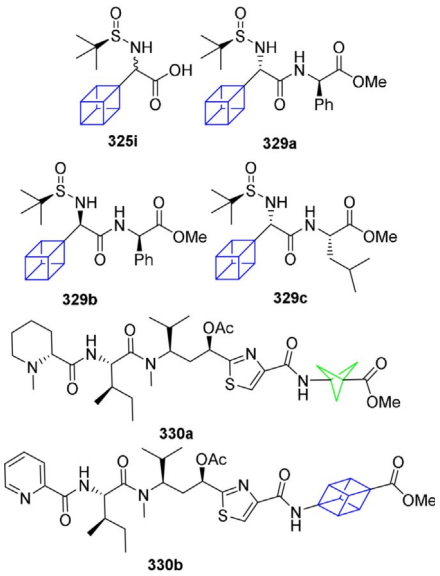

Figure 72. Non-natural peptides.

embryonic kidney cell line. These highly potent cytotoxic compounds have application as antibody–drug conjugates and other drug delivery systems for personalized targeted cancer chemotherapies.

One of the first examples of amino acids containing a BCP moiety are 2-(3′-substituted-BCP)glycines **331** (Figure 73).[393,396]

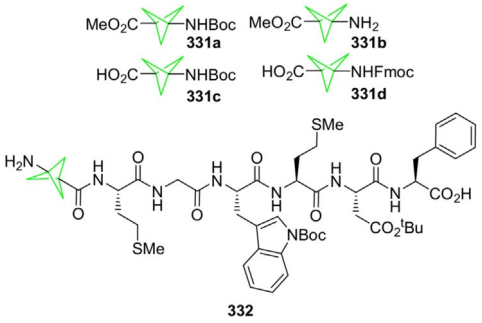

Figure 73. A BCP peptide.

Inspired by this work, four derivatives of 3-aminoBCP-1-carboxylic acid **331 a**–**d** were prepared to act as rigid analogues of 4-aminobutyric acid, which has been shown to act as a neurotransmitter in the brain.[423] These analogues were then incorporated into linear and cyclic peptides using solution chemistry and solid-phase techniques. Moreover, the sequences for the BCP peptide **332** were derived from the neuropeptide cholecystokinine (CCK), to be used as a ligand for the CCK-B subreceptor in the brain that acts as neurotransmitter and neuromodulator. The shortest natural CCK fragment that exhibits a high affinity for the CCK-B receptor is the C-terminal CCK-4 that has the sequence Trp-Met-Asp-Phe. Classic coupling methods as well as by solid-phase techniques were employed to synthesize the peptide.

In recent years, peptides have emerged as promising novel antibiotics due to their wide applicability against a broad spectrum of pathogens. Toxicity, instability and high production costs are big obstacles for the practical implementation of large peptides. To overcome these issues, smaller antibacterial peptides with adequate metabolic stability are required. While few examples are known in the literature, *N*-acetylated hexapeptides such as Ac-RRWWRF-NH_2 have been identified.[424] The size, shape, and character of the side chains influence the antimicrobial effect, as does cyclization of the peptide through reducing the likelihood of proteolysis.

To investigate the influence of lipophilic, nonaromatic amino acid side chains on antimicrobial and hemolytic activity a number of corresponding linear and cyclic peptides were synthesized that contain non-natural amino acids with a BCP moiety.[425] Linear and cyclic hexapeptides of the type Arg-Arg-Xaa-Yaa-Arg-Phe **334** containing the BCP amino acid **333** as a replacement for two tryptophan residues were prepared by SPPS (Figure 74). Results showed that the antimicrobial effect

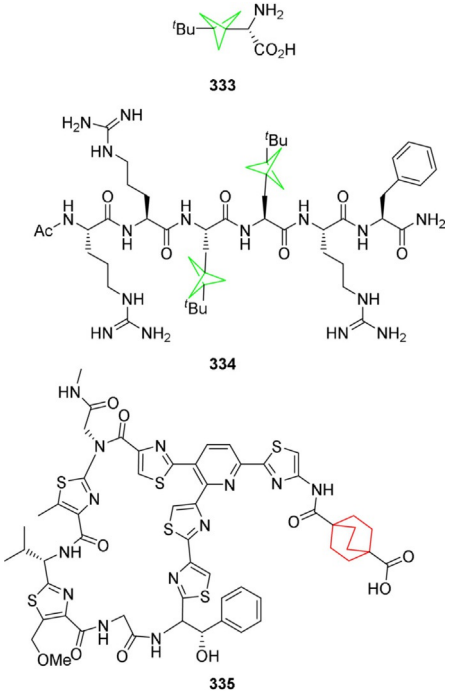

Figure 74. BCP and BCO antimicrobial peptides.

of the non-natural peptides markedly increased due to the presence of the bulky and hydrophobic BCP amino acids confirming the importance of having hydrophobicity in the hexapeptides. Unexpectedly, cyclization was detrimental to the activity of the BCP-substituted derivatives, likely due to its high global hydrophobicity eliminating the activity-enhancing effect of cyclization-induced amphipathicity.[426] The chiral BCP amino acid was synthesized over nine steps from the tetrahalide; key steps involved addition of a Grignard reagent to from the BCP scaffold and an asymmetric Strecker reaction to form two glycinonitriles.

One of the significant areas of antibiotic resistance involves Gram-positive skin and soft-tissue infections. GE2270, an isolated thiopeptide-based natural product was found to inhibit the prokaryotic chaperone elongation factor Tu (EF-Tu).[427] The antibiotic profile was remarkable, with minimum inhibitory concentrations below 1 $\mu g\,mL^{-1}$ but drawbacks included low water solubility and instability of the macrocycle. Hence, in order to increase the intrinsic aqueous solubility and improve the cellular antibacterial activity, a variety of linkers, spacers, and termini, including the BCO spacer, were examined to further chemically stabilize the 4-aminothiazole macrocyclic **335**.[428] SAR results showed improvements in the solubility and efficacy profiles over previous analogues and GE2270 although the cyclohexane derivative proved to be more effective than the rigid BCO counterpart.

Hepatitus C virus (HCV) is a positive-stranded RNA virus that causes several serious liver conditions such as liver cirrhosis, chronic hepatitis, and hepatocellular carcinoma.[429] A potential therapeutic target for the treatment of HCV is the HCV NS5A protein as it plays a critical role in regulating HCV replication.[430,431] The first-in-class HCV NS5A inhibitor Daclatasvir **336**[432] contains a C_2-symmetric biphenyl bisimidazole motif, and a biphenyl central unit (Figure 75). Alternative rigid bio-

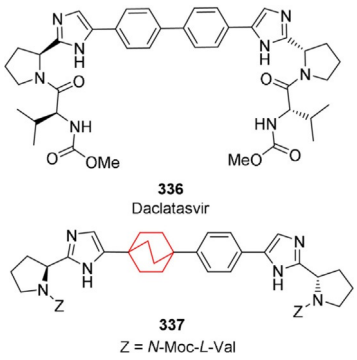

Figure 75. HCV NS5A inhibitors.

isosteres, such as the BCO analogue **337**, were employed to improve the pharmacokinetic properties of the compound.[433] Results showed good solubility and potency at the target. Additionally, the BCO derivative **337** possessed good bioavailability and high concentrations in liver tissues and saw increased solubility compared with the parent compound. The 10- to 20-fold less reduction in potency relative to Daclatasvir **336** suggests that the biphenyl unit may be interacting with the NS5A protein and not just merely acting as a spacer.

8. Perspective of Linkers

The systems we have presented all share the common theme of being linear and disubstituted, ranging from bridgehead-to-bridgehead distances of 1.85 Å in BCP to 2.79 Å in cubane (Figure 76).

With regards to rigidity, being able to arrange functional groups in a spatial defined manner, many other hydrocarbons

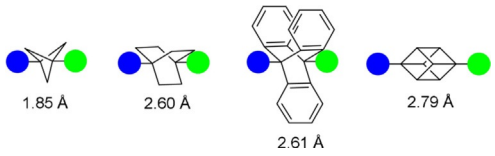

Figure 76. Scope of distances within the 180° void.

enter the stage, spanning a full range of different angles and distances. The family of bicyclic [*x.y.z*]-hydrocarbons seems to be perfect candidates for a wide spectrum of angles and distances (Figure 77). With *x*, *y*, *z* in the range of 1 to 3, this group covers a range from 2.01 to 3.02 Å, and a geometrical arrangement from 132 to 177°.

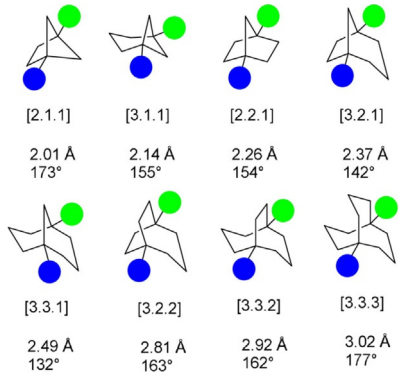

Figure 77. Different angles and distances within the [*x.y.z*]-hydrocarbon series. Estimated values assuming standard bond angles and length, for non-specific functional groups.

The potential for various orientations becomes even more complicated and exciting with the introduction of more than two functional groups. New geometric arrangements and isomers can be realized to generate desired functions. Expanding on this, a four-fold substituted system, with a tetrahedrane-like shape, would even introduce a new chiral opportunity. Chiral adamantane or cubane-systems seem to be ideal candidates to explore the tetrahedral space and progress has already been made in this area, with the synthesis of tetrahalogenated asymmetric adamantane[434] and cubane[435] (Figure 78).

Implementing the use of multidimensional arrays with Chauvin's concept of carbomers,[436] is a logical process to achieve the various linker lengths and geometries. A "cubamere", the

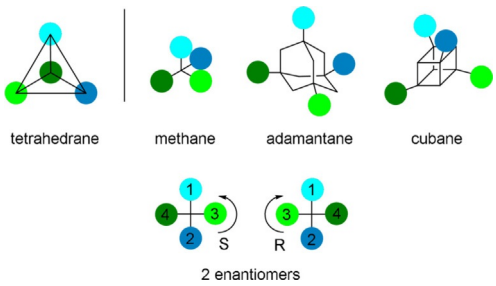

Figure 78. The tetrahedral space.

nonconjugated counterpart to Feldman's tetraethynylmethane[437] is just one thinkable structure with unexplored properties. Like the tetraethynylmethane, the synthesis of the corresponding cubamer would be a remarkable challenge, but with promising possibilities (Figure 79). In addition, just like the plethora of polyacetylenic linked molecules and their triumphal procession in material chemistry,[438] their nonconjugated counterparts would build the bridge over unknown waters for many desirable functions. Again, there is no set limit to the tetrahedral space as well, many different polysubstituted linker systems being possible (Figure 80): Octasubstituted BCP with a trigonal bipyramidal motif (6+2), octadodecasubstituted triptycene (4+4+4+2), or even an octasubstituted cubane with eight different substituents.

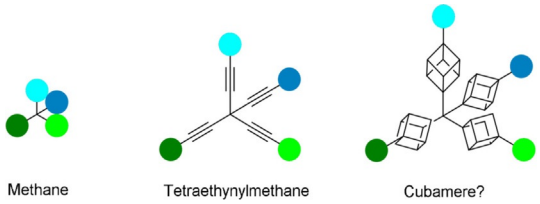

Figure 79. Expanding methane from carbomers to cubamers.

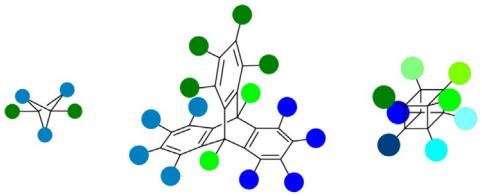

Figure 80. Possible geometrical arrangements of different substituents (indicated by different colors) for key framework molecules.

A rather futuristic approach lies within utilizing rigid linker systems in a dynamic fashion–order and turmoil in one molecule. One might need molecules to be arranged in a certain geometry, but would it not be even more covetable to use a dynamic, covalent approach? Breaking and mending bonds, but still in a defined conformational and, therefore, geometrical distinct fashion. This would create the possibility to use the rigid, but still flexible conformation of the linker molecules to cope with the specialties of the environment. One could imagine a linker which can adjust the overall geometric arrangement of the pharmacophores, to specifically fit into a protein binding pocket? Current work utilizing this shape shifting approach was presented by the Bode group.[439] They incorporated a single ^{13}C-label into the bullvalene backbone and were able to differentiate dissimilar polyols by small changes in the chemical shift and intensities (Figure 81).[440] With the recently developed method by the Fallon group, disubstituted bullvalenes are easily available now and their computational network analysis is a useful tool to understand the energetic landscape of the various isomers.[441]

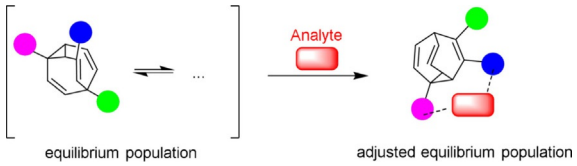

Figure 81. Shape-shifting bullvalene as a dynamic chemical sensor.

A few more examples focus on reversible carbon–carbon bond formations without the presence of heteroatoms are catalyzed olefin[442] or alkyne metathesis[443] or cycloadditions,[444] as shown below (Scheme 31).[445] These systems are interesting since they combine the rigidness of their arrangement with the flexible control of their formation.

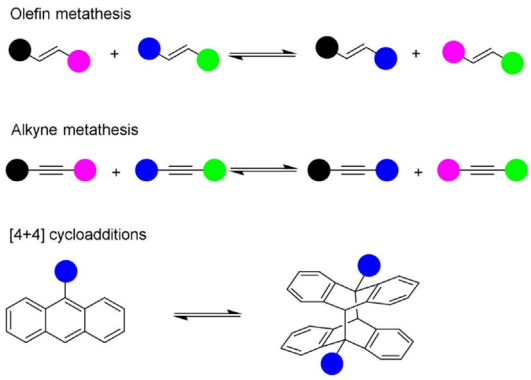

Scheme 31. Dynamic covalent C–C bond formations.

9. Conclusions

In this Review article, the chemistry and applications of different, rigid, nonconjugated, linear hydrocarbons are highlighted. It is hoped that this comprehensive study compiles the relevant information about BCP, BCO, triptycene, and cubane into a "handbook" to provide chemists with the knowledge required to select an appropriate hydrocarbon, depending on their unique needs, whether it be for electron-transfer studies, MOF or liquid crystal constructions, molecular rotors or rods, bioisosteres or drug motifs. What is more, the relevance of these systems has been long overlooked and disregarded because of their different chemistry when compared to the omnipresent benzene or acetylene motifs; thus, their chemistry has been highlighted once more. We hope this Review inspires chemists to develop new and expanding methodologies to access these molecules. The use of these unique scaffolds[446] will leave their shadow-existence once more robust cross-coupling methodologies (sp^3-sp, sp^3-sp^2, sp^3-sp^3) have been developed. Nevertheless, the already prepared systems show highly interesting and unique properties in diverse areas, from bioisosteres to rigid rods. The rapid development within recent years clearly shows the rising interest in these hydrocarbons with many more fascinating developments emerging.

Naturally, there are more compounds that fulfill the requirements of this Review article, such as the rigid-linear hydrocar-

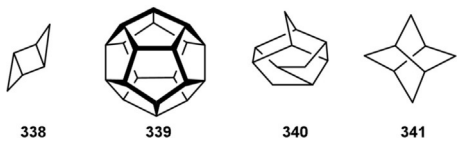

Figure 82. Other rigid hydrocarbons.

bons tricyclo[2.1.0.0^{2,5}]pentane[447] **338**, dodecahedrane[448] **339**, and trishomocubane[449] **340** (Figure 82). Although, in the case of tricyclo[2.1.0.0^{2,5}]pentane, while it satisfies the criteria for this review, the stability of the plain hydrocarbon is too low to be of practical use.[447] Similarly, dodecahedrane has great potential to be used as a linear linker, although its 23 step synthesis and its size limit its applicability in many of the areas outlined. In addition, the chemistry of trishomocubane is underdeveloped, again limiting its use. Additionally, bisnoradamantane **341**, while non-linear, affords four equivalent bridgeheads offering unique opportunities to be used as a rigid hydrocarbon scaffold.[450]

Acknowledgements

This work was supported by grants from the Science Foundation Ireland (SFI IvP 13/IA/1894) and the Irish Research Council (GOIPG/2015/3700).

Conflict of interest

The authors declare no conflict of interest.

Keywords: crystal engineering · electron transfer · liquid crystals · metal–organic frameworks · porphyrins

[1] a) R. Chinchilla, C. Najera, *Chem. Rev.* **2007**, *107*, 874 – 922; b) N. Miyaura, A. Suzuki, *Chem. Rev.* **1995**, *95*, 2457 – 2483.
[2] K. F. Biegasiewicz, J. R. Griffiths, G. P. Savage, J. Tsanaktsidis, R. Priefer, *Chem. Rev.* **2015**, *115*, 6719 – 6745.
[3] A. M. Dilmaç, E. Spuling, A. de Meijere, S. Bräse, *Angew. Chem. Int. Ed.* **2017**, *56*, 5684 – 5718; *Angew. Chem.* **2017**, *129*, 5778 – 5813.
[4] V. Richards, *Nat. Chem.* **2016**, *8*, 1090.
[5] K. B. Wiberg, D. S. Connor, G. M. Lampman, *Tetrahedron Lett.* **1964**, *5*, 531 – 534.
[6] K. B. Wiberg, D. S. Connor, *J. Am. Chem. Soc.* **1966**, *88*, 4437 – 4441.
[7] M. D. Levin, P. Kaszynski, J. Michl, *Chem. Rev.* **2000**, *100*, 169 – 234.
[8] a) K. Semmler, G. Szeimies, J. Belzner, *J. Am. Chem. Soc.* **1985**, *107*, 6410 – 6411; b) J. Belzner, U. Bunz, K. Semmler, G. Szeimies, K. Opitz, A.-D. Schlüter, *Chem. Ber.* **1989**, *122*, 397 – 398; c) M. Werner, D. S. Stephenson, G. Szeimies, *Liebigs Ann.* **1996**, *1996*, 1705 – 1715; d) K. R. Mondanaro, W. P. Dailey, *Org. Synth.* **1998**, *75*, 98.
[9] J. Altman, E. Babad, J. Itzchaki, D. Ginsburg, *Tetrahedron* **1966**, *22*, 279 – 304.
[10] J. F. Chiang, S. H. Bauer, *J. Am. Chem. Soc.* **1970**, *92*, 1614 – 1617.
[11] A. Almenningen, B. Andersen, B. A. Nyhus, P. Beronius, J. E. Engebretsen, L. Ehrenberg, *Acta Chem. Scand.* **1971**, *25*, 1217 – 1223.
[12] K. B. Wiberg, C. M. Hadad, S. Sieber, P. V. R. Schleyer, *J. Am. Chem. Soc.* **1992**, *114*, 5820 – 5828.
[13] K. B. Wiberg, *Angew. Chem. Int. Ed. Engl.* **1986**, *25*, 312 – 322; *Angew. Chem.* **1986**, *98*, 312 – 322.
[14] K. B. Wiberg, *Tetrahedron Lett.* **1985**, *26*, 599 – 602.
[15] H. A. Bent, *Chem. Rev.* **1961**, *61*, 275 – 311.
[16] S. Shahbazian, *Chem. Eur. J.* **2018**, *24*, 5401 – 5405.
[17] M. Messerschmidt, S. Scheins, L. Grubert, M. Pätzel, G. Szeimies, C. Paulmann, P. Luger, *Angew. Chem. Int. Ed.* **2005**, *44*, 3925 – 3928; *Angew. Chem.* **2005**, *117*, 3993 – 3997.
[18] W. Wu, J. Gu, J. Song, S. Shaik, P. C. Hiberty, *Angew. Chem. Int. Ed.* **2009**, *48*, 1407 – 1410; *Angew. Chem.* **2009**, *121*, 1435 – 1438.
[19] V. Galasso, *Chem. Phys. Lett.* **1994**, *230*, 387 – 391.
[20] a) M. Bremer, H. Untenecker, P. A. Gunchenko, A. A. Fokin, P. R. Schreiner, *J. Org. Chem.* **2015**, *80*, 6520 – 6524; b) D. R. Huntley, G. Markopoulos, P. M. Donovan, L. T. Scott, R. Hoffmann, *Angew. Chem. Int. Ed.* **2005**, *44*, 7549 – 7553; *Angew. Chem.* **2005**, *117*, 7721 – 7725.
[21] R. Srinivasan, *J. Am. Chem. Soc.* **1968**, *90*, 2752 – 2754.
[22] K. B. Wiberg, *Chem. Rev.* **1989**, *89*, 975 – 983.
[23] K. Alder, G. Stein, *Justus Liebigs Ann. Chem.* **1934**, *514*, 1 – 13.
[24] O. Diels, K. Alder, *Justus Liebigs Ann. Chem.* **1930**, *478*, 137 – 154.
[25] K. B. Wiberg, G. A. Epling, M. Jason, *J. Am. Chem. Soc.* **1974**, *96*, 912 – 915.
[26] J. J. Dannenberg, T. M. Prociv, C. Hutt, *J. Am. Chem. Soc.* **1974**, *96*, 913 – 914.
[27] W. D. Stohrer, R. Hoffmann, *J. Am. Chem. Soc.* **1972**, *94*, 779 – 786.
[28] A. F. Cameron, G. Ferguson, D. G. Morris, *J. Chem Soc. Chem. Commun.* **1968**, 316 – 316.
[29] O. Ermer, J. D. Dunitz, *J. Chem Soc. Chem. Commun.* **1968**, 567 – 568.
[30] R. B. Turner, W. R. Meador, R. E. Winkler, *J. Am. Chem. Soc.* **1957**, *79*, 4116 – 4121.
[31] J. B. Hendrickson, *J. Am. Chem. Soc.* **1961**, *83*, 4537 – 4547.
[32] a) P. Brüesch, *Spectrochim. Acta* **1966**, *22*, 867 – 875; b) J. J. Macfarlane, I. G. Ross, *J. Chem. Soc.* **1960**, 4169 – 4176; c) A. H. Nethercot, A. Javan, *J. Chem. Phys.* **1953**, *21*, 363 – 364.
[33] P. Brüesch, *Spectrochim. Acta* **1966**, *22*, 861 – 865.
[34] O. Ermer, J. D. Dunitz, *Helv. Chim. Acta* **1969**, *52*, 1861 – 1886.
[35] G. J. Gleicher, P. v. R. Schleyer, *J. Am. Chem. Soc.* **1967**, *89*, 582 – 593.
[36] E. Müller, G. Fiedler, *Chem. Ber.* **1965**, *98*, 3493 – 3500.
[37] L. Zhao, Z. Li, T. Wirth, *Chem. Lett.* **2010**, *39*, 658 – 667.
[38] J. H. Chong, M. J. MacLachlan, *Chem. Soc. Rev.* **2009**, *38*, 3301 – 3315.
[39] P. D. Bartlett, M. J. Ryan, S. G. Cohen, *J. Am. Chem. Soc.* **1942**, *64*, 2649 – 2653.
[40] P. D. Bartlett, L. H. Knox, *J. Am. Chem. Soc.* **1939**, *61*, 3184 – 3192.
[41] P. D. Bartlett, S. G. Cohen, *J. Am. Chem. Soc.* **1940**, *62*, 1183 – 1189.
[42] a) G. Wittig, *Org. Synth.* **1959**, *39*, 75; b) A. Wiehe, M. O. Senge, H. Kurreck, *Liebigs Ann.* **1997**, 1951 – 1963; c) A. Wiehe, M. O. Senge, A. Schäfer, M. Speck, S. Tannert, H. Kurreck, B. Röder, *Tetrahedron* **2001**, *57*, 10089 – 10110.
[43] H. E. Zimmerman, R. M. Paufler, *J. Am. Chem. Soc.* **1960**, *82*, 1514 – 1515.
[44] H. E. Zimmerman, D. Armesto, *Chem. Rev.* **1996**, *96*, 3065 – 3112.
[45] a) L. M. Frutos, U. Sancho, O. Castaño, *Org. Lett.* **2004**, *6*, 1229 – 1231; b) X. Li, T. Liao, L. W. Chung, *J. Am. Chem. Soc.* **2017**, *139*, 16438 – 16441; c) R. A. Matute, K. N. Houk, *Angew. Chem. Int. Ed.* **2012**, *51*, 13097 – 13100; *Angew. Chem.* **2012**, *124*, 13274 – 13277.
[46] H. E. Zimmerman, G. L. Grunewald, *J. Am. Chem. Soc.* **1966**, *88*, 183 – 184.
[47] H. E. Zimmerman, G. L. Grunewald, R. M. Paufler, M. A. Sherwin, *J. Am. Chem. Soc.* **1969**, *91*, 2330 – 2338.
[48] a) H. S. Rzepa, *Chem. Rev.* **2005**, *105*, 3697 – 3715; b) E. Haselbach, L. Neuhaus, R. P. Johnson, K. N. Houk, M. N. Paddon-Row, *Helv. Chim. Acta* **1982**, *65*, 1743 – 1751; c) A. Y. Meyer, R. Pasternak, *Tetrahedron* **1977**, *33*, 3233 – 3237; d) H. E. Zimmerman, *Acc. Chem. Res.* **1971**, *4*, 272 – 280.
[49] R. B. Turner, *J. Am. Chem. Soc.* **1964**, *86*, 3586 – 3589.
[50] a) S. Cossu, S. Battaggia, O. de Lucchi, *J. Org. Chem.* **1997**, *62*, 4162 – 4163; b) M. W. Wagaman, E. Bellmann, M. Cucullu, R. H. Grubbs, *J. Org. Chem.* **1997**, *62*, 9076 – 9082.
[51] E. R. Davidson, *J. Am. Chem. Soc.* **1997**, *119*, 1449 – 1449.
[52] P. E. Eaton, T. W. Cole, *J. Am. Chem. Soc.* **1964**, *86*, 3157 – 3158.
[53] P. E. Eaton, T. W. Cole, *J. Am. Chem. Soc.* **1964**, *86*, 962 – 964.
[54] M. Francl, *Nat. Chem.* **2018**, *10*, 1 – 2.
[55] W. Weltner, *J. Am. Chem. Soc.* **1953**, *75*, 4224 – 4231.
[56] W. v. E. Doering, W. R. Roth, R. Breuckmann, L. Figge, H.-W. Lennartz, W.-D. Fessner, H. Prinzbach, *Chem. Ber.* **1988**, *121*, 1 – 9.
[57] a) N. B. Chapman, J. M. Key, K. J. Toyne, *J. Org. Chem.* **1970**, *35*, 3860 – 3867; b) M. Bliese, J. Tsanaktsidis, *Aust. J. Chem.* **1997**, *50*, 189 – 192;

c) M. J. Falkiner, S. W. Littler, K. J. McRae, G. P. Savage, J. Tsanaktsidis, *Org. Process Res. Dev.* **2013**, *17*, 1503 – 1509.
[58] a) A. de Meijere, S. Redlich, D. Frank, J. Magull, A. Hofmeister, H. Menzel, B. König, J. Svoboda, *Angew. Chem. Int. Ed.* **2007**, *46*, 4658 – 4660; *Angew. Chem.* **2007**, *119*, 4574 – 4576; b) J. C. Barborak, L. Watts, R. Pettit, *J. Am. Chem. Soc.* **1966**, *88*, 1328 – 1329; c) L. F. Pelosi, W. T. Miller, *J. Am. Chem. Soc.* **1976**, *98*, 4311 – 4312; d) R. Gleiter, M. Karcher, *Angew. Chem. Int. Ed. Engl.* **1988**, *27*, 840 – 841; *Angew. Chem.* **1988**, *100*, 851 – 852; e) R. Gleiter, S. Brand, *Tetrahedron Lett.* **1994**, *35*, 4969 – 4972.
[59] P. E. Eaton, J. Tsanaktsidis, *J. Am. Chem. Soc.* **1990**, *112*, 876 – 878.
[60] K. Hassenruck, J. G. Radziszewski, V. Balaji, G. S. Murthy, A. J. McKinley, D. E. David, V. M. Lynch, H. D. Martin, J. Michl, *J. Am. Chem. Soc.* **1990**, *112*, 873 – 874.
[61] D. A. Hrovat, W. T. Borden, *J. Am. Chem. Soc.* **1990**, *112*, 875 – 876.
[62] P. E. Eaton, *Angew. Chem. Int. Ed. Engl.* **1992**, *31*, 1421 – 1436; *Angew. Chem.* **1992**, *104*, 1447 – 1462.
[63] L. Hedberg, K. Hedberg, P. E. Eaton, N. Nodari, A. G. Robiette, *J. Am. Chem. Soc.* **1991**, *113*, 1514 – 1517.
[64] E. B. Fleischer, *J. Am. Chem. Soc.* **1964**, *86*, 3889 – 3890.
[65] A. Almenningen, T. Jonvik, H. D. Martin, T. Urbanek, *J. Mol. Struct.* **1985**, *128*, 239 – 247.
[66] Z. Li, S. L. Anderson, *J. Phys. Chem. A* **2003**, *107*, 1162 – 1174.
[67] B. D. Kybett, S. Carroll, P. Natalis, D. W. Bonnell, J. L. Margrave, J. L. Franklin, *J. Am. Chem. Soc.* **1966**, *88*, 626 – 626.
[68] M. V. Roux, G. Martín-Valcarcel, R. Notario, S. Kini, J. S. Chickos, J. F. Liebman, *J. Chem. Eng. Data* **2011**, *56*, 1220 – 1228.
[69] a) G. W. Griffin, A. P. Marchand, *Chem. Rev.* **1989**, *89*, 997 – 1010; b) F. Agapito, R. C. Santos, R. M. Borges dos Santos, J. A. Martinho Simões, *J. Phys. Chem. A* **2015**, *119*, 2998 – 3007.
[70] a) H. Hopf, in *Classics in Hydrocarbon Chemistry: Syntheses, Concepts, Perspectives*, Wiley-VCH, Weinheim, **2000**, p. 547; b) H. Hopf, J. F. Liebman, H. M. Perks, in *The Chemistry of Functional Groups* (Eds.: Z. Rappoport, J. F. Liebman), Wiley, Chichester, **2005**, pp. 1061 – 1109; c) A. Bashir-Hashemi, H. Higuchi, in *The Chemistry of Functional Groups* (Eds.: Z. Rappoport, J. F. Liebman), Wiley, Chichester, **2005**, pp. 873 – 921.
[71] S. Toyota, *Chem. Rev.* **2010**, *110*, 5398 – 5424.
[72] W. F. Sanjuan-Szklarz, A. A. Hoser, M. Gutmann, A. Ø. Madsen, K. Woźniak, *IUCrJ* **2016**, *3*, 61 – 70.
[73] T. Yildirim, P. M. Gehring, D. A. Neumann, P. E. Eaton, T. Emrick, *Carbon* **1998**, *36*, 809 – 815.
[74] B. A. Chalmers, H. Xing, S. Houston, C. Clark, S. Ghassabian, A. Kuo, B. Cao, A. Reitsma, C.-E. P. Murray, J. E. Stok, G. M. Boyle, C. J. Pierce, S. W. Littler, D. A. Winkler, P. V. Bernhardt, C. Pasay, J. J. De Voss, J. McCarthy, P. G. Parsons, G. H. Walter, M. T. Smith, H. M. Cooper, S. K. Nilsson, J. Tsanaktsidis, G. P. Savage, C. M. Williams, *Angew. Chem. Int. Ed.* **2016**, *55*, 3580 – 3585; *Angew. Chem.* **2016**, *128*, 3644 – 3649.
[75] G. S. Murthy, K. Hassenruck, V. M. Lynch, J. Michl, *J. Am. Chem. Soc.* **1989**, *111*, 7262 – 7263.
[76] J. D. Rehm, B. Ziemer, G. Szeimies, *Eur. J. Org. Chem.* **1999**, 2079 – 2085.
[77] J. L. Adcock, A. A. Gakh, J. L. Pollitte, C. Woods, *J. Am. Chem. Soc.* **1992**, *114*, 3980 – 3981.
[78] P. R. Schreiner, L. V. Chernish, P. A. Gunchenko, E. Y. Tikhonchuk, H. Hausmann, M. Serafin, S. Schlecht, J. E. P. Dahl, R. M. K. Carlson, A. A. Fokin, *Nature* **2011**, *477*, 308 – 311.
[79] N. Muller, D. E. Pritchard, *J. Chem. Phys.* **1959**, *31*, 768 – 780.
[80] H. E. Gottlieb, V. Kotlyar, A. Nudelman, *J. Org. Chem.* **1997**, *62*, 7512 – 7515.
[81] a) A. Yoshimura, J. M. Fuchs, K. R. Middleton, A. V. Maskaev, G. T. Rohde, A. Saito, P. S. Postnikov, M. S. Yusubov, V. N. Nemykin, V. V. Zhdankin, *Chem. Eur. J.* **2017**, *23*, 16738 – 16742; b) R. Mello, M. Fiorentino, C. Fusco, R. Curci, *J. Am. Chem. Soc.* **1989**, *111*, 6749 – 6757.
[82] E. W. Della, P. T. Hine, H. K. Patney, *J. Org. Chem.* **1977**, *42*, 2940 – 2941.
[83] E. W. Della, E. Cotsaris, P. T. Hine, P. E. Pigou, *Aust. J. Chem.* **1981**, *34*, 913 – 916.
[84] C. J. Rhodes, J. C. Walton, E. W. Della, *J. Chem. Soc. Perkin Trans. 2* **1993**, 2125 – 2128.
[85] a) Z. B. Maksić, M. Eckert-Maksić, *Tetrahedron* **1969**, *25*, 5113 – 5114; b) T.-Y. Luh, L. M. Stock, *J. Am. Chem. Soc.* **1974**, *96*, 3712 – 3713.
[86] R. E. Dixon, A. Streitwieser, P. G. Williams, P. E. Eaton, *J. Am. Chem. Soc.* **1991**, *113*, 357 – 358.
[87] A. Streitwieser, Jr., W. R. Young, *J. Am. Chem. Soc.* **1969**, *91*, 529 – 530.
[88] T. W. Cole, C. J. Mayers, L. M. Stock, *J. Am. Chem. Soc.* **1974**, *96*, 4555 – 4557.
[89] W. Adcock, Y. Baran, A. Filippi, M. Speranza, N. A. Trout, *J. Org. Chem.* **2005**, *70*, 1029 – 1034.
[90] a) W. Adcock, A. V. Blokhin, G. M. Elsey, N. H. Head, A. R. Krstic, M. D. Levin, J. Michl, J. Munton, E. Pinkhassik, M. Robert, J.-M. Savéant, A. Shtarev, I. Stibo, *J. Org. Chem.* **1999**, *64*, 2618 – 2625; b) K. Bowden, D. C. Parkin, *Can. J. Chem.* **1969**, *47*, 177 – 183.
[91] K. B. Wiberg, *J. Org. Chem.* **2002**, *67*, 1613 – 1617.
[92] F. H. Allen, *Acta Crystallogr. Sect. B* **1984**, *40*, 64 – 72.
[93] H. Irngartinger, S. Strack, F. Gredel, A. Dreuw, E. W. Della, *Eur. J. Org. Chem.* **1999**, 1253 – 1264.
[94] T. Koopmans, *Physica* **1934**, *1*, 104 – 113.
[95] P. Bischof, P. E. Eaton, R. Gleiter, E. Heilbronner, T. B. Jones, H. Musso, A. Schmelzer, R. Stober, *Helv. Chim. Acta* **1978**, *61*, 547 – 557.
[96] E. Honegger, E. Heilbronner, T. Urbanek, H.-D. Martin, *Helv. Chim. Acta* **1985**, *68*, 23 – 38.
[97] E. Honegger, E. Heilbronner, N. Heß, H.-D. Martin, *Chem. Ber.* **1987**, *120*, 187 – 193.
[98] R. Gleiter, K.-H. Pfeifer, G. Szeimies, U. Bunz, *Angew. Chem. Int. Ed. Engl.* **1990**, *29*, 413 – 415; *Angew. Chem.* **1990**, *102*, 418 – 420.
[99] M. Ehara, S. Fukawa, H. Nakatsuji, D. E. David, E. Z. Pinkhassik, M. D. Levin, M. Apostol, J. Michl, *Chem. Asian J.* **2007**, *2*, 1007 – 1019.
[100] M. Braga, *Chem. Phys.* **1996**, *213*, 159 – 164.
[101] O. Schafer, M. Allan, G. Szeimies, M. Sanktjohanser, *Chem. Phys. Lett.* **1992**, *195*, 293 – 297.
[102] a) J. R. Winkler, H. B. Gray, *J. Am. Chem. Soc.* **2014**, *136*, 2930 – 2939; b) C. Liang, M. D. Newton, *J. Phys. Chem.* **1993**, *97*, 3199 – 3211; c) M. N. Paddon-Row, K. D. Jordan, *J. Am. Chem. Soc.* **1993**, *115*, 2952 – 2960.
[103] A. Baeyer, *Ber. Dtsch. Chem. Ges.* **1885**, *18*, 2269 – 2281.
[104] a) K. S. Pitzer, *J. Chem. Phys.* **1937**, *5*, 473; b) J. D. Kemp, K. S. Pitzer, *J. Chem. Phys.* **1936**, *4*, 749 – 750.
[105] J. D. Dunitz, V. Prelog, *Angew. Chem.* **1960**, *72*, 896 – 902.
[106] J. W. Knowlton, F. D. Rossini, *J. Res. Natl. Bur. Stand.* **1949**, *43*, 113 – 115.
[107] S. W. Slayden, J. F. Liebman, *Chem. Rev.* **2001**, *101*, 1541 – 1566.
[108] E. J. Prosen, W. H. Johnson, F. D. Rossini, *J. Res. Natl. Bur. Stand.* **1946**, *37*, 51 – 56.
[109] K. B. Wiberg, G. Bonneville, R. Dempsey, *Isr. J. Chem.* **1983**, *23*, 85 – 92.
[110] W.-K. Wong, E. F. Westrum, *J. Phys. Chem.* **1970**, *74*, 1303 – 1308.
[111] D. L. Rodgers, E. F. Westrum, J. T. S. Andrews, *J. Chem. Thermodyn.* **1973**, *5*, 733 – 739.
[112] J. F. Liebman, A. Greenberg, *Chem. Rev.* **1976**, *76*, 311 – 365.
[113] I. Alkorta, N. Campillo, I. Rozas, J. Elguero, *J. Org. Chem.* **1998**, *63*, 7759 – 7763.
[114] J. I.-C. Wu, P. v. R. Schleyer, *Pure Appl. Chem.* **2013**, *85*, 921 – 940.
[115] D. A. Hrovat, W. T. Borden, *J. Am. Chem. Soc.* **1990**, *112*, 3227 – 3228.
[116] J. M. Lehn, G. Wipff, *Chem. Phys. Lett.* **1972**, *15*, 450 – 454.
[117] a) K. B. Wiberg, Z. van Williams, *J. Am. Chem. Soc.* **1967**, *89*, 3373 – 3374; b) K. B. Wiberg, N. McMurdie, *J. Am. Chem. Soc.* **1994**, *116*, 11990 – 11998.
[118] a) S. Vázquez, P. Camps, *Tetrahedron* **2005**, *61*, 5147 – 5208; b) D. A. Hrovat, W. T. Borden, *J. Am. Chem. Soc.* **1988**, *110*, 4710 – 4718.
[119] P. E. Eaton, J. P. Zhou, *J. Am. Chem. Soc.* **1992**, *114*, 3118 – 3120.
[120] R. M. Moriarty, S. M. Tuladhar, R. Penmasta, A. K. Awasthi, *J. Am. Chem. Soc.* **1990**, *112*, 3228 – 3230.
[121] W. T. Borden, *Chem. Rev.* **1989**, *89*, 1095 – 1109.
[122] P. E. Eaton, C. X. Yang, Y. Xiong, *J. Am. Chem. Soc.* **1990**, *112*, 3225 – 3226.
[123] R. J. Doedens, P. E. Eaton, E. B. Fleischer, *Eur. J. Org. Chem.* **2017**, 2627 – 2630.
[124] Y. P. Auberson, C. Brocklehurst, M. Furegati, T. C. Fessard, G. Koch, A. Decker, L. La Vecchia, E. Briard, *ChemMedChem* **2017**, *12*, 590 – 598.
[125] D. N. Kevill, M. J. D'Souza, R. M. Moriarty, S. M. Tuladhar, R. Penmasta, A. K. Awasthi, *J. Chem. Soc. Chem. Commun.* **1990**, 623 – 624.
[126] S. Jalife, S. Mondal, J. L. Cabellos, G. Martinez-Guajardo, M. A. Fernandez-Herrera, G. Merino, *Chem. Commun.* **2016**, *52*, 3403 – 3405.
[127] C. W. Jefford, R. M. McCreadie, P. Muller, B. Siegfried, *J. Chem. Educ.* **1971**, *48*, 708 – 710.

[128] J. W. Wilt, T. P. Malloy, *J. Org. Chem.* **1972**, *37*, 2781 – 2782.
[129] T. W. Cole, PhD Thesis, University of Chicago, Chicago, IL, **1966**.
[130] B. J. Smith, J. Tsanaktsidis, *J. Org. Chem.* **1997**, *62*, 5709 – 5712.
[131] Z. Tian, S. R. Kass, *Chem. Rev.* **2013**, *113*, 6986 – 7010.
[132] C. H. DePuy, S. Gronert, S. E. Barlow, V. M. Bierbaum, R. Damrauer, *J. Am. Chem. Soc.* **1989**, *111*, 1968 – 1973.
[133] a) C. H. DePuy, V. M. Bierbaum, L. A. Flippin, J. J. Grabowski, G. K. King, R. J. Schmitt, *J. Am. Chem. Soc.* **1979**, *101*, 6443 – 6445; b) C. H. DePuy, V. M. Bierbaum, L. A. Flippin, J. J. Grabowski, G. K. King, R. J. Schmitt, S. A. Sullivan, *J. Am. Chem. Soc.* **1980**, *102*, 5012 – 5015.
[134] E. E. Ferguson, F. C. Fehsenfeld, A. L. Schmeltekopf, in *Advances in Atomic, Molecular, and Optical Physics* (Ed.: D. R. Bates), Academic Press, Boston, **1965**, pp. 1 – 56.
[135] J. L. Beauchamp, L. R. Anders, J. D. Baldeschwieler, *J. Am. Chem. Soc.* **1967**, *89*, 4569 – 4577.
[136] C. H. DePuy, V. M. Bierbaum, R. Damrauer, *J. Am. Chem. Soc.* **1984**, *106*, 4051 – 4053.
[137] A. Fattahi, L. Lis, Z. A. Tehrani, S. S. Marimanikkuppam, S. R. Kass, *J. Org. Chem.* **2012**, *77*, 1909 – 1914.
[138] X.-S. Xue, P. Ji, B. Zhou, J.-P. Cheng, *Chem. Rev.* **2017**, *117*, 8622 – 8648.
[139] A. Fattahi, R. E. McCarthy, M. R. Ahmad, S. R. Kass, *J. Am. Chem. Soc.* **2003**, *125*, 11746 – 11750.
[140] a) R. A. Seburg, R. R. Squires, *Int. J. Mass. Spectrom.* **1997**, *167 – 168*, 541 – 557; b) D. R. Reed, S. R. Kass, K. R. Mondanaro, W. P. Dailey, *J. Am. Chem. Soc.* **2002**, *124*, 2790 – 2795; c) M. Hare, T. Emrick, P. E. Eaton, S. R. Kass, *J. Am. Chem. Soc.* **1997**, *119*, 237 – 238; d) R. R. Sauers, *Tetrahedron* **1999**, *55*, 10013 – 10026.
[141] J. M. Lehn, G. Wipff, *Tetrahedron Lett.* **1980**, *21*, 159 – 162.
[142] J. Bredt, *Justus Liebigs Ann. der Chem.* **1924**, *437*, 1 – 13.
[143] J. C. Walton, *Chem. Soc. Rev.* **1992**, *21*, 105 – 112.
[144] E. W. Della, G. M. Elsey, N. J. Head, J. C. Walton, *J. Chem. Soc. Chem. Commun.* **1990**, 1589 – 1591.
[145] R. R. Sauers, *Comput. Theor. Chem.* **2011**, *970*, 73 – 78.
[146] B. Maillard, J. C. Walton, *J. Chem. Soc. Chem. Commun.* **1983**, *16*, 900 – 901.
[147] M. Ohsaku, A. Imamura, K. Hirao, T. Kawamura, *Tetrahedron* **1979**, *35*, 701 – 706.
[148] J. W. Verhoeven, *Recl. Trav. Chim. Pays-Bas* **1980**, *99*, 369 – 379.
[149] G. T. Binmore, J. C. Walton, W. Adcock, C. I. Clark, A. R. Kristic, *Magn. Reson. Chem.* **1995**, *33*, S53 – S59.
[150] P. J. Krusic, T. A. Rettig, P. v. R. Schleyer, *J. Am. Chem. Soc.* **1972**, *94*, 995 – 997.
[151] J. C. Walton, *J. Chem. Soc. Perkin Trans. 2* **1987**, *2*, 231 – 235.
[152] a) P. R. Schreiner, A. Wittkopp, P. A. Gunchenko, A. I. Yaroshinsky, S. A. Peleshanko, A. A. Fokin, *Chem. Eur. J.* **2001**, *7*, 2739 – 2744; b) X. Z. Qin, A. D. Trifunac, P. E. Eaton, Y. Xiong, *J. Am. Chem. Soc.* **1990**, *112*, 4565 – 4567; c) A. Marcinek, J. Rogowski, J. Gébicki, G.-F. Chen, F. Williams, *J. Phys. Chem. A* **2000**, *104*, 5265 – 5268.
[153] H.-D. Martin, T. Urbanek, P. Pföhler, R. Walsh, *J. Chem. Soc. Chem. Commun.* **1985**, 964 – 965.
[154] P. E. Eaton, L. Cassar, J. Halpern, *J. Am. Chem. Soc.* **1970**, *92*, 6366 – 6368.
[155] a) S. Moss, B. T. King, A. de Meijere, S. I. Kozhushkov, P. E. Eaton, J. Michl, *Org. Lett.* **2001**, *3*, 2375 – 2377; b) G. Durkó, I. Jalsovszky, *Tetrahedron* **2013**, *69*, 5160 – 5163.
[156] L. Cassar, P. E. Eaton, J. Halpern, *J. Am. Chem. Soc.* **1970**, *92*, 3515 – 3518.
[157] K. B. Wiberg, S. T. Waddell, *J. Am. Chem. Soc.* **1990**, *112*, 2194 – 2216.
[158] D. H. R. Barton, D. Crich, W. B. Motherwell, *J. Chem. Soc. Chem. Commun.* **1983**, 939 – 942.
[159] P. E. Eaton, Y. C. Yip, *J. Am. Chem. Soc.* **1991**, *113*, 7692 – 7697.
[160] S. Y. Choi, P. E. Eaton, M. Newcomb, Y. C. Yip, *J. Am. Chem. Soc.* **1992**, *114*, 6326 – 6329.
[161] B. P. Branchaud, A. G. Glenn, H. C. Stiasny, *J. Org. Chem.* **1991**, *56*, 6656 – 6659.
[162] P. E. Eaton, K. L. Hoffmann, *J. Am. Chem. Soc.* **1987**, *109*, 5285 – 5286.
[163] N. Chen, M. Jones, *J. Phys. Org. Chem.* **1988**, *1*, 305 – 308.
[164] P. E. Eaton, R. B. Appell, *J. Am. Chem. Soc.* **1990**, *112*, 4055 – 4057.
[165] N. Chen, M. Jones, W. R. White, M. S. Platz, *J. Am. Chem. Soc.* **1991**, *113*, 4981 – 4992.
[166] R. Stober, H. Musso, *Angew. Chem. Int. Ed. Engl.* **1977**, *16*, 415 – 416; *Angew. Chem.* **1977**, *89*, 430 – 431.
[167] R. Stober, H. Musso, E. Ōsawa, *Tetrahedron* **1986**, *42*, 1757 – 1761.
[168] A. J. H. Klunder, B. Zwanenburg, *Tetrahedron* **1975**, *31*, 1419 – 1426.
[169] V. M. Carroll, D. N. Harpp, R. Priefer, *Tetrahedron Lett.* **2008**, *49*, 2677 – 2680.
[170] A. Fasolini, *Master Thesis*, University of Bologna, Bologna, **2016**.
[171] A.-D. Schlüter, *Macromolecules* **1988**, *21*, 1208 – 1211; A.-D. Schlüter, *Angew. Chem. Int. Ed. Engl.* **1988**, *27*, 296 – 298; *Angew. Chem.* **1988**, *100*, 283 – 285.
[172] R. M. Bär, S. Kirschner, M. Nieger, S. Bräse, *Chem. Eur. J.* **2018**, *24*, 1373 – 1382.
[173] P. Kaszynski, J. Michl, *The Chemistry of the Cyclopropyl Group: Supplement*, Wiley, Chichester, **1995**.
[174] J. Waser, E. M. Carreira, *Angew. Chem. Int. Ed.* **2004**, *43*, 4099 – 4102; *Angew. Chem.* **2004**, *116*, 4191 – 4194.
[175] K. D. Bunker, N. W. Sach, Q. Huang, P. F. Richardson, *Org. Lett.* **2011**, *13*, 4746 – 4748.
[176] J. Kanazawa, K. Maeda, M. Uchiyama, *J. Am. Chem. Soc.* **2017**, *139*, 17791 – 17794.
[177] R. Gianatassio, J. M. Lopchuk, J. Wang, C.-M. Pan, L. R. Malins, L. Prieto, T. A. Brandt, M. R. Collins, G. M. Gallego, N. W. Sach, J. E. Spangler, H. Zhu, J. Zhu, P. S. Baran, *Science* **2016**, *351*, 241 – 246.
[178] M. Messner, S. I. Kozhushkov, A. de Meijere, *Eur. J. Org. Chem.* **2000**, 1137 – 1155.
[179] I. S. Makarov, C. E. Brocklehurst, K. Karaghiosoff, G. Koch, P. Knochel, *Angew. Chem. Int. Ed.* **2017**, *56*, 12774 – 12777; *Angew. Chem.* **2017**, *129*, 12949 – 12953.
[180] D. F. J. Caputo, C. Arroniz, A. B. Dürr, J. J. Mousseau, A. F. Stepan, S. J. Mansfield, E. A. Anderson, *Chem. Sci.* **2018**, *9*, 5295 – 5300.
[181] R. J. Ranson, R. M. G. Roberts, *J. Organomet. Chem.* **1976**, *107*, 295 – 300.
[182] V. I. Dodero, M. B. Faraoni, D. C. Gerbino, L. C. Koll, A. E. Zúñiga, T. N. Mitchell, J. C. Podestá, *Organometallics* **2005**, *24*, 1992 – 1995.
[183] Y. Kawada, H. Iwamura, *J. Org. Chem.* **1981**, *46*, 3357 – 3359.
[184] Z. Zielinski, N. Presseau, R. Amorati, L. Valgimigli, D. A. Pratt, *J. Am. Chem. Soc.* **2014**, *136*, 1570 – 1578.
[185] T. Nakamoto, S. Hayashi, W. Nakanishi, *J. Org. Chem.* **2008**, *73*, 9259 – 9263.
[186] R. J. Baker, M. Brym, C. Jones, M. Waugh, *J. Organomet. Chem.* **2004**, *689*, 781 – 790.
[187] P. D. Bartlett, F. D. Greene, *J. Am. Chem. Soc.* **1954**, *76*, 1088 – 1096.
[188] K. Okada, K. Okamoto, M. Oda, *J. Chem. Soc. Chem. Commun.* **1989**, 1636 – 1637.
[189] M. J. S. Dewar, R. S. Goldberg, *J. Am. Chem. Soc.* **1970**, *92*, 1582 – 1586.
[190] K. B. Wiberg, W. E. Pratt, W. F. Bailey, *J. Am. Chem. Soc.* **1977**, *99*, 2297 – 2302.
[191] K. Higashiguchi, K. Yumoto, K. Matsuda, *Org. Lett.* **2010**, *12*, 5284 – 5286.
[192] W. Adcock, G. B. Kok, *J. Org. Chem.* **1985**, *50*, 1079 – 1087.
[193] X. Qian, A. Auffrant, A. Felouat, C. Gosmini, *Angew. Chem. Int. Ed.* **2011**, *50*, 10402 – 10405; *Angew. Chem.* **2011**, *123*, 10586 – 10589.
[194] W. Adam, F. Mazenod, Y. Nishizawa, P. S. Engel, S. A. Baughman, W.-K. Chae, D. W. Horsey, H. Quast, B. Seiferling, *J. Am. Chem. Soc.* **1983**, *105*, 6141 – 6145.
[195] R. H. Pouwer, J. B. Harper, K. Vyakaranam, J. Michl, C. M. Williams, C. H. Jessen, P. V. Bernhardt, *Eur. J. Org. Chem.* **2007**, 241 – 248.
[196] F. Toriyama, J. Cornella, L. Wimmer, T.-G. Chen, D. D. Dixon, G. Creech, P. S. Baran, *J. Am. Chem. Soc.* **2016**, *138*, 11132 – 11135.
[197] C. Li, J. Wang, L. M. Barton, S. Yu, M. Tian, D. S. Peters, M. Kumar, A. W. Yu, K. A. Johnson, A. K. Chatterjee, M. Yan, P. S. Baran, *Science* **2017**, *356*, eaam7355.
[198] A. Fawcett, J. Pradeilles, Y. Wang, T. Mutsuga, E. L. Myers, V. K. Aggarwal, *Science* **2017**, *357*, 283 – 286.
[199] J. M. Smith, T. Qin, R. R. Merchant, J. T. Edwards, L. R. Malins, Z. Liu, G. Che, Z. Shen, S. A. Shaw, M. D. Eastgate, P. S. Baran, *Angew. Chem. Int. Ed.* **2017**, *56*, 11906 – 11910; *Angew. Chem.* **2017**, *129*, 12068 – 12072.
[200] J. T. Edwards, R. R. Merchant, K. S. McClymont, K. W. Knouse, T. Qin, L. R. Malins, B. Vokits, S. A. Shaw, D.-H. Bao, F.-L. Wei, T. Zhou, M. D. Eastgate, P. S. Baran, *Nature* **2017**, *545*, 213 – 218.

[201] R. R. Merchant, J. T. Edwards, T. Qin, M. M. Kruszyk, C. Bi, G. Che, D.-H. Bao, W. Qiao, L. Sun, M. R. Collins, O. O. Fadeyi, G. M. Gallego, J. J. Mousseau, P. Nuhant, P. S. Baran, *Science* **2018**, *360*, 75 – 80.
[202] D. W. C. MacMillan, Y. Liang, X. Zhang, Decarboxylative sp^3 C–N Coupling via Dual Copper/Photoredox Catalysis, ChemRxiv, **2018**.
[203] T. Patra, D. Maiti, *Chem. Eur. J.* **2017**, *23*, 7382 – 7401.
[204] R. M. Moriarty, J. S. Khosrowshahi, T. M. Dalecki, *J. Chem. Soc. Chem. Commun.* **1987**, 675 – 676.
[205] G. A. Olah, C. S. Lee, G. K. S. Prakash, R. M. Moriarty, M. S. C. Rao, *J. Am. Chem. Soc.* **1993**, *115*, 10728 – 10732.
[206] J. Wlochal, R. D. M. Davies, J. Burton, *Org. Lett.* **2014**, *16*, 4094 – 4097.
[207] S. Plunkett, K. J. Flanagan, B. Twamley, M. O. Senge, *Organometallics* **2015**, *34*, 1408 – 1414.
[208] S. Bernhard, G. Locke, S. Plunkett, A. Meindl, K. Flanagan, M. O. Senge, *Chem. Eur. J.* **2018**, *24*, 1026 – 1030.
[209] T. Qin, L. R. Malins, J. T. Edwards, R. R. Merchant, A. J. E. Novak, J. Z. Zhong, R. B. Mills, M. Yan, C. Yuan, M. D. Eastgate, P. S. Baran, *Angew. Chem. Int. Ed.* **2017**, *56*, 260 – 265; *Angew. Chem.* **2017**, *129*, 266 – 271.
[210] R. Gianatassio, S. Kawamura, C. L. Eprile, K. Foo, J. Ge, A. C. Burns, M. R. Collins, P. S. Baran, *Angew. Chem. Int. Ed.* **2014**, *53*, 9851 – 9855; *Angew. Chem.* **2014**, *126*, 10009 – 10013.
[211] a) G. M. Locke, M. O. Senge, *ECS Trans.* **2016**, *72*, 1 – 11; b) A. A. Ryan, M. O. Senge, *Photochem. Photobiol. Sci.* **2015**, *14*, 638 – 660.
[212] a) G. McDermott, S. M. Prince, A. A. Freer, A. M. Hawthornthwaite-Lawless, M. Z. Papiz, R. J. Cogdell, N. W. Isaacs, *Nature* **1995**, *374*, 517 – 521; b) M. O. Senge, A. A. Ryan, K. A. Letchford, S. A. MacGowan, T. Mielke, *Symmetry* **2014**, *6*, 781 – 843; c) M. R. Wasielewski, *Chem. Rev.* **1992**, *92*, 435 – 461; d) H. Kurreck, M. Huber, *Angew. Chem. Int. Ed. Engl.* **1995**, *34*, 849 – 866; *Angew. Chem.* **1995**, *107*, 929 – 947; e) D. Gust, T. A. Moore, A. L. Moore, *Acc. Chem. Res.* **1995**, *28*, 40 – 48; f) Q. F. Yan, Z. Y. Luo, K. Cai, Y. G. Ma, D. H. Zhao, *Chem. Soc. Rev.* **2014**, *43*, 4199 – 4221.
[213] H. E. Zimmerman, T. D. Goldman, T. K. Hirzel, S. P. Schmidt, *J. Org. Chem.* **1980**, *45*, 3933 – 3951.
[214] H. E. Zimmerman, Y. A. Lapin, E. E. Nesterov, G. A. Sereda, *J. Org. Chem.* **2000**, *65*, 7740 – 7746.
[215] H. Hokari, U. Akiba, M. Fujihira, *J. Chem. Soc. Chem. Commun.* **1995**, *180*, 2139 – 2140.
[216] H. Langhals, A. J. Esterbauer, A. Walter, E. Riedle, I. Pugliesi, *J. Am. Chem. Soc.* **2010**, *132*, 16777 – 16782.
[217] A. de Meijere, L. Zhao, V. N. Belov, M. Bossi, M. Noltemeyer, S. W. Hell, *Chem. Eur. J.* **2007**, *13*, 2503 – 2516.
[218] A. Karimata, H. Kawauchi, S. Suzuki, M. Kozaki, N. Ikeda, K. Keyaki, K. Nozaki, K. Akiyama, K. Okada, *Chem. Lett.* **2013**, *42*, 794 – 830.
[219] D. E. Stasiw, J. Zhang, G. Wang, R. Dangi, B. W. Stein, D. A. Shultz, M. L. Kirk, L. Wojtas, R. D. Sommer, *J. Am. Chem. Soc.* **2015**, *137*, 9222 – 9225.
[220] R. H. Goldsmith, J. Vura-Weis, A. M. Scott, S. Borkar, A. Sen, M. A. Ratner, M. R. Wasielewski, *J. Am. Chem. Soc.* **2008**, *130*, 7659 – 7669.
[221] H. E. Zimmerman, R. D. McKelvey, *J. Am. Chem. Soc.* **1971**, *93*, 3638 – 3645.
[222] a) R. A. Keller, L. J. Dolby, *J. Am. Chem. Soc.* **1969**, *91*, 1293 – 1299; b) S. A. Latt, H. T. Cheung, E. R. Blout, *J. Am. Chem. Soc.* **1965**, *87*, 995 – 1003; c) A. A. Lamola, *J. Am. Chem. Soc.* **1969**, *91*, 4786 – 4790.
[223] H. E. Zimmerman, R. K. King, M. B. Meinhardt, *J. Org. Chem.* **1992**, *57*, 5484 – 5492.
[224] a) D. J. Wold, R. Haag, M. A. Rampi, C. D. Frisbie, *J. Phys. Chem. B* **2002**, *106*, 2813 – 2816; b) T. Ishida, W. Mizutani, Y. Aya, H. Ogiso, S. Sasaki, H. Tokumoto, *J. Phys. Chem. B* **2002**, *106*, 5886 – 5892.
[225] B. Schlicke, P. Belser, L. de Cola, E. Sabbioni, V. Balzani, *J. Am. Chem. Soc.* **1999**, *121*, 4207 – 4214.
[226] a) E. A. Weiss, M. J. Ahrens, L. E. Sinks, A. V. Gusev, M. A. Ratner, M. R. Wasielewski, *J. Am. Chem. Soc.* **2004**, *126*, 5577 – 5584; b) W. Wang, S. Wang, X. Li, J.-P. Collin, J. Liu, P. N. Liu, N. Lin, *J. Am. Chem. Soc.* **2010**, *132*, 8774 – 8778.
[227] B. O. Jahn, H. Ottosson, M. Galperin, J. Fransson, *ACS Nano* **2013**, *7*, 1064 – 1071.
[228] K. E. Drexler, Nanosystems: Moleculur Machinery, Manufacturing and Computation, Wiley, New York, **1992**.
[229] F. Vögtle, M. Frank, P. Belser, A. von Zelewsky, V. Balzani, L. de Cola, F. Barigelletti, L. Flamigni, M. Nieger, *Angew. Chem. Int. Ed. Engl.* **1993**, *32*, 1643 – 1646; *Angew. Chem.* **1993**, *105*, 1706 – 1709.
[230] a) L. Hammarström, F. Barigelletti, L. Flamigni, N. Armaroli, A. Sour, J.-P. Collin, J.-P. Sauvage, *J. Am. Chem. Soc.* **1996**, *118*, 11972 – 11973; b) F. Barigelletti, L. Flamigni, J.-P. Collin, J.-P. Sauvage, *Chem. Commun.* **1997**, 333 – 410.
[231] Q. Wei, E. Galoppini, *Tetrahedron* **2004**, *60*, 8497 – 8508.
[232] G. Vives, A. Gonzalez, J. Jaud, J.-P. Launay, G. Rapenne, *Chem. Eur. J.* **2007**, *13*, 5622 – 5631.
[233] P. F. H. Schwab, M. D. Levin, J. Michl, *Chem. Rev.* **1999**, *99*, 1863 – 1934.
[234] A. Carella, G. Rapenne, J.-P. Launay, *New J. Chem.* **2005**, *29*, 288 – 290.
[235] A. Juris, V. Balzani, F. Barigelletti, S. Campagna, P. Belser, A. von Zelewsky, *Coord. Chem. Rev.* **1988**, *84*, 85 – 277.
[236] A. Beyeler, P. Belser, *Coord. Chem. Rev.* **2002**, *230*, 29 – 39.
[237] a) M. O. Senge, *Chem. Commun.* **2006**, 243 – 256; b) M. O. Senge, *Chem. Commun.* **2011**, *47*, 1943 – 1960; c) M. O. Senge, S. A. MacGowan, J. M. O'Brien, *Chem. Commun.* **2015**, *51*, 17031 – 17063.
[238] a) J. R. Bolton, T.-F. Ho, S. Liauw, A. Siemiarczuk, C. S. K. Wan, A. C. Weedon, *J. Chem. Soc. Chem. Commun.* **1985**, 559 – 560; b) D. N. Beratan, *J. Am. Chem. Soc.* **1986**, *108*, 4321 – 4326; c) A. D. Joran, B. A. Leland, G. G. Geller, J. J. Hopfield, P. B. Dervan, *J. Am. Chem. Soc.* **1984**, *106*, 6090 – 6092.
[239] a) L. M. Urner, M. Sekita, N. Trapp, W. B. Schweizer, M. Wörle, J.-P. Gisselbrecht, C. Boudon, D. M. Guldi, F. Diederich, *Eur. J. Org. Chem.* **2015**, 91 – 108; b) T. A. Reekie, M. Sekita, L. M. Urner, S. Bauroth, L. Ruhlmann, J.-P. Gisselbrecht, C. Boudon, N. Trapp, T. Clark, D. M. Guldi, F. Diederich, *Chem. Eur. J.* **2017**, *23*, 6357 – 6369.
[240] a) A. Osuka, R.-P. Zhang, K. Maruyama, N. Mataga, Y. Tanaka, T. Okada, *Chem. Phys. Lett.* **1993**, *215*, 179 – 184; b) A. Osuka, R.-P. Zhang, K. Maruyama, T. Ohno, K. Nozaki, *Bull. Chem. Soc. Jpn.* **1993**, *66*, 3773 – 3782.
[241] C. F. Portela, J. Brunckova, J. L. Richards, B. Schöllhorn, Y. Iamamoto, D. Magde, T. G. Traylor, C. L. Perrin, *J. Phys. Chem. A* **1999**, *103*, 10540 – 10552.
[242] J. Andréasson, G. Kodis, T. Ljungdahl, A. L. Moore, T. A. Moore, D. Gust, J. Mårtensson, B. Albinsson, *J. Phys. Chem. A* **2003**, *107*, 8825 – 8833.
[243] K. Pettersson, K. Kilså, J. Mårtensson, B. Albinsson, *J. Am. Chem. Soc.* **2004**, *126*, 6710 – 6719.
[244] K. Pettersson, A. Kyrychenko, E. Rönnow, T. Ljungdahl, J. Mårtensson, B. Albinsson, *J. Phys. Chem. A* **2006**, *110*, 310 – 318.
[245] a) H. Lodish, S. L. Zipursky, P. Matsudaira, D. Baltimore, J. Darnell, *Molecular Cell Biology*, W. H. Freeman and Company, New York, **2000**; b) D. Bray, *Cell Movements: From Molecules to Mobility*, Garland, New York, **2001**; c) J. Howard, *Mechanics of Motor Proteins and the Cytoskeleton*, Sinauer Associates, Sunderland, **2001**; d) M. Schliwa, G. Woehlke, *Nature* **2003**, *422*, 759 – 765; e) A. B. Kolomeisky, M. E. Fisher, *Annu. Rev. Phys. Chem.* **2007**, *58*, 675 – 695; f) V. Balzani, M. Gómez-López, J. F. Stoddart, *Acc. Chem. Res.* **1998**, *31*, 405 – 414; g) K. Kinbara, T. Aida, *Chem. Rev.* **2005**, *105*, 1377 – 1400.
[246] A. G. Douglass, B. Both, P. Kaszynski, *J. Mater. Chem.* **1999**, *9*, 683 – 686.
[247] H. M. Abdullah, G. W. Gray, K. J. Toyne, *Mol. Cryst. Liq. Cryst.* **1985**, *124*, 105 – 114.
[248] a) D. Demus, H.-J. Deutscher, F. Kuschel, H. Schubert, DDR Patent: 1974/105,701; b) D. Demus, *Son-emissive Electrooptic Displays*, Plenum, New York, **1976**.
[249] G. W. Gray, S. M. Kelly, *J. Chem. Soc. Perkin Trans. 2* **1981**, 26 – 31.
[250] G. W. Gray, S. M. Kelly, *J. Chem. Soc. Chem. Commun.* **1979**, 974 – 975.
[251] a) G. W. Gray, S. M. Kelly, *Angew. Chem. Int. Ed. Engl.* **1981**, *20*, 393 – 394; *Angew. Chem.* **1981**, *93*, 412 – 415; b) G. W. Gray, *Advances in Liquid Crystals*, Academic Press, New York, **1976**.
[252] G. W. Gray, S. M. Kelly, *Mol. Cryst. Liq. Cryst.* **1981**, *75*, 95 – 108.
[253] G. W. Gray, S. M. Kelly, *J. Mater. Chem.* **1999**, *9*, 2037 – 2050.
[254] H. J. Deutscher, R. Frach, C. Tschierske, H. Zaschke, in *Selected Topics in Liquid Crystal Research* (Ed.: H.-D. Koswig), Akademie, Berlin, **1990**.
[255] P. Kaszynski, A. Januszko, K. Ohta, T. Nagamine, P. Potaczek, V. G. Young, Y. Endo, *Liq. Cryst.* **2008**, *35*, 1169 – 1190.
[256] A. Jankowiak, P. Kaszynski, W. R. Tilford, K. Ohta, A. Januszko, T. Nagamine, Y. Endo, *Beilstein J. Org. Chem.* **2009**, *5*, 83.
[257] G. W. Gray, M. Hird, K. J. Toyne, *Mol. Cryst. Liq. Cryst.* **1991**, *204*, 91 – 110.
[258] R. C. Geivandov, V. Mezhnev, T. Geivandova, *Mol. Cryst. Liq. Cryst.* **2011**, *542*, 106 – 114.
[259] a) A. Januszko, K. L. Glab, P. Kaszynski, K. Patel, R. A. Lewis, G. H. Mehl, M. D. Wand, *J. Mater. Chem.* **2006**, *16*, 3183 – 3192; b) M. Jasinski, A.

Jankowiak, A. Januszko, M. Bremer, D. Pauluth, P. Kaszynski, *Liq. Cryst.* **2008**, *35*, 343 – 350.
[260] A. Januszko, K. L. Glab, P. Kaszynski, *Liq. Cryst.* **2008**, *35*, 549 – 553.
[261] A. de Meijere, M. Messner, V. Vill, *Mol. Cryst. Liq. Cryst. Sci. Technol. Sect. A* **1994**, *257*, 161 – 167.
[262] C. Ramireddy, V. S. Reddy, P. Munk, C. N. Wu, *Macromolecules* **1991**, *24*, 1387 – 1391.
[263] K. J. Toyne, *Thermotropic Liquid Crystals*, Wiley, New York, **1987**.
[264] P. Kaszynski, A. C. Friedli, J. Michl, *Mol. Cryst. Liq. Cryst. Lett.* **1988**, *6*, 27 – 33.
[265] V. Reiffenrath, F. Z. Schneider, *Z. Naturforsch.* **1981**, *36a*, 1006 – 1008.
[266] S. S. Kuduva, D. C. Craig, A. Nangia, G. R. Desiraju, *J. Am. Chem. Soc.* **1999**, *121*, 1936 – 1944.
[267] D. Das, R. K. R. Jetti, R. Boese, G. R. Desiraju, *Cryst. Growth Des.* **2003**, *3*, 675 – 681.
[268] S. S. Kuduva, D. Bläser, R. Boese, G. R. Desiraju, *J. Org. Chem.* **2001**, *66*, 1621 – 1626.
[269] J. Echeverría, G. Aullón, D. Danovich, S. Shaik, S. Alvarez, *Nat. Chem.* **2011**, *3*, 323 – 330.
[270] S. Pekker, E. Kováts, G. Oszlányi, G. Bényei, G. Klupp, G. Bortel, I. Jalsovszky, E. Jakab, F. Borondics, K. Kamarás, M. Bokor, G. Kriza, K. Tompa, G. Faigel, *Nat. Mater.* **2005**, *4*, 764 – 767.
[271] G. Bortel, S. Pekker, É. Kováts, *Cryst. Growth Des.* **2011**, *11*, 865 – 874.
[272] a) R. Freudenberger, W. Lamer, A. D. Schlueter, *J. Org. Chem.* **1993**, *58*, 6497 – 6498; b) P. Kaszynski, J. Michl, *J. Am. Chem. Soc.* **1988**, *110*, 5225 – 5226.
[273] P. Kaszynski, A. C. Friedli, J. Michl, *J. Am. Chem. Soc.* **1992**, *114*, 601 – 620.
[274] H. Bothe, A.-D. Schlüter, *Adv. Mater.* **1991**, *3*, 440 – 442.
[275] J. D. D. Rehm, B. Ziemer, G. Szeimies, *Eur. J. Org. Chem.* **2001**, 1049 – 1052.
[276] C. Mazal, A. J. Paraskos, J. Michl, *J. Org. Chem.* **1998**, *63*, 2116 – 2119.
[277] J. Kaleta, Z. Janoušek, M. Nečas, C. Mazal, *Organometallics* **2015**, *34*, 967 – 972.
[278] P. F. H. Schwab, B. C. Noll, J. Michl, *J. Org. Chem.* **2002**, *67*, 5476 – 5485.
[279] G. Nuding, F. Voegtle, K. Danielmeier, E. Steckhan, *Synthesis* **1996**, 71 – 76.
[280] P. E. Eaton, E. Galoppini, R. Gilardi, *J. Am. Chem. Soc.* **1994**, *116*, 7588 – 7596.
[281] P. E. Eaton, K. Pramod, T. Emrick, R. Gilardi, *J. Am. Chem. Soc.* **1999**, *121*, 4111 – 4123.
[282] Y. Chauvin, L. Saussine, *Macromolecules* **1996**, *29*, 1163 – 1166.
[283] T. Kakuchi, W. Hirahat, S. Yano, H. Kaga, *Polym. Bull.* **1997**, *38*, 651 – 655.
[284] R. Priefer, S. Nguyen, P. G. Farrell, D. N. Harpp, *Macromolecules* **2003**, *36*, 5435 – 5436.
[285] N.-H. Yeh, C.-W. Chen, S.-L. Lee, H.-J. Wu, C.-h. Chen, T.-Y. Luh, *Macromolecules* **2012**, *45*, 2662 – 2667.
[286] P. I. Dron, K. Zhao, J. Kaleta, Y. Shen, J. Wen, R. K. Shoemaker, C. T. Rogers, J. Michl, *Adv. Funct. Mater.* **2016**, *26*, 5718 – 5732.
[287] C. Lemouchi, K. Iliopoulos, L. Zorina, S. Simonov, P. Wzietek, T. Cauchy, A. Rodríguez-Fortea, E. Canadell, J. Kaleta, J. Michl, D. Gindre, M. Chrysos, P. Batail, *J. Am. Chem. Soc.* **2013**, *135*, 9366 – 9376.
[288] G. Bastien, C. Lemouchi, P. Wzietek, S. Simonov, L. Zorina, A. Rodríguez-Fortea, E. Canadell, P. Batail, *Z. Anorg. Allg. Chem.* **2014**, *640*, 1127 – 1133.
[289] J. Kaleta, J. Michl, C. Mézière, S. Simonov, L. Zorina, P. Wzietek, A. Rodríguez-Fortea, E. Canadell, P. Batail, *CrystEngComm* **2015**, *17*, 7829 – 7834.
[290] C. Lemouchi, P. Batail, *Beilstein J. Org. Chem.* **2015**, *11*, 1881 – 1885.
[291] J. Kaleta, G. Bastien, I. Císařová, P. Batail, J. Michl, *Eur. J. Org. Chem.* **2018**, 5137 – 5142.
[292] H. Iwamura, K. Mislow, *Acc. Chem. Res.* **1988**, *21*, 175 – 182.
[293] Y. Kawada, H. Sakai, M. Oguri, G. Koga, *Tetrahedron Lett.* **1994**, *35*, 139 – 142.
[294] a) Nobel Prize (2016) The Nobel Prize in Chemistry. Available at www.nobelprize.org/nobel_prizes/chemistry/laureates/2016/; Accessed November 20, **2016**; b) D. A. Leigh, *Angew. Chem. Int. Ed.* **2016**, *55*, 14506 – 14508; *Angew. Chem.* **2016**, *128*, 14722 – 14724.
[295] J. E. Walker, *Angew. Chem. Int. Ed.* **1998**, *37*, 2308 – 2319; *Angew. Chem.* **1998**, *110*, 2438 – 2450.
[296] F. Chérioux, O. Galangau, F. Palmino, G. Rapenne, *ChemPhysChem* **2016**, *17*, 1742 – 1751.
[297] X. Jiang, B. Rodríguez-Molina, N. Nazarian, M. A. Garcia-Garibay, *J. Am. Chem. Soc.* **2014**, *136*, 8871 – 8874.
[298] G. Jimenez-Bueno, G. Rapenne, *Tetrahedron Lett.* **2003**, *44*, 6261 – 6263.
[299] G. Rapenne, G. Jimenez-Bueno, *Tetrahedron* **2007**, *63*, 7018 – 7026.
[300] H.-P. Jacquot de Rouville, R. Garbage, R. E. Cook, A. R. Pujol, A. M. Sirven, G. Rapenne, *Chem. Eur. J.* **2012**, *18*, 3023 – 3031.
[301] C. Lemouchi, H. M. Yamamoto, R. Kato, S. Simonov, L. Zorina, A. Rodríguez-Fortea, E. Canadell, P. Wzietek, K. Iliopoulos, D. Gindre, M. Chrysos, P. Batail, *Cryst. Growth Des.* **2014**, *14*, 3375 – 3383.
[302] C. E. Godinez, G. Zepeda, M. A. Garcia-Garibay, *J. Am. Chem. Soc.* **2002**, *124*, 4701 – 4707.
[303] C. E. Godinez, G. Zepeda, C. J. Mortko, H. Dang, M. A. Garcia-Garibay, *J. Org. Chem.* **2004**, *69*, 1652 – 1662.
[304] S. D. Karlen, C. E. Godinez, M. A. Garcia-Garibay, *Org. Lett.* **2006**, *8*, 3417 – 3420.
[305] C. S. Vogelsberg, M. A. Garcia-Garibay, *Chem. Soc. Rev.* **2012**, *41*, 1892 – 1910.
[306] B. Rodríguez-Molina, S. Pérez-Estrada, M. A. Garcia-Garibay, *J. Am. Chem. Soc.* **2013**, *135*, 10388 – 10395.
[307] M. A. Garcia-Garibay, *Proc. Natl. Acad. Sci. USA* **2005**, *102*, 10771 – 10776.
[308] a) T.-A. V. Khuong, G. Zepeda, R. Ruiz, S. I. Khan, M. A. Garcia-Garibay, *Cryst. Growth Des.* **2004**, *4*, 15 – 18; b) M. A. Garcia-Garibay, C. E. Godinez, *Cryst. Growth Des.* **2009**, *9*, 3124 – 3128.
[309] A. V. Akimov, A. B. Kolomeisky, *J. Phys. Chem. C* **2011**, *115*, 13584 – 13591.
[310] K. Nikitin, H. Müller-Bunz, Y. Ortin, W. Risse, M. J. McGlinchey, *Eur. J. Org. Chem.* **2008**, 3079 – 3084.
[311] S. Toyota, T. Shimizu, T. Iwanaga, K. Wakamatsu, *Chem. Lett.* **2011**, *40*, 312 – 314.
[312] D. K. Frantz, A. Linden, K. K. Baldridge, J. S. Siegel, *J. Am. Chem. Soc.* **2012**, *134*, 1528 – 1535.
[313] F. Huang, G. Wang, L. Ma, Y. Wang, X. Chen, Y. Che, H. Jiang, *J. Org. Chem.* **2017**, *82*, 12106 – 12111.
[314] A. M. Stevens, C. J. Richards, *Tetrahedron Lett.* **1997**, *38*, 7805 – 7808.
[315] M. Oki, *Angew. Chem. Int. Ed. Engl.* **1976**, *15*, 87 – 93; *Angew. Chem.* **1976**, *88*, 67 – 74.
[316] S. Toyota, K. Kawahata, K. Sugahara, K. Wakamatsu, T. Iwanaga, *Eur. J. Org. Chem.* **2017**, 5696 – 5707.
[317] G. Wang, H. Xiao, J. He, J. Xiang, Y. Wang, X. Chen, Y. Che, H. Jiang, *J. Org. Chem.* **2016**, *81*, 3364 – 3371.
[318] T. R. Kelly, M. C. Bowyer, K. V. Bhaskar, D. Bebbington, A. Garcia, F. Lang, M. H. Kim, M. P. Jette, *J. Am. Chem. Soc.* **1994**, *116*, 3657 – 3658.
[319] T. R. Kelly, *Acc. Chem. Res.* **2001**, *34*, 514 – 522.
[320] a) T. R. Kelly, J. P. Sestelo, I. Tellitu, *J. Org. Chem.* **1998**, *63*, 3655 – 3665; b) T. R. Kelly, I. Tellitu, J. P. Sestelo, *Angew. Chem. Int. Ed. Engl.* **1997**, *36*, 1866 – 1868; *Angew. Chem.* **1997**, *109*, 1969 – 1972.
[321] T. R. Kelly, H. de Silva, R. A. Silva, *Nature* **1999**, *401*, 150 – 152.
[322] a) K. Nikitin, H. Müller-Bunz, Y. Ortin, M. J. McGlinchey, *Org. Biomol. Chem.* **2007**, *5*, 1952 – 1960; b) K. Nikitin, C. Fleming, H. Müller-Bunz, Y. Ortin, M. J. McGlinchey, *Eur. J. Org. Chem.* **2010**, 5203 – 5216; c) L. E. Harrington, L. S. Cahill, M. J. McGlinchey, *Organometallics* **2004**, *23*, 2884 – 2891; d) K. Nikitin, C. Bothe, H. Müller-Bunz, Y. Ortin, M. J. McGlinchey, *Organometallics* **2012**, *31*, 6183 – 6198.
[323] K. Nikitin, H. Müller-Bunz, Y. Ortin, J. Muldoon, M. J. McGlinchey, *J. Am. Chem. Soc.* **2010**, *132*, 17617 – 17622.
[324] K. Nikitin, J. Muldoon, H. Müller-Bunz, M. J. McGlinchey, *Chem. Eur. J.* **2015**, *21*, 4664 – 4670.
[325] M. O'Keeffe, O. M. Yaghi, *Chem. Rev.* **2012**, *112*, 675 – 702.
[326] R. Ballesteros-Garrido, A. P. da Costa, P. Atienzar, M. Alvaro, C. Baleizão, H. García, *RSC Adv.* **2016**, *6*, 35191 – 35196.
[327] P. J. Llabres-Campaner, J. Pitarch-Jarque, R. Ballesteros-Garrido, B. Abarca, R. Ballesteros, E. García-España, *Dalton Trans.* **2017**, *46*, 7397 – 7402.
[328] X. Jiang, H.-B. Duan, S. I. Khan, M. A. Garcia-Garibay, *ACS Cent. Sci.* **2016**, *2*, 608 – 613.
[329] a) S. I. Vagin, A. K. Ott, S. D. Hoffmann, D. Lanzinger, B. Rieger, *Chem. Eur. J.* **2009**, *15*, 5845 – 5853; b) S. Vagin, A. Ott, H.-C. Weiss, A. Karbach, D. Volkmer, B. Rieger, *Eur. J. Inorg. Chem.* **2008**, 2601 – 2609.

[330] a) H. Chun, D. N. Dybtsev, H. Kim, K. Kim, *Chem. Eur. J.* **2005**, *11*, 3521 – 3529; b) B.-Q. Ma, K. L. Mulfort, J. T. Hupp, *Inorg. Chem.* **2005**, *44*, 4912 – 4914.
[331] E. I. Volkova, A. V. Vakhrushev, M. Suyetin, *Chem. Phys.* **2015**, *459*, 14 – 18.
[332] A. Kuc, A. Enyashin, G. Seifert, *J. Phys. Chem. B* **2007**, *111*, 8179 – 8186.
[333] a) M. R. Pérez, I. Pavlovic, C. Barriga, J. Cornejo, M. C. Hermosín, M. A. Ulibarri, *Appl. Clay Sci.* **2006**, *32*, 245 – 251; b) F. Cavani, F. Trifirb, A. Vaccari, *Catal. Today* **1991**, *11*, 173 – 301.
[334] a) F. A. Rad, Z. Rezvani, *RSC Adv.* **2015**, *5*, 67384 – 67393; b) Z. Rezvani, F. Arjomandi Rad, F. Khodam, *Dalton Trans.* **2015**, *44*, 988 – 996.
[335] F. A. Cotton, L. M. Daniels, C. Lin, C. A. Murillo, S.-Y. Yu, *J. Chem. Soc. Dalton Trans.* **2001**, 502 – 504.
[336] a) A. F. Stepan, C. Subramanyam, I. V. Efremov, J. K. Dutra, T. J. O'Sullivan, K. J. DiRico, W. S. McDonald, A. Won, P. H. Dorff, C. E. Nolan, S. L. Becker, L. R. Pustilnik, D. R. Riddell, G. W. Kauffman, B. L. Kormos, L. Zhang, Y. Lu, S. H. Capetta, M. E. Green, K. Karki, E. Sibley, K. P. Atchison, A. J. Hallgren, C. E. Oborski, A. E. Robshaw, B. Sneed, C. J. O'Donnell, *J. Med. Chem.* **2012**, *55*, 3414 – 3424; b) K. C. Nicolaou, D. Vourloumis, S. Totokotsopoulos, A. Papakyriakou, H. Karsunky, H. Fernando, J. Gavrilyuk, D. Webb, A. F. Stepan, *ChemMedChem* **2016**, *11*, 31 – 37.
[337] For a recent comprehensive review on this topic, see: T. A. Reekie, C. M. Williams, L. M. Rendina, M. Kassiou, *J. Med. Chem.* **2018**, in press, DOI https://doi.org/10.1021/acs.jmedchem.8b00888.
[338] N. A. Meanwell, *J. Med. Chem.* **2011**, *54*, 2529 – 2591.
[339] T. J. Ritchie, S. J. F. Macdonald, *Drug Discovery Today* **2009**, *14*, 1011 – 1020.
[340] N. T. Thirumoorthi, C. Jia Shen, V. A. Adsool, *Chem. Commun.* **2015**, *51*, 3139 – 3142.
[341] D. E. Applequist, T. L. Renken, J. W. Wheeler, *J. Org. Chem.* **1982**, *47*, 4985 – 4995.
[342] a) Y. P. Auberson, E. Briard, D. Sykes, J. Reilly, M. Healy, *ChemMedChem* **2016**, *11*, 1415 – 1427; b) F. Assmus, A. Seelig, L. Gobbi, E. Borroni, P. Glaentzlin, H. Fischer, *Eur. J. Pharm. Sci.* **2015**, *79*, 27 – 35.
[343] R. C. Reynolds, C. A. Johnson, J. R. Piper, F. M. Sirotnak, *Eur. J. Med. Chem.* **2001**, *36*, 237 – 242.
[344] A. Rosowsky, in *Progress in Medicinal Chemistry*, Vol. 29 (Eds.: G. P. Ellis, G. B. West), Elsevier, Amsterdam, **1989**, pp. 1 – 252.
[345] a) S. Sinha, I. Lieberburg, *Proc. Natl. Acad. Sci. USA* **1999**, *96*, 11049 – 11053; b) B. A. Bergmans, B. de Strooper, *Lancet Neurol.* **2010**, *9*, 215 – 226; c) M. S. Wolfe, *Biochemistry* **2006**, *45*, 7931 – 7939.
[346] a) R. Kopan, M. X. G. Ilagan, *Nat. Rev. Mol. Cell Biol.* **2004**, *5*, 499 – 504; b) A. J. Beel, C. R. Sanders, *Cell. Mol. Life Sci.* **2008**, *65*, 1311 – 1334.
[347] a) A. F. Kreft, R. Martone, A. Porte, *J. Med. Chem.* **2009**, *52*, 6169 – 6188; b) R. E. Olson, C. F. Albright, *Curr. Top. Med. Chem.* **2008**, *8*, 17 – 33; c) K. W. Gillman, J. E. Starrett, M. F. Parker, K. Xie, J. J. Bronson, L. R. Marcin, K. E. McElhone, C. P. Bergstrom, R. A. Mate, R. Williams, J. E. Meredith, Jr., C. R. Burton, D. M. Barten, J. H. Toyn, S. B. Roberts, K. A. Lentz, J. G. Houston, R. Zaczek, C. F. Albright, C. P. Decicco, J. E. Macor, R. E. Olson, *ACS Med. Chem. Lett.* **2010**, *1*, 120 – 124.
[348] a) G. Staurenghi, L. Ye, M. H. Magee, R. P. Danis, J. Wurzelmann, P. Adamson, M. M. McLaughlin, *Ophthalmology* **2015**, *122*, 990 – 996; b) G. Maher-Edwards, J. De'Ath, C. Barnett, A. Lavrov, A. Lockhart, *Alzheimer's Dementia* **2015**, *1*, 131 – 140.
[349] J. A. Blackie, J. C. Bloomer, M. J. B. Brown, H. Y. Cheng, B. Hammond, D. M. B. Hickey, R. J. Ife, C. A. Leach, V. A. Lewis, C. H. Macphee, K. J. Milliner, K. E. Moores, I. L. Pinto, S. A. Smith, I. G. Stansfield, S. J. Stanway, M. A. Taylor, C. J. Theobald, *Bioorg. Med. Chem. Lett.* **2003**, *13*, 1067 – 1070.
[350] R. J. Young, D. V. S. Green, C. N. Luscombe, A. P. Hill, *Drug Discovery Today* **2011**, *16*, 822 – 830.
[351] N. D. Measom, K. D. Down, D. J. Hirst, C. Jamieson, E. S. Manas, V. K. Patel, D. O. Somers, *ACS Med. Chem. Lett.* **2017**, *8*, 43 – 48.
[352] M. H. Keylor, B. S. Matsuura, C. R. J. Stephenson, *Chem. Rev.* **2015**, *115*, 8976 – 9027.
[353] L. G. Carter, J. A. D'Orazio, K. J. Pearson, *Endocr.-Relat. Cancer* **2014**, *21*, R209 – 225.
[354] J. M. Smoliga, O. Blanchard, *Molecules* **2014**, *19*, 17154 – 17172.
[355] L. A. Stivala, M. Savio, F. Carafoli, P. Perucca, L. Bianchi, G. Maga, L. Forti, U. M. Pagnoni, A. Albini, E. Prosperi, V. Vannini, *J. Biol. Chem.* **2001**, *276*, 22586 – 22594.
[356] Y. L. Goh, Y. T. Cui, V. Pendharkar, V. A. Adsool, *ACS Med. Chem. Lett.* **2017**, *8*, 516 – 520.
[357] N. T. Thirumoorthi, V. A. Adsool, *Org. Biomol. Chem.* **2016**, *14*, 9485 – 9489.
[358] a) A. Levitzki, E. Mishani, *Annu. Rev. Biochem.* **2006**, *75*, 93 – 109; b) T. Hunter, *J. Clin. Invest.* **2007**, *117*, 2036 – 2043.
[359] V. M. Richon, *Br. J. Cancer* **2006**, *95*, S2 – S6.
[360] P. J. Middlemiss, A. J. Glasky, M. P. Rathbone, E. Werstuik, S. Hindley, J. Gysbers, *Neurosci. Lett.* **1995**, *199*, 131 – 134.
[361] M. J. O'Neil, *The Merck Index: An Encyclopedia of Chemicals, Drugs, and Biologicals*, RSC, Cambridge, **2013**.
[362] M. R. Barbachyn, D. K. Hutchinson, D. S. Toops, R. J. Reid, G. E. Zurenko, B. H. Yagi, R. D. Schaadt, J. W. Allison, *Bioorg. Med. Chem. Lett.* **1993**, *3*, 671 – 676.
[363] D. Bouzard, P. Di Cesare, M. Essiz, J. P. Jacquet, J. R. Kiechel, P. Remuzon, A. Weber, T. Oki, M. Masuyoshi, R. E. Kessler, *J. Med. Chem.* **1990**, *33*, 1344 – 1352.
[364] L. J. Rubin, D. B. Badesch, R. J. Barst, N. Galie, C. M. Black, A. Keogh, T. Pulido, A. Frost, S. Roux, I. Leconte, M. Landzberg, G. Simonneau, *New Engl. J. Med.* **2002**, *346*, 896 – 903.
[365] K. O. Arseneau, F. Cominelli, *Expert Opin. Invest. Drugs* **2013**, *22*, 907 – 913.
[366] M. V. Westphal, B. T. Wolfstädter, J.-M. Plancher, J. Gatfield, E. M. Carreira, *ChemMedChem* **2015**, *10*, 461 – 469.
[367] J. M. Lopchuk, K. Fjelbye, Y. Kawamata, L. R. Malins, C.-M. Pan, R. Gianatassio, J. Wang, L. Prieto, J. Bradow, T. A. Brandt, M. R. Collins, J. Elleraas, J. Ewanicki, W. Farrell, O. O. Fadeyi, G. M. Gallego, J. J. Mousseau, R. Oliver, N. W. Sach, J. K. Smith, J. E. Spangler, H. Zhu, J. Zhu, P. S. Baran, *J. Am. Chem. Soc.* **2017**, *139*, 3209 – 3226.
[368] L. Zehnder, M. Bennett, J. Meng, B. Huang, S. Ninkovic, F. Wang, J. Braganza, J. Tatlock, T. Jewell, J. Z. Zhou, B. Burke, J. Wang, K. Maegley, P. P. Mehta, M.-J. Yin, K. S. Gajiwala, M. J. Hickey, S. Yamazaki, E. Smith, P. Kang, A. Sistla, E. Dovalsantos, M. R. Gehring, R. Kania, M. Wythes, P.-P. Kung, *J. Med. Chem.* **2011**, *54*, 3368 – 3385.
[369] a) A. Pagano, D. Ruegg, S. Litschig, N. Stoehr, C. Stierlin, M. Heinrich, P. Floersheim, L. Prezèau, F. Carroll, J. P. Pin, A. Cambria, I. Vranesic, P. Josef Flor, F. Gasparini, R. Kuhn, *J. Biol. Chem.* **2000**, *275*, 33750 – 33758; b) P. M. Lea, A. I. Faden, *CNS Drug Rev.* **2006**, *12*, 149 – 166.
[370] C.-Y. Cheng, L.-W. Hsin, Y.-P. Lin, P.-L. Tao, T.-T. Jong, *Bioorg. Med. Chem.* **1996**, *4*, 73 – 80.
[371] a) B. Sperlágh, P. Illes, *Purinergic Signal.* **2007**, *3*, 117 – 127; b) J. P. Hughes, J. P. Hatcher, I. P. Chessell, *Purinergic Signal.* **2007**, *3*, 163 – 169.
[372] K. Inoue, *Purinergic Signal.* **2007**, *3*, 135 – 144.
[373] H. Gunosewoyo, J. L. Guo, M. R. Bennett, M. J. Coster, M. Kassiou, *Bioorg. Med. Chem. Lett.* **2008**, *18*, 3720 – 3723.
[374] V. A. Zammit, L. K. Buckett, A. V. Turnbull, H. Wure, A. Proven, *Pharmacol. Ther.* **2008**, *118*, 295 – 302.
[375] B. M. Fox, N. Furukawa, X. Hao, K. Iio, T. Inaba, S. M. Jackson, F. Kayser, M. Labelle, K. Li, T. Matsui, D. L. Mcminn, N. Ogawa, S. M. Rubenstein, S. Sagawa, K. Sugimoto, M. Suzuki, M. Tanaka, G. Ye, A. Yoshida, J. Zhang (Tularik Inc & Japan Tobacco Inc) U.S. & Japan Patent WO 2004047755.
[376] A. V. Stachulski, J. R. Harding, J. C. Lindon, J. L. Maggs, B. K. Park, I. D. Wilson, *J. Med. Chem.* **2006**, *49*, 6931 – 6945.
[377] A. M. Birch, S. Birtles, L. K. Buckett, P. D. Kemmitt, G. J. Smith, T. J. D. Smith, A. V. Turnbull, S. J. Y. Wang, *J. Med. Chem.* **2009**, *52*, 1558 – 1568.
[378] J. G. Barlind, U. A. Bauer, A. M. Birch, S. Birtles, L. K. Buckett, R. J. Butlin, R. D. M. Davies, J. W. Eriksson, C. D. Hammond, R. Hovland, P. Johannesson, M. J. Johansson, P. D. Kemmitt, B. T. Lindmark, P. M. Gutierrez, T. A. Noeske, A. Nordin, C. J. O'Donnell, A. U. Petersson, A. Redzic, A. V. Turnbull, J. Vinblad, *J. Med. Chem.* **2012**, *55*, 10610 – 10629.
[379] F. Cameron, M. Sanford, *Drugs* **2014**, *74*, 263 – 271.
[380] B. B. Lerman, L. Belardinelli, *Circulation* **1991**, *83*, 1499 – 1509.
[381] X. Gao, J. Wang, J. Liu, D. Guiadeen, A. Krikorian, S. B. Boga, A.-B. Alhassan, O. Selyutin, W. Yu, Y. Yu, R. Anand, S. Liu, C. Yang, H. Wu, J. Cai, A. Cooper, H. Zhu, K. Maloney, Y.-D. Gao, T. O. Fischmann, J. Presland, M. Mansueto, Z. Xu, E. Leccese, J. Zhang-Hoover, I. Knemeyer, C. G. Garlisi, N. Bays, P. Stivers, P. E. Brandish, A. Hicks, R. Kim, J. A. Kozlowski, *Bioorg. Med. Chem. Lett.* **2017**, *27*, 1471 – 1477.

[382] R. Al Hussainy, J. Verbeek, D. van der Born, A. H. Braker, J. E. Leysen, R. J. Knol, J. Booij, J. K. D. M. Herscheid, *J. Med. Chem.* **2011**, *54*, 3480 – 3491.

[383] a) R. Al Hussainy, J. Verbeek, D. van der Born, J. Booij, J. K. D. M. Herscheid, *Eur. J. Med. Chem.* **2011**, *46*, 5728 – 5735; b) R. Al Hussainy, J. Verbeek, D. van der Born, C. Molthoff, J. Booij, J. K. D. M. Herscheid, *Nucl. Med. Biol.* **2012**, *39*, 1068 – 1076.

[384] G. Reaven, *Circulation* **2002**, *106*, 286 – 288.

[385] J. R. Seckl, B. R. Walker, *Endocrinology* **2001**, *142*, 1371 – 1376.

[386] a) X. Gu, J. Dragovic, G. C. Koo, S. L. Koprak, C. LeGrand, S. S. Mundt, K. Shah, M. S. Springer, E. Y. Tan, R. Thieringer, A. Hermanowski-Vosatka, H. J. Zokian, J. M. Balkovec, S. T. Waddell, *Bioorg. Med. Chem. Lett.* **2005**, *15*, 5266 – 5269; b) M. Maletic, A. Leeman, M. Szymonifka, S. S. Mundt, H. J. Zokian, K. Shah, J. Dragovic, K. Lyons, R. Thieringer, A. H. Vosatka, J. Balkovec, S. T. Waddell, *Bioorg. Med. Chem. Lett.* **2011**, *21*, 2568 – 2572.

[387] S. T. Waddell, G. M. Santorelli, M. M. Milana, A. H. Leeman, X. Gu, D. W. Graham, J. M. Balkovec, S. D. Aster (Merck & Co Inc.) US Patent: US 2004133011 (A1).

[388] W. A. Gregory (E. I. du Pont de Nemours and Co.) US Patent 3558704.

[389] F. Bordi, A. Ugolini, *Prog. Neurobiol.* **1999**, *59*, 55 – 79.

[390] J. P. Pin, R. Duvoisin, *Neuropharmacology* **1995**, *34*, 1 – 26.

[391] S. A. Eaton, D. E. Jane, P. L. St.J. Jones, R. H. P. Porter, P. C.-K. Pook, D. C. Sunter, P. M. Udvarhelyi, P. J. Roberts, T. E. Salt, J. C. Watkins, *Eur. J. Pharmacol.* **1993**, *244*, 195 – 197.

[392] J. Watkins, G. Collingridge, *Trends Pharmacol. Sci.* **1994**, *15*, 333 – 342.

[393] R. Pellicciari, M. Raimondo, M. Marinozzi, B. Natalini, G. Costantino, C. Thomsen, *J. Med. Chem.* **1996**, *39*, 2874 – 2876.

[394] R. Pellicciari, G. Costantino, E. Giovagnoni, L. Mattoli, I. Brabet, J.-P. Pin, *Bioorg. Med. Chem. Lett.* **1998**, *8*, 1569 – 1574.

[395] S. R. Baker, T. C. Hancox, *Tetrahedron Lett.* **1999**, *40*, 781 – 784.

[396] G. Costantino, K. Maltoni, M. Marinozzi, E. Camaioni, L. Prezeau, J.-P. Pin, R. Pellicciari, *Bioorg. Med. Chem.* **2001**, *9*, 221 – 227.

[397] R. Pellicciari, R. Filosa, M. C. Fulco, M. Marinozzi, A. Macchiarulo, C. Novak, B. Natalini, M. B. Hermit, S. Nielsen, T. N. Sager, T. B. Stensbøl, C. Thomsen, *ChemMedChem* **2006**, *1*, 358 – 365.

[398] Y. Tanabe, A. Nomura, M. Masu, R. Shigemoto, N. Mizuno, S. Nakanishi, *J. Neurosci.* **1993**, *13*, 1372 – 1378.

[399] a) R. Filosa, M. Marinozzi, G. Costantino, M. B. Hermit, C. Thomsen, R. Pellicciari, *Bioorg. Med. Chem.* **2006**, *14*, 3811 – 3817; b) R. Filosa, M. Carmela Fulco, M. Marinozzi, N. Giacchè, A. Macchiarulo, A. Peduto, A. Massa, P. de Caprariis, C. Thomsen, C. T. Christoffersen, R. Pellicciari, *Bioorg. Med. Chem.* **2009**, *17*, 242 – 250.

[400] L. J. Loeffler, S. F. Britcher, W. Baumgarten, *J. Med. Chem.* **1970**, *13*, 926 – 935.

[401] J. Wlochal, R. Davies, J. Burton, *Synlett* **2016**, *27*, 919 – 923.

[402] Q. I. Churches, R. J. Mulder, J. M. White, J. Tsanaktsidis, P. J. Duggan, *Aust. J. Chem.* **2012**, *65*, 690 – 693.

[403] D. Steer, R. Lew, P. Perlmutter, A. I. Smith, M.-I. Aguilar, *Biochemistry* **2002**, *41*, 10819 – 10826.

[404] D. Seebach, J. L. Matthews, *Chem. Commun.* **1997**, 2015 – 2022.

[405] M. A. Danielson, J. J. Falke, *Annu. Rev. Biophys. Biomol. Struct.* **1996**, *25*, 163 – 195.

[406] R. W. Glaser, C. Sachse, U. H. N. Dürr, P. Wadhwani, S. Afonin, E. Strandberg, A. S. Ulrich, *Biophys. J.* **2005**, *88*, 3392 – 3397.

[407] R. W. Glaser, C. Sachse, U. H. N. Dürr, P. Wadhwani, A. S. Ulrich, *J. Magn. Reson.* **2004**, *168*, 153 – 163.

[408] P. Wadhwani, J. Reichert, E. Strandberg, J. Bürck, J. Misiewicz, S. Afonin, N. Heidenreich, S. Fanghänel, P. K. Mykhailiuk, I. V. Komarov, A. S. Ulrich, *Phys. Chem. Chem. Phys.* **2013**, *15*, 8962 – 8971.

[409] P. Wadhwani, E. Strandberg, N. Heidenreich, J. Bürck, S. Fanghänel, A. S. Ulrich, *J. Am. Chem. Soc.* **2012**, *134*, 6512 – 6515.

[410] J. Blazyk, R. Wiegand, J. Klein, J. Hammer, R. M. Epand, R. F. Epand, W. L. Maloy, U. P. Kari, *J. Biol. Chem.* **2001**, *276*, 27899 – 27906.

[411] M. Meier, J. Seelig, *J. Am. Chem. Soc.* **2008**, *130*, 1017 – 1024.

[412] S. O. Kokhan, A. V. Tymtsunik, S. L. Grage, S. Afonin, O. Babii, M. Berditsch, A. V. Strizhak, D. Bandak, M. O. Platonov, I. V. Komarov, A. S. Ulrich, P. K. Mykhailiuk, *Angew. Chem. Int. Ed.* **2016**, *55*, 14788 – 14792; *Angew. Chem.* **2016**, *128*, 15008 – 15012.

[413] P. K. Mikhailiuk, S. Afonin, A. N. Chernega, E. B. Rusanov, M. O. Platonov, G. G. Dubinina, M. Berditsch, A. S. Ulrich, I. V. Komarov, *Angew. Chem. Int. Ed.* **2006**, *45*, 5659 – 5661; *Angew. Chem.* **2006**, *118*, 5787 – 5789.

[414] S. L. Grage, X. Xu, M. Schmitt, P. Wadhwani, A. S. Ulrich, *J. Phys. Chem. Lett.* **2014**, *5*, 4256 – 4259.

[415] a) O. Toke, R. D. O'Connor, T. K. Weldeghiorghis, W. L. Maloy, R. W. Glaser, A. S. Ulrich, J. Schaefer, *Biophys. J.* **2004**, *87*, 675 – 687; b) J. Salgado, S. L. Grage, L. H. Kondejewski, R. S. Hodges, R. N. McElhaney, A. S. Ulrich, *J. Biomol. NMR* **2001**, *21*, 191 – 208; c) A. N. Tkachenko, P. K. Mykhailiuk, D. S. Radchenko, O. Babii, S. Afonin, A. S. Ulrich, I. V. Komarov, *Eur. J. Org. Chem.* **2014**, 3584 – 3591.

[416] D. Bandak, O. Babii, R. Vasiuta, I. V. Komarov, P. K. Mykhailiuk, *Org. Lett.* **2015**, *17*, 226 – 229.

[417] K. Richter, H. Aschauer, G. Kreil, *Peptides* **1985**, *6*, 17 – 21.

[418] K. Schmidt-Rohr, E. R. deAzevedo, T. J. Bonagamba, in *Centerband-Only Detection of Exchange (CODEX)*, Wiley, Chichester, **2007**.

[419] a) E. Strandberg, P. Wadhwani, P. Tremouilhac, U. H. N. Dürr, A. S. Ulrich, *Biophys. J.* **2006**, *90*, 1676 – 1686; b) D. S. Radchenko, S. Kattge, S. Kara, A. S. Ulrich, S. Afonin, *Biochim. Biophys. Acta Biomembr.* **2016**, *1858*, 2019 – 2027.

[420] S. Horvat, K. Mlinarić-Majerski, L. Glavas-Obrovac, A. Jakas, J. Veljković, S. Marczi, G. Kragol, M. Roscić, M. Matković, A. Milostić-Srb, *J. Med. Chem.* **2006**, *49*, 3136 – 3142.

[421] V. V. Kapoerchan, A. D. Knijnenburg, M. Niamat, E. Spalburg, A. J. de Neeling, P. H. Nibbering, R. H. Mars-Groenendijk, D. Noort, J. M. Otero, A. L. Llamas-Saiz, M. J. van Raaij, G. A. van der Marel, H. S. Overkleeft, M. Overhand, *Chem. Eur. J.* **2010**, *16*, 12174 – 12181.

[422] K. C. Nicolaou, J. Yin, D. Mandal, R. D. Erande, P. Klahn, M. Jin, M. Aujay, J. Sandoval, J. Gavrilyuk, D. Vourloumis, *J. Am. Chem. Soc.* **2016**, *138*, 1698 – 1708.

[423] a) P. Gaudreau, R. Quirion, S. St-Pierre, C. B. Pert, *Peptides* **1983**, *4*, 755 – 762; b) M. Pätzel, M. Sanktjohanser, A. Doss, P. Henklein, G. Szeimies, *Eur. J. Org. Chem.* **2004**, 493 – 498.

[424] S. E. Blondelle, E. Takahashi, K. T. Dinh, R. A. Houghten, *J. Appl. Bacteriol.* **1995**, *78*, 39 – 46.

[425] S. Pritz, M. Pätzel, G. Szeimies, M. Dathe, M. Bienert, *Org. Biomol. Chem.* **2007**, *5*, 1789 – 1794.

[426] A. Wessolowski, M. Bienert, M. Dathe, *J. Pept. Res.* **2004**, *64*, 159 – 169.

[427] E. Selva, G. Beretta, N. Montanini, G. S. Saddler, L. Gastaldo, P. Ferrari, R. Lorenzetti, P. Landini, F. Ripamonti, B. P. Goldstein, *J. Antibiot.* **1991**, *44*, 693 – 701.

[428] M. J. LaMarche, J. A. Leeds, K. Amaral, J. T. Brewer, S. M. Bushell, J. M. Dewhurst, J. Dzink-Fox, E. Gangl, J. Goldovitz, A. Jain, S. Mullin, G. Neckermann, C. Osborne, D. Palestrant, M. A. Patane, E. M. Rann, M. Sachdeva, J. Shao, S. Tiamfook, L. Whitehead, D. Yu, *J. Med. Chem.* **2011**, *54*, 8099 – 8109.

[429] a) Q. L. Choo, G. Kuo, A. J. Weiner, L. R. Overby, D. W. Bradley, M. Houghton, *Science* **1989**, *244*, 359 – 362; b) G. Kuo, Q. L. Choo, H. J. Alter, G. L. Gitnick, A. G. Redeker, R. H. Purcell, T. Miyamura, J. L. Dienstag, M. J. Alter, C. E. Stevens, *Science* **1989**, *244*, 362 – 364.

[430] A. Macdonald, M. Harris, *J. Gen. Virol.* **2004**, *85*, 2485 – 2502.

[431] J. L. Romine, D. R. St. Laurent, J. E. Leet, S. W. Martin, M. H. Serrano-Wu, F. Yang, M. Gao, D. R. O'Boyle, J. A. Lemm, J.-H. Sun, P. T. Nower, X. S. Huang, M. S. Deshpande, N. A. Meanwell, L. B. Snyder, *ACS Med. Chem. Lett.* **2011**, *2*, 224 – 229.

[432] M. Gao, R. E. Nettles, M. Belema, L. B. Snyder, V. N. Nguyen, R. A. Fridell, M. H. Serrano-Wu, D. R. Langley, J.-H. Sun, D. R. O'Boyle, J. A. Lemm, C. Wang, J. O. Knipe, C. Chien, R. J. Colonno, D. M. Grasela, N. A. Meanwell, L. G. Hamann, *Nature* **2010**, *465*, 96 – 100.

[433] M. Zhong, E. Peng, N. Huang, Q. Huang, A. Huq, M. Lau, R. Colonno, L. Li, *Bioorg. Med. Chem. Lett.* **2016**, *26*, 4508 – 4512.

[434] P. R. Schreiner, A. A. Fokin, O. Lauenstein, Y. Okamoto, T. Wakita, C. Rinderspacher, G. H. Robinson, J. K. Vohs, C. F. Campana, *J. Am. Chem. Soc.* **2002**, *124*, 13348 – 13349.

[435] A. A. Fokin, P. R. Schreiner, R. Berger, G. H. Robinson, P. Wei, C. F. Campana, *J. Am. Chem. Soc.* **2006**, *128*, 5332 – 5333.

[436] a) R. Chauvin, *Tetrahedron Lett.* **1995**, *36*, 397 – 400; b) V. Maraval, R. Chauvin, *New J. Chem.* **2007**, *31*, 1853 – 1873.

[437] K. S. Feldman, C. M. Kraebel, M. Parvez, *J. Am. Chem. Soc.* **1993**, *115*, 3846 – 3847.

[438] a) S. Szafert, J. A. Gladysz, *Chem. Rev.* **2006**, *106*, 1 – 33; b) A. Orita, J. Otera, *Chem. Rev.* **2006**, *106*, 5387 – 5412.
[439] K. K. Larson, M. He, J. F. Teichert, A. Naganawa, J. W. Bode, *Chem. Sci.* **2012**, *3*, 1825 – 1828.
[440] J. F. Teichert, D. Mazunin, J. W. Bode, *J. Am. Chem. Soc.* **2013**, *135*, 11314 – 11321.
[441] O. Yahiaoui, L. F. Pašteka, B. Judeel, T. Fallon, *Angew. Chem. Int. Ed.* **2018**, *57*, 2570 – 2574; *Angew. Chem.* **2018**, *130*, 2600 – 2604.
[442] P. C. M. van Gerven, J. A. A. W. Elemans, J. W. Gerritsen, S. Speller, R. J. M. Nolte, A. E. Rowan, *Chem. Commun.* **2005**, 3535 – 3537.
[443] Q. Wang, C. Yu, C. Zhang, H. Long, S. Azarnoush, Y. Jin, W. Zhang, *Chem. Sci.* **2016**, *7*, 3370 – 3376.
[444] J.-F. Xu, Y.-Z. Chen, L.-Z. Wu, C.-H. Tung, Q.-Z. Yang, *Org. Lett.* **2013**, *15*, 6148 – 6151.
[445] Y. Jin, C. Yu, R. J. Denman, W. Zhang, *Chem. Soc. Rev.* **2013**, *42*, 6634 – 6654.
[446] R. Hoffmann, H. Hopf, *Angew. Chem. Int. Ed.* **2008**, *47*, 4474 – 4481; *Angew. Chem.* **2008**, *120*, 4548 – 4556.
[447] P. Dowd, H. Irngartinger, *Chem. Rev.* **1989**, *89*, 985 – 996.
[448] L. A. Paquette, R. J. Ternansky, D. W. Balogh, G. Kentgen, *J. Am. Chem. Soc.* **1983**, *105*, 5446 – 5450.
[449] G. J. Kent, S. A. Godleski, E. Osawa, P. v. R. Schleyer, *J. Org. Chem.* **1977**, *42*, 3852 – 3859.
[450] B. R. Vogt, S. R. Suter, J. R. E. Hoover, *Tetrahedron Lett.* **1968**, *13*, 1609 – 1612.

Manuscript received: August 19, 2018
Revised manuscript received: October 20, 2018
Accepted manuscript online: November 2, 2018
Version of record online: January 14, 2019

